Part H : Gamma-ray bursts

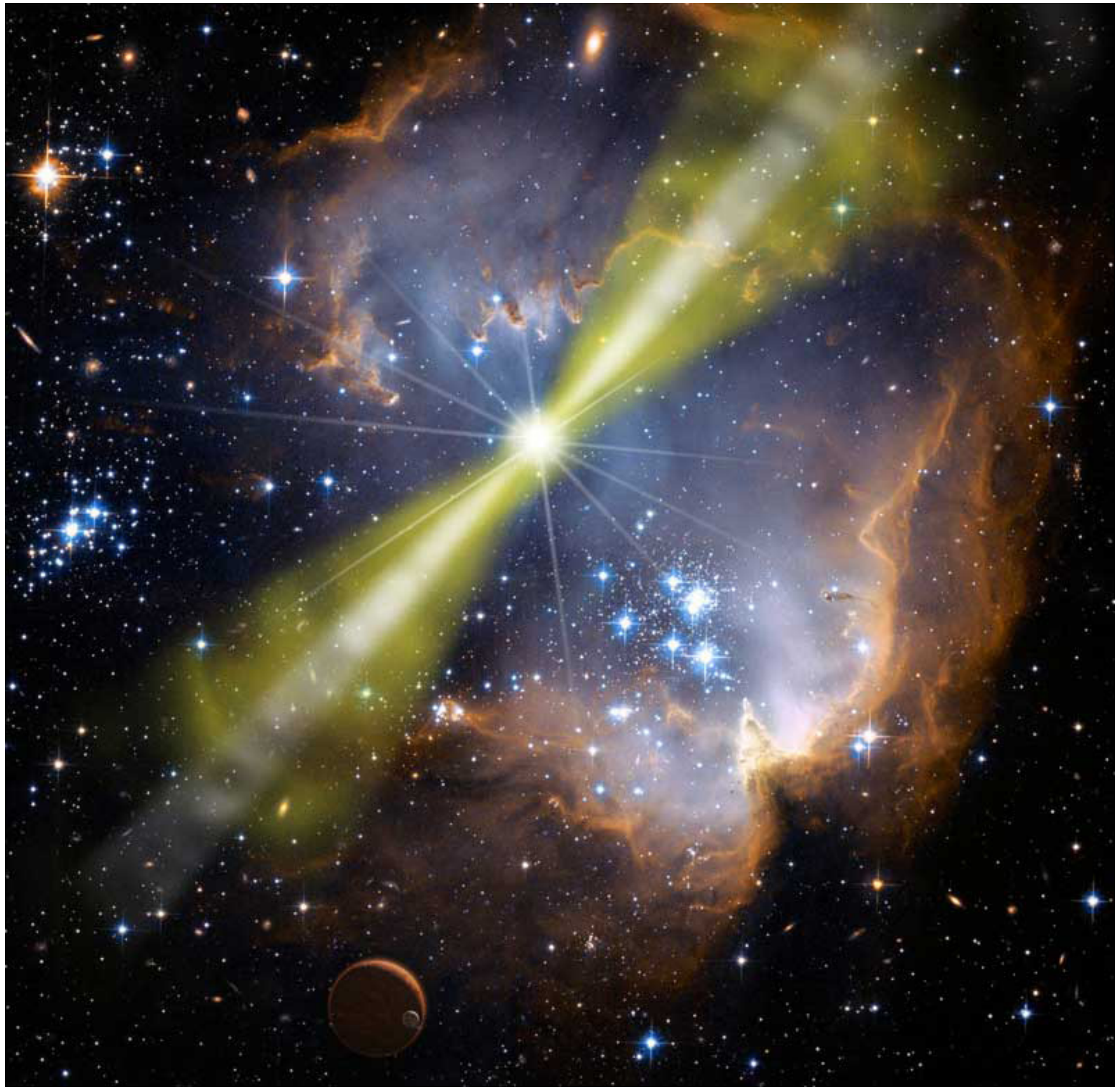

Discovered in 1967 by the military Vela satellites.

Initially classified, published only in 1973 (73 bursts in total).

Strong bursts of gamma rays (E > 30 keV), lasting for a few seconds, coming from all directions.

For over 25 years (until late 1990s) unclear whether originating in Milky Way/local Universe events (e.g. comets impacting neutron stars) or from cosmological distances.

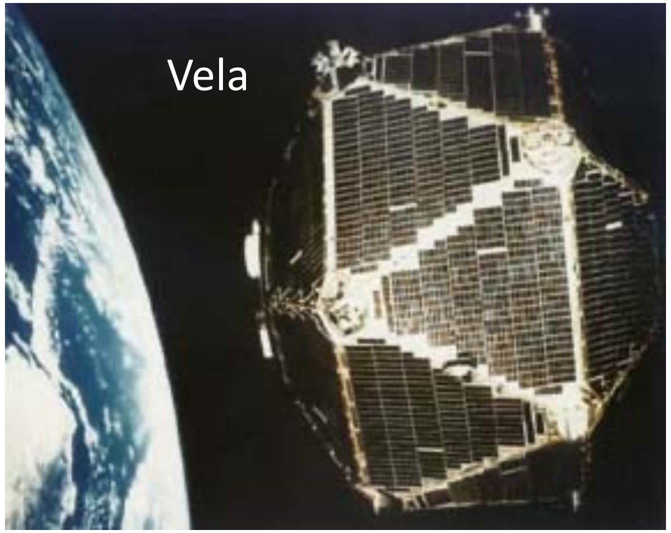

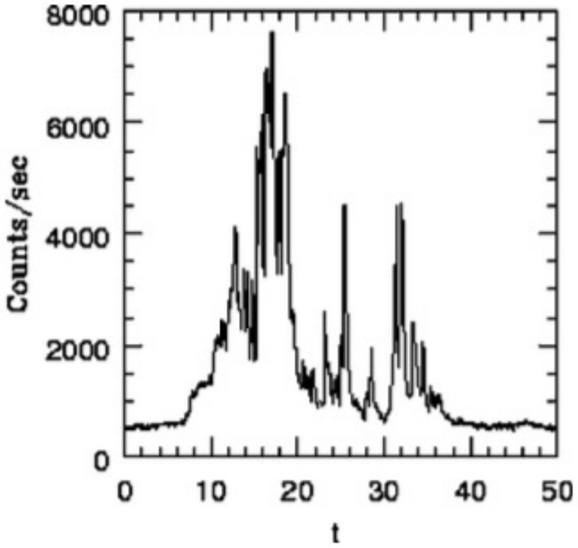

COMPTON BATSE (1991-2000). 20 keV - 30 GeV


Detected ~3000 GRBs, but not very accurate sky positions.

BeppoSAX (1996 - 2002)
0.1 - 300 keV


Allowed accurate enough localization to search for counterparts.

SWIFT (2004 - current)
15 - 150 keV + Xray/UV/optical.
Follow-up capability within 2 min.

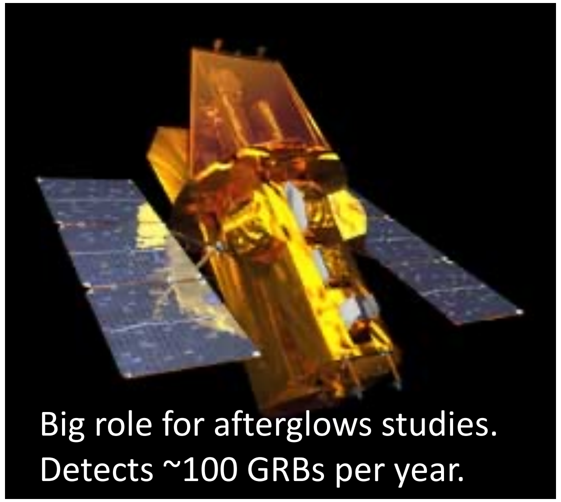
Big role for afterglows studies.
Detects ~100 GRBs per year.

FERMI (2008 - current)
8 keV – 100 GeV.

Probes the very high energy range.

*Others: **HETE-2, AGILE, Konus-Wind***

Bursts emit at keV to > GeV energies

Abdo+2009, Science
(burst observed with FERMI)

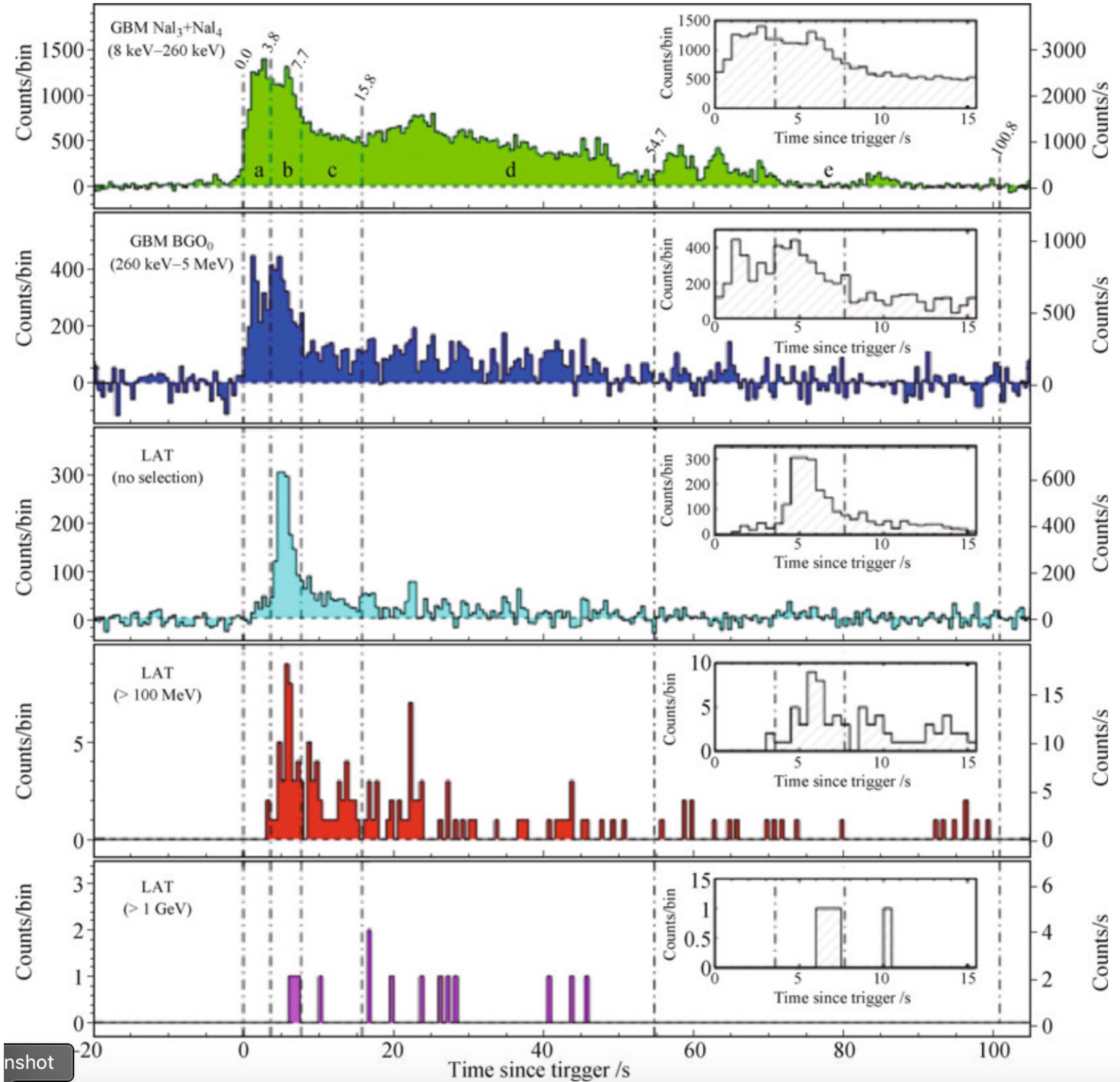

Kouveliotou+1993

Properties

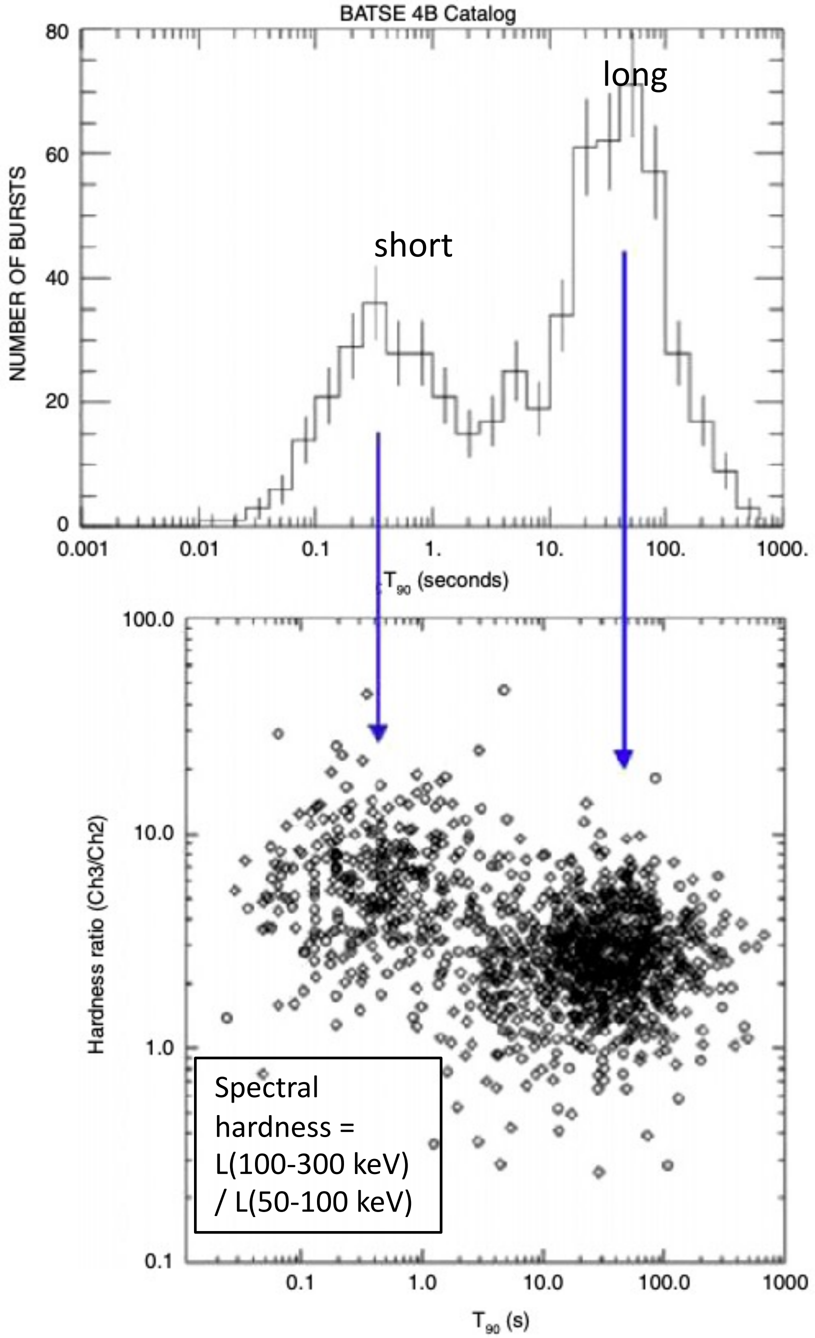

Spectral hardness = L(100-300 keV) / L(50-100 keV)

- A **bimodal duration distribution**: ***short*** (~0.1 - 2s) and ***long*** (~2 - 200s) bursts, as measured by "T90" (the time over which 90% of the total emission has been received).

- The short bursts have on average somewhat harder (higher energy photon) emission.

- **Brightness**: Large variation in light curve morphologies.

Clearly the emission process can be repeatable.

- **Variability:** on many timescales, down to milliseconds.

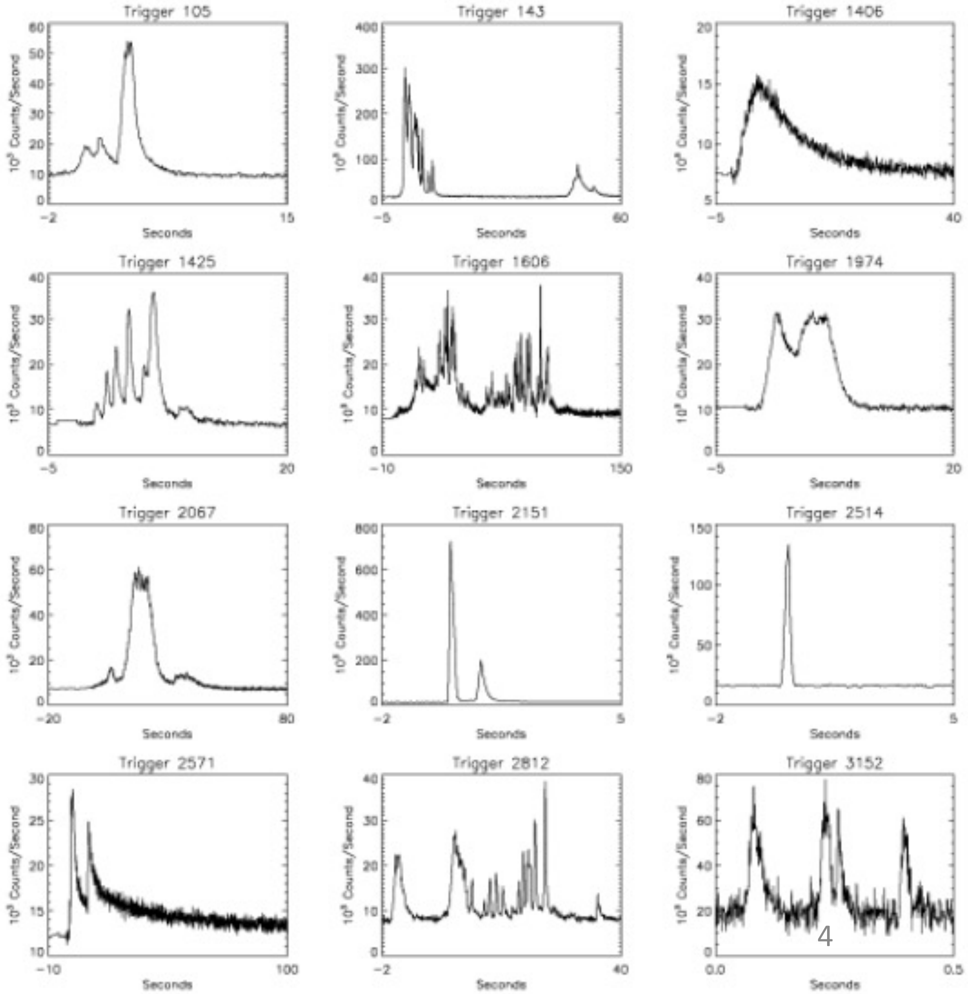

Kumar 2015

Long burst examples

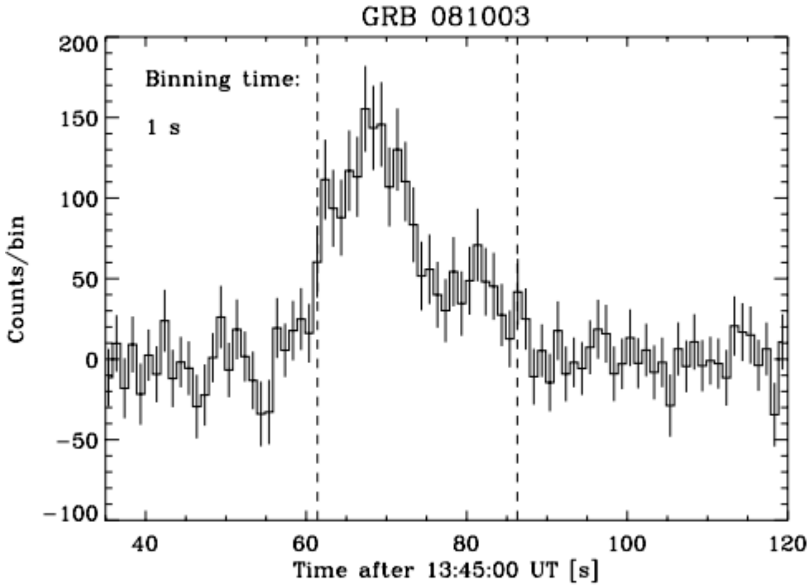
GRB 081003

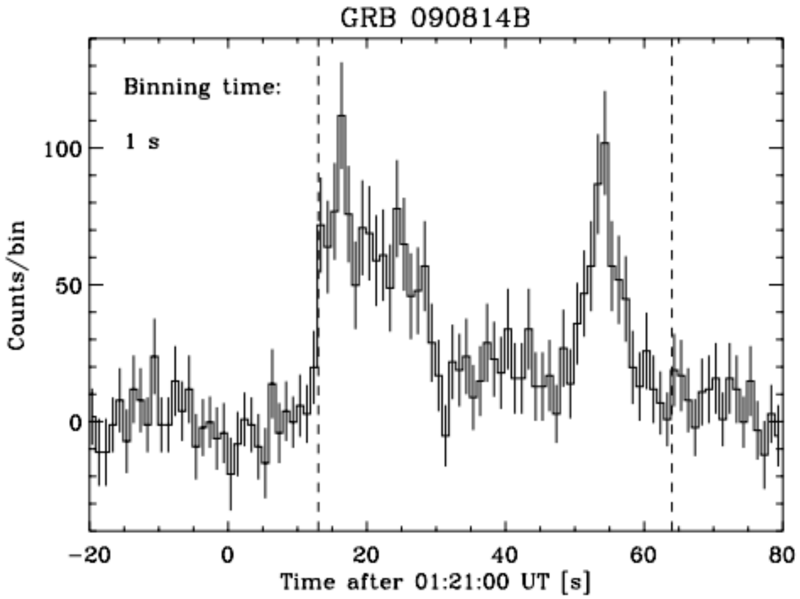
GRB 090814B

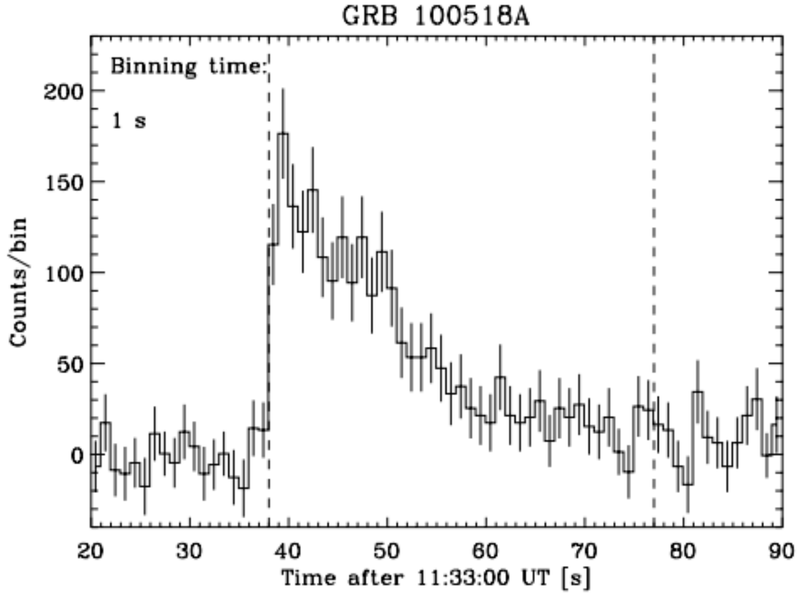
GRB 100518A

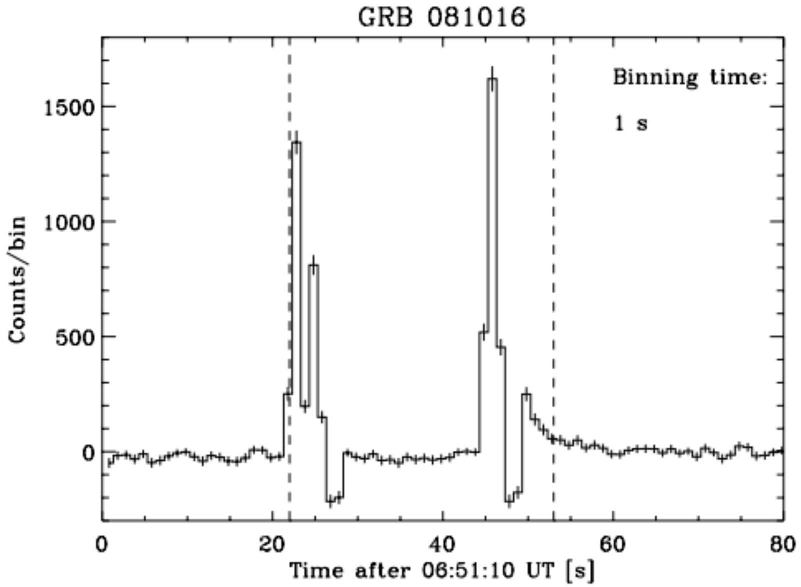
GRB 081016

Bosnjak+2014

Long burst examples

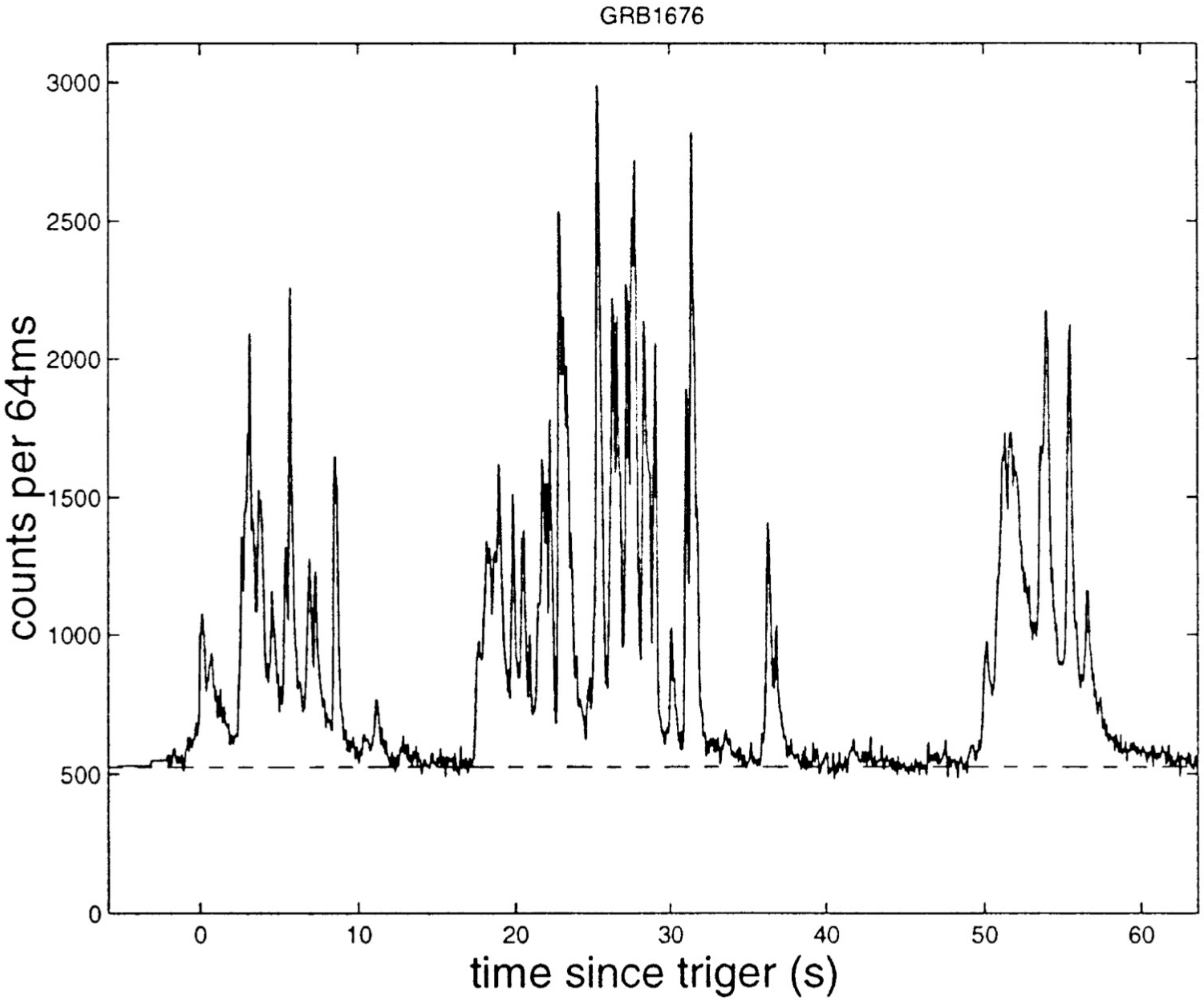

Piran 1999

Spectral Energy Distribution (SED) : non-thermal

Care whether *N(E)*, or $F_\nu (\propto E * N(E))$, or $\upsilon F_\nu (\propto E^2 * N(E))$ plotted.

N(E)

$E^2 * N(E)$

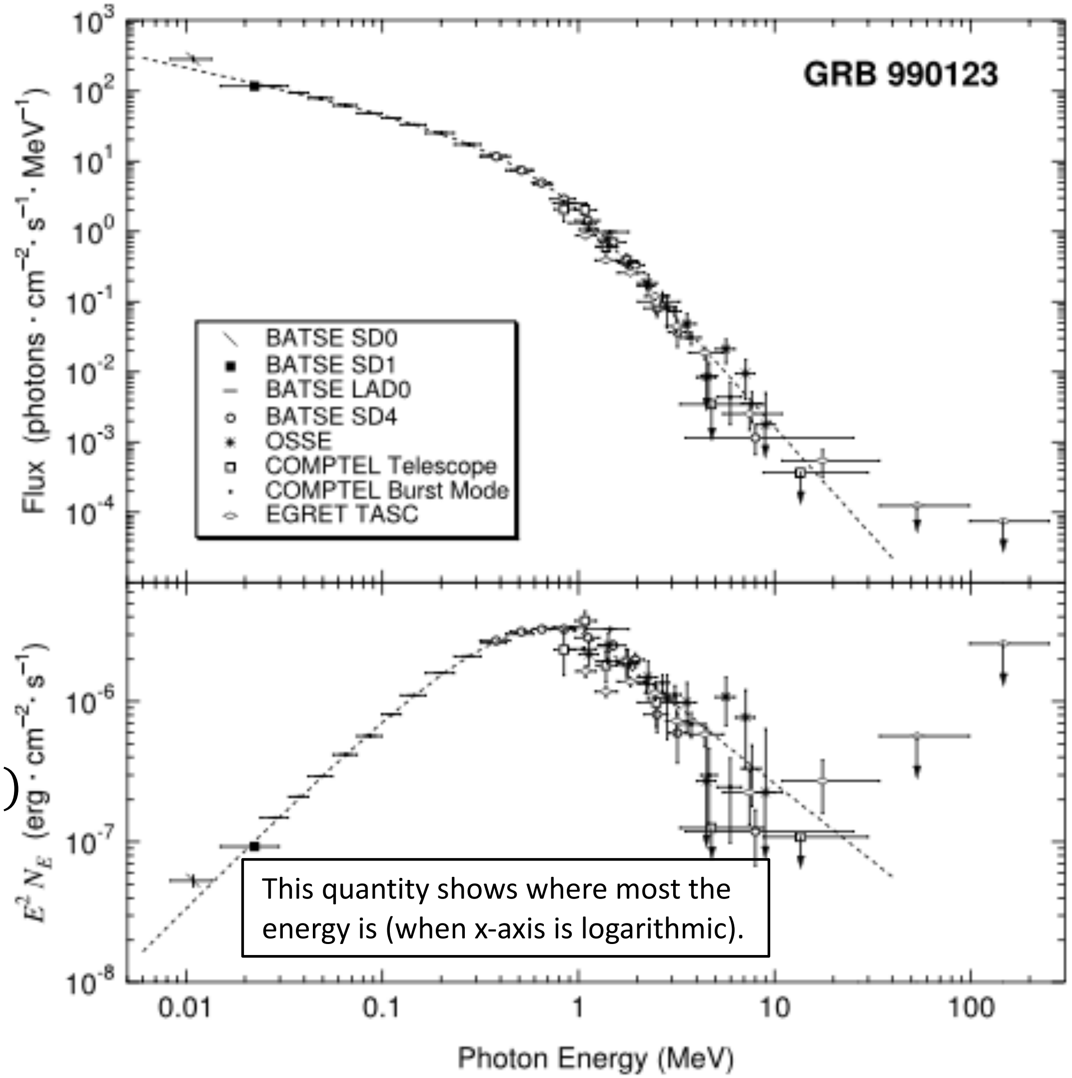

This quantity shows where most the energy is (when x-axis is logarithmic).

Kumar 2015

For most GRBs, only a time-integrated SED available. Brightest bursts → time-resolved.

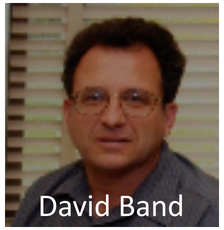

David Band

"**Band function**": 4-parameter broken power law:

$$N(E) = \begin{cases} A\left(\frac{E}{100\ \mathrm{keV}}\right)^{\alpha} \exp\left(-\frac{E}{E_0}\right), & E < (\alpha-\beta)E_0, \\ A\left[\frac{(\alpha-\beta)E_0}{100\ \mathrm{keV}}\right]^{\alpha-\beta} \exp(\beta-\alpha)\left(\frac{E}{100\ \mathrm{keV}}\right)^{\beta}, & E \geq (\alpha-\beta)E_0, \end{cases}$$

Fits give $\alpha = -1 \pm 1, \beta = -2^{+1}_{-2}$.

E_0 is called the "**break energy**". Peak of $E^2 N(E)$ is called the "**peak energy**", E_p. Can show $E_p = (2+\alpha)E_0$.

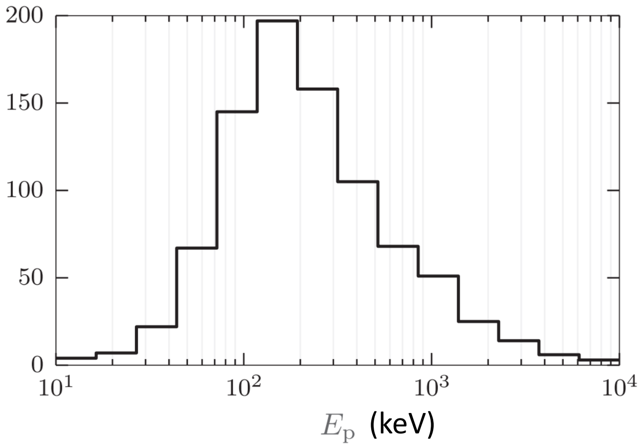

Burgess+2015.

Afterglows

A cosmological origin was established in 1997 when **afterglows** were detected for the first time. Spectral lines in these revealed a large redshift z = 0.835 (distance 5.4 GPc) for GRB 970508.

The vast majority of burst have afterglows: >95% in X-rays, >60% in optical,~10% in radio. Most of the radiated afterglow energy lies in the X-ray band.

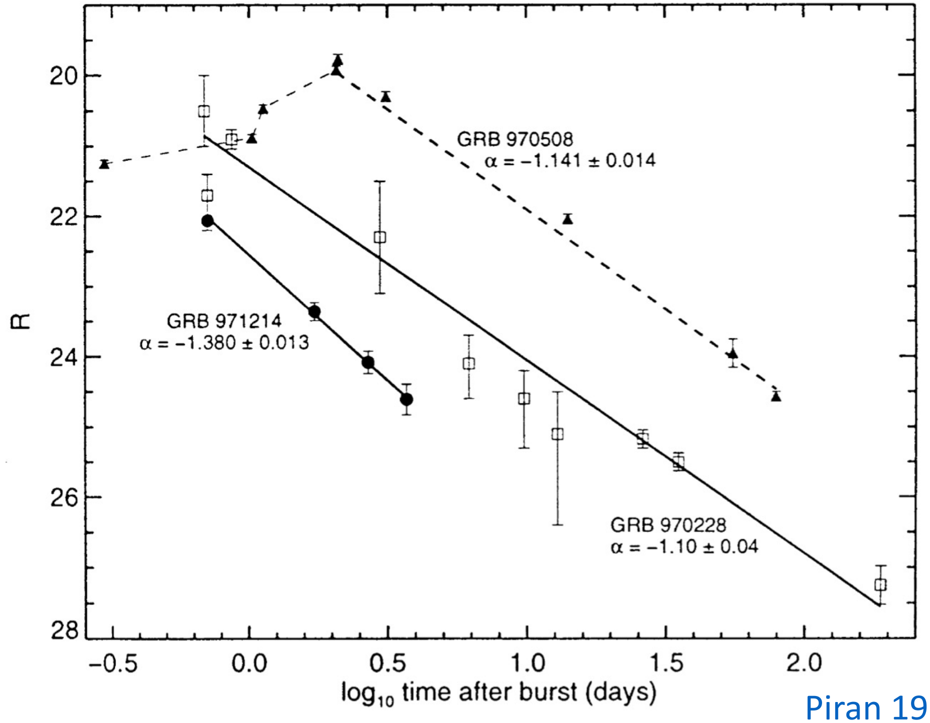

Piran 1999

(note alpha is here the time ev. power law).

Immediate consequence: **Equivalent isotropic energy E_{iso} ≡ $4\pi d^2 \int F(t)dt = \sim 10^{53}$ erg long bursts, $\sim 10^{51}$ erg short.**

What kind of objects can release this kind of energy on a time scale of seconds?

Only **black holes** and **neutron stars**.

$$E_{grav} \sim \frac{GM^2}{R} = 10^{53}\left(\frac{M}{M_\odot}\right)\left(\frac{R}{10\,R_S}\right)^{-1} \text{erg}$$

$$\tau_{hydro} = \frac{1}{2\sqrt{G\rho}} \sim 10^{-3}\text{s}\left(\frac{M}{M_\odot}\right)\left(\frac{R}{10\,R_S}\right)^{-3/2}$$

Too short? More later..

Schwarzschild radius $R_S = 2GM/c^2 = 3$ km*(M/M_{sun})

Equivalent isotropic energy (prompt emission)

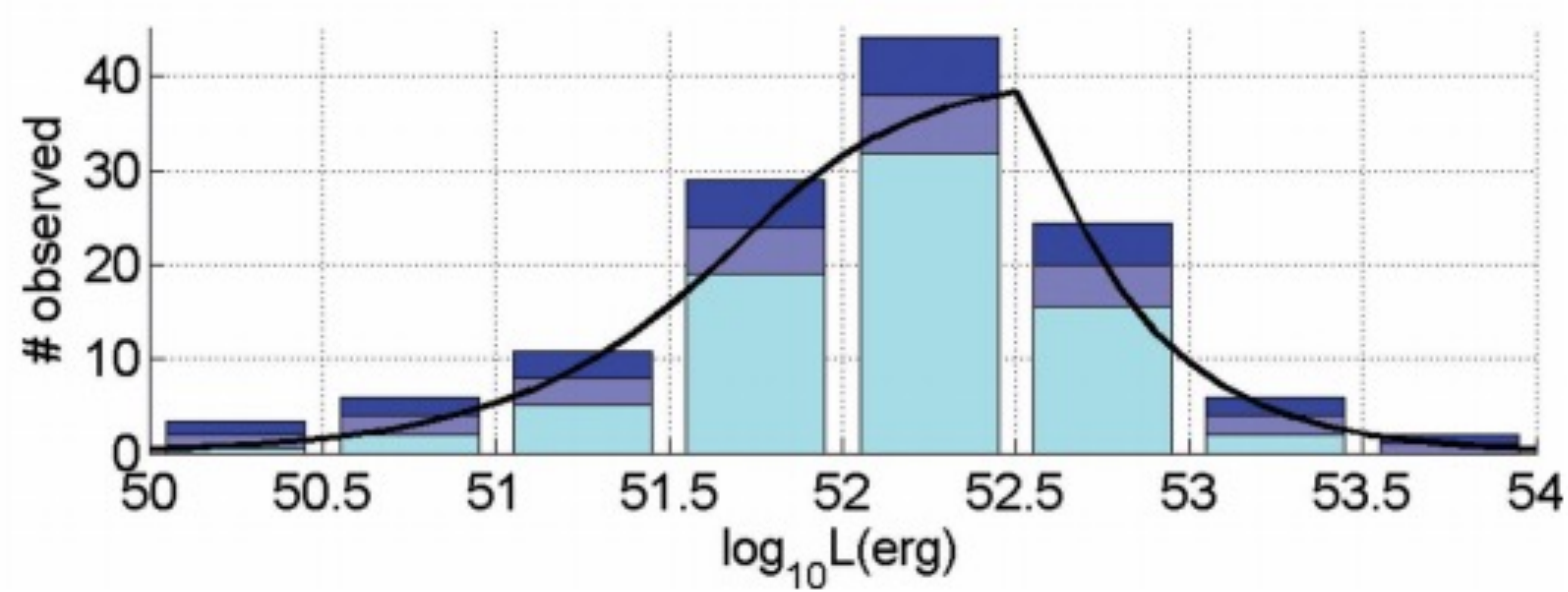

Wanderman 2010

(long bursts)

Redshift distribution

GRBs occur mostly at high z, not because something very different is happening there but just more volume of space.

Universe age
2 billion years

Universe age
500 million years

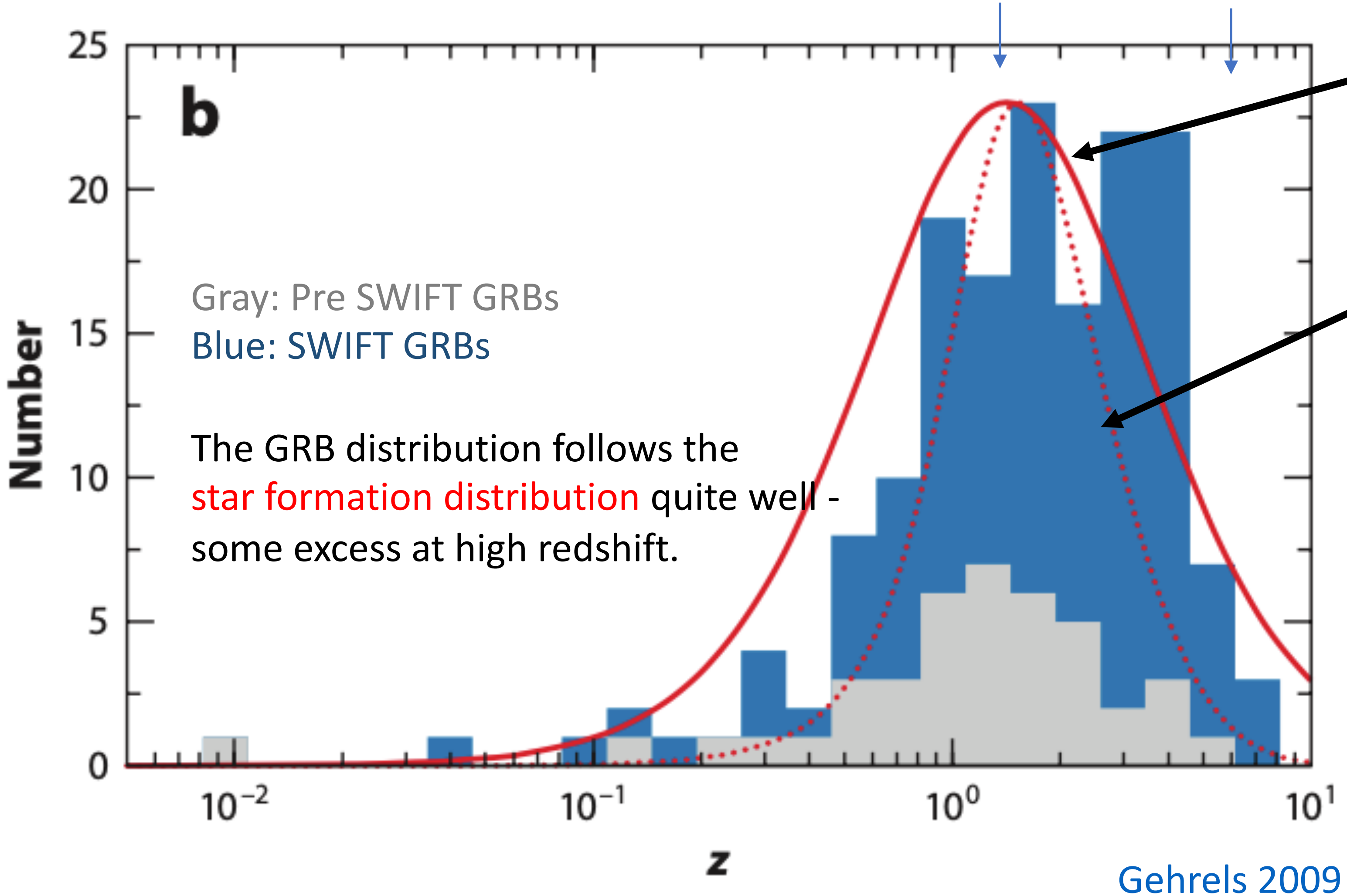

Gray: Pre SWIFT GRBs
Blue: SWIFT GRBs

The GRB distribution follows the star formation distribution quite well - some excess at high redshift.

Solid red line:
Evolution of comoving volume, dV_C/dz.

Dotted red line:
dV_C/dz convolved with star- formation rate.

Gehrels 2009

Afterglows

Afterglow properties:

- Duration minutes to years.
- Emission across the electromagnetic spectrum, from radio to X-rays (most energy in X-rays).
- Relatively smoothly declining luminosity evolution (typically $\sim t^{-1}$), but flares can be seen.

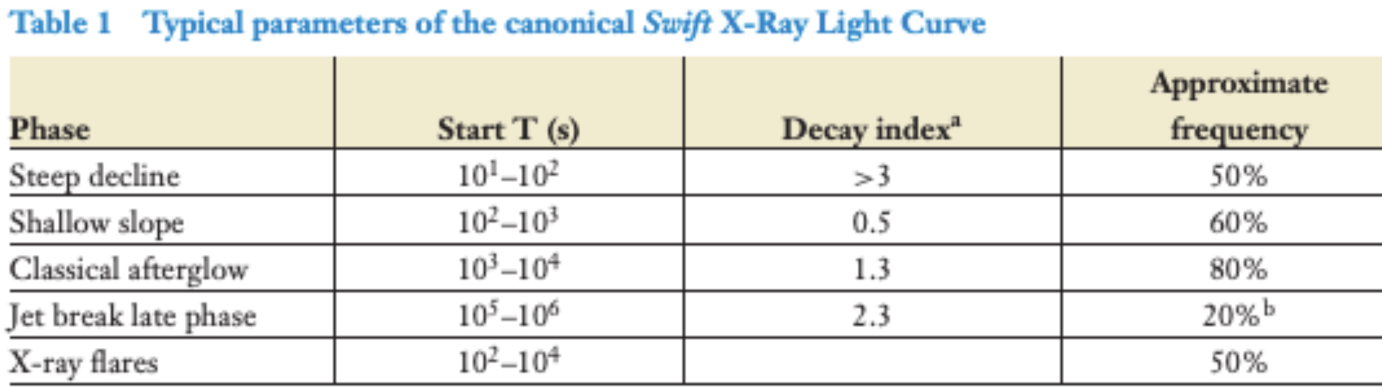

Table 1 Typical parameters of the canonical *Swift* X-Ray Light Curve

Phase	Start T (s)	Decay index[a]	Approximate frequency
Steep decline	10^1–10^2	>3	50%
Shallow slope	10^2–10^3	0.5	60%
Classical afterglow	10^3–10^4	1.3	80%
Jet break late phase	10^5–10^6	2.3	20%[b]
X-ray flares	10^2–10^4		50%

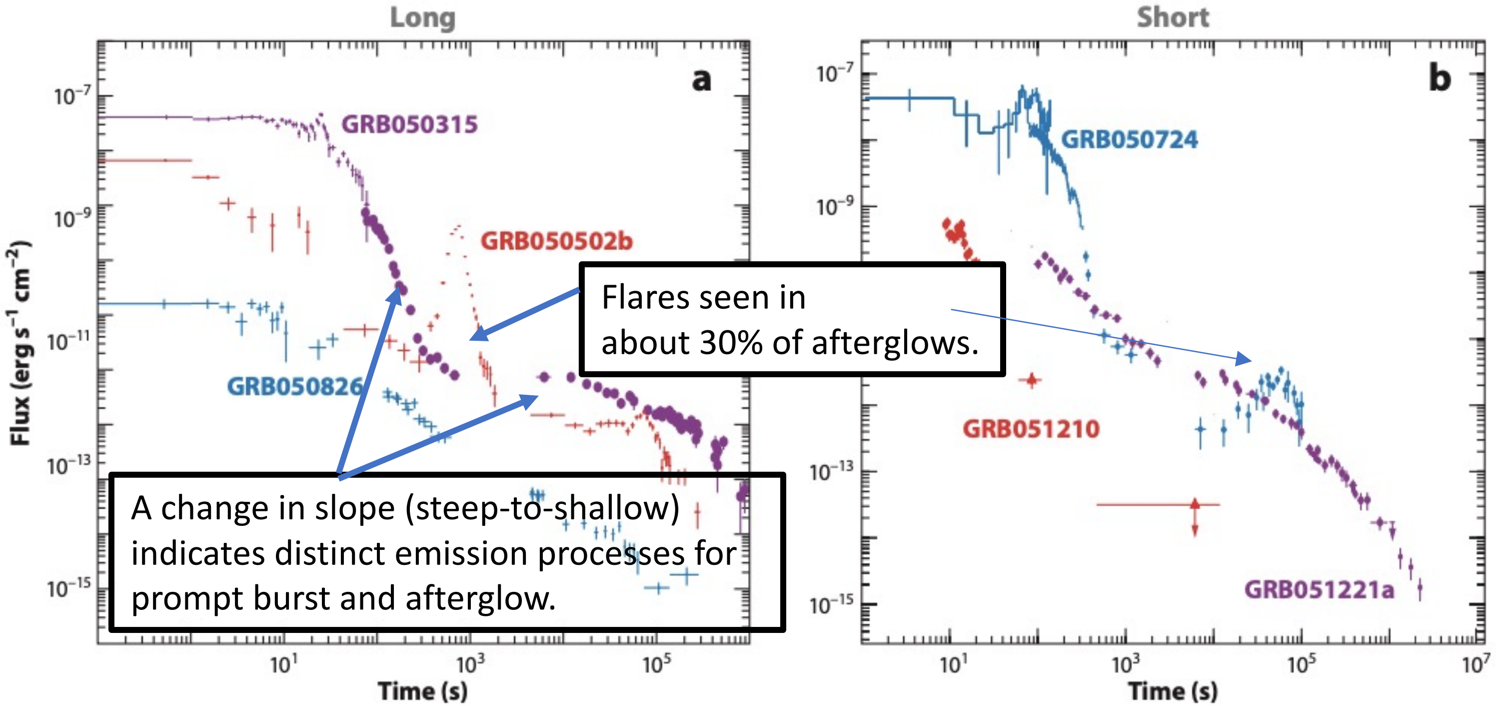

Flares seen in about 30% of afterglows.

A change in slope (steep-to-shallow) indicates distinct emission processes for prompt burst and afterglow.

SWIFT revealed a large diversity in afterglow properties.

Figure 6

Representative examples of X-ray afterglows of (*a*) long and (*b*) short *Swift* events with steep-to-shallow transitions (GRB050315, 050724), large X-ray flares (GRB050502B, 050724), and rapidly declining (GRB051210) and gradually declining (GRB051221a, 050826; flux scale divided by 100 for clarity) afterglows.

Gehrels 2009

Temporal evolution of prompt and afterglow emission (X-rays)

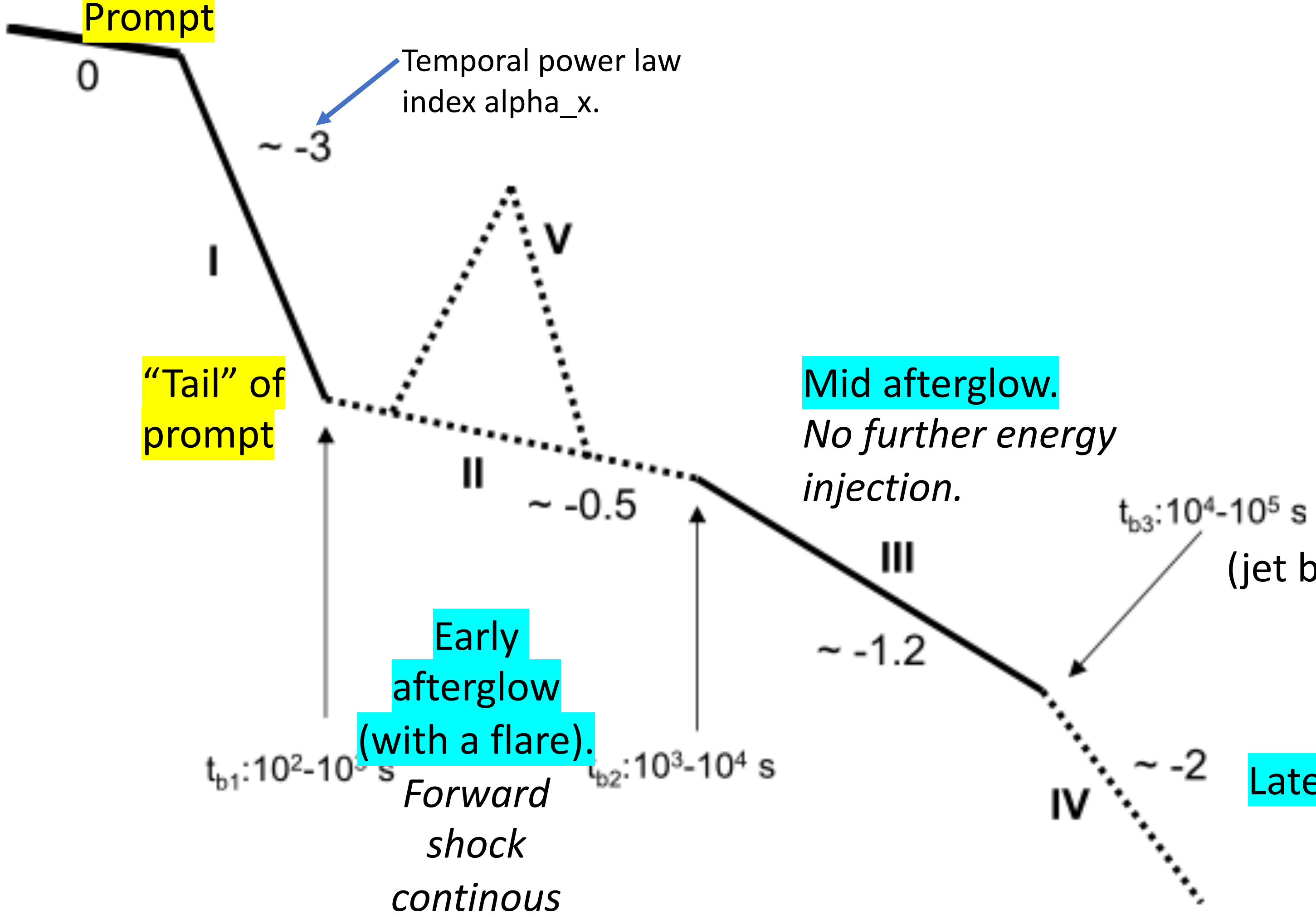

Prompt

Temporal power law index alpha_x.

“Tail” of prompt

Early afterglow (with a flare).

Forward shock continous energy injection.

Mid afterglow.

No further energy injection.

(jet break time)

Late afterglow

Zhang 2006

Afterglow SEDs

Broken power laws.

Simple **synchrotron emission** model (relativistic electrons gyrating in magnetic fields) from a power law distribution of electrons, $N(\gamma)d\gamma = \gamma^{-p}d\gamma$, fits well.

Lorentz factor of electrons

Three break frequencies (which evolve with time):

- $\boldsymbol{\nu_c}$: Characteristic cooling frequency.
- $\boldsymbol{\nu_m}$: Peak frequency (for F_ν).
- $\boldsymbol{\nu_a}$: Self-absorption frequency (somewhere in radio band).

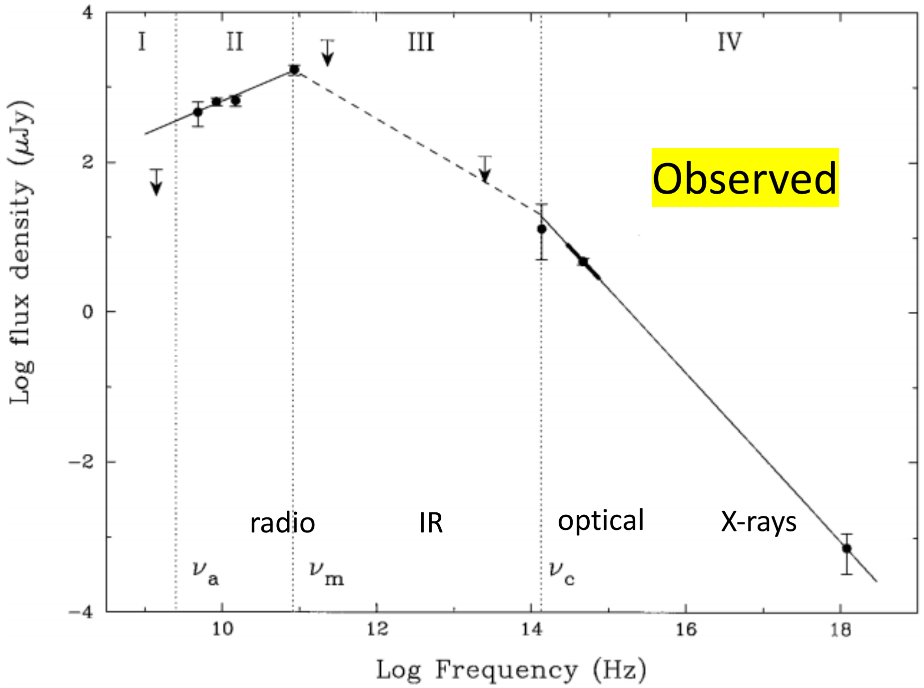

Galama 1998

GRB970508 at 12d

p typically fit in 2-3 range.
(note *p* > 2 needed to give a finite energy).

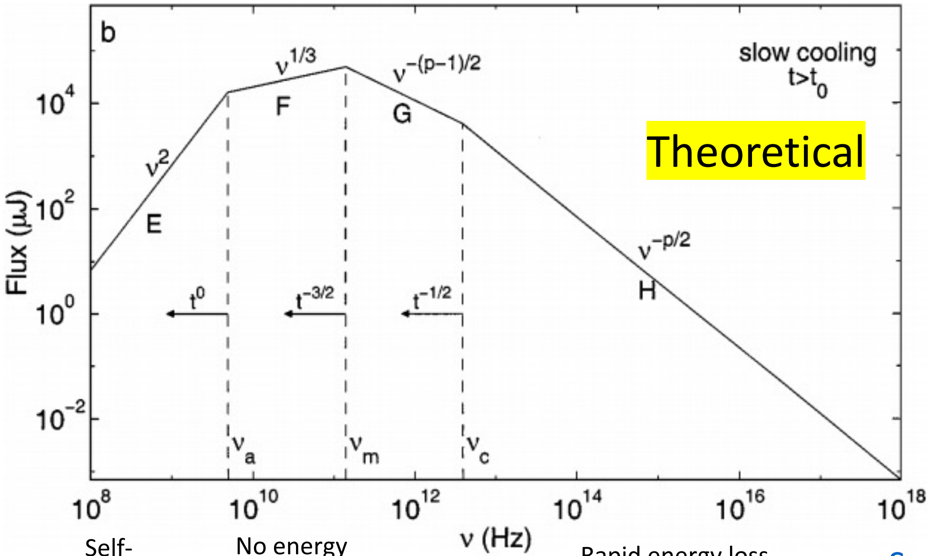

Self-absorption.

No energy loss.

Some energy loss.

Rapid energy loss.

Sari 1998

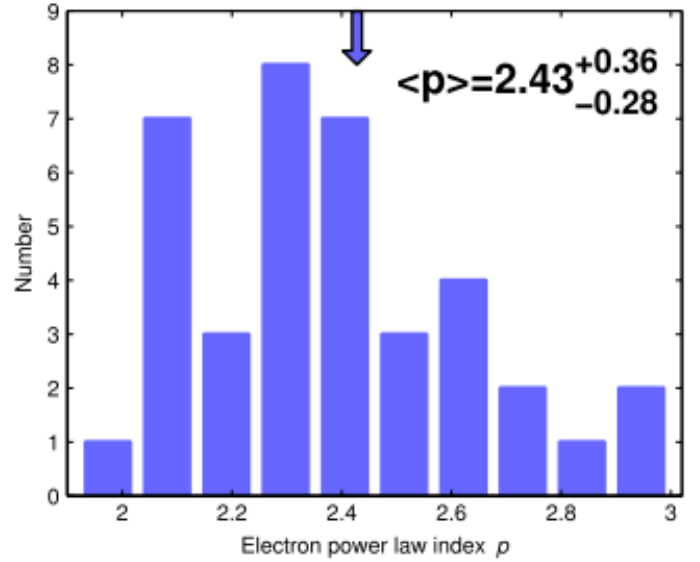

Figure 2. Histogram of electron power law index, *p*, for 38 short GRBs as inferred from the X-ray temporal and spectral indices. The weighted mean and 1σ uncertainties for the population (blue arrow) is $\langle p \rangle = 2.43^{+0.36}_{-0.28}$. These values correspond to those listed in Table 3.

Fong 2015

Theory somewhat different depending on whether

- Slow cooling ($\nu_c > \nu_m$) or fast cooling ($\nu_c < \nu_m$).
- ISM (ρ = constant) or CSM ($\rho \sim r^{-2}$) circumburst medium (CBM).
- Continous energy injection active or inactive.

→ 8 possible combinations (6 listed in the table here).

Zhang 2006

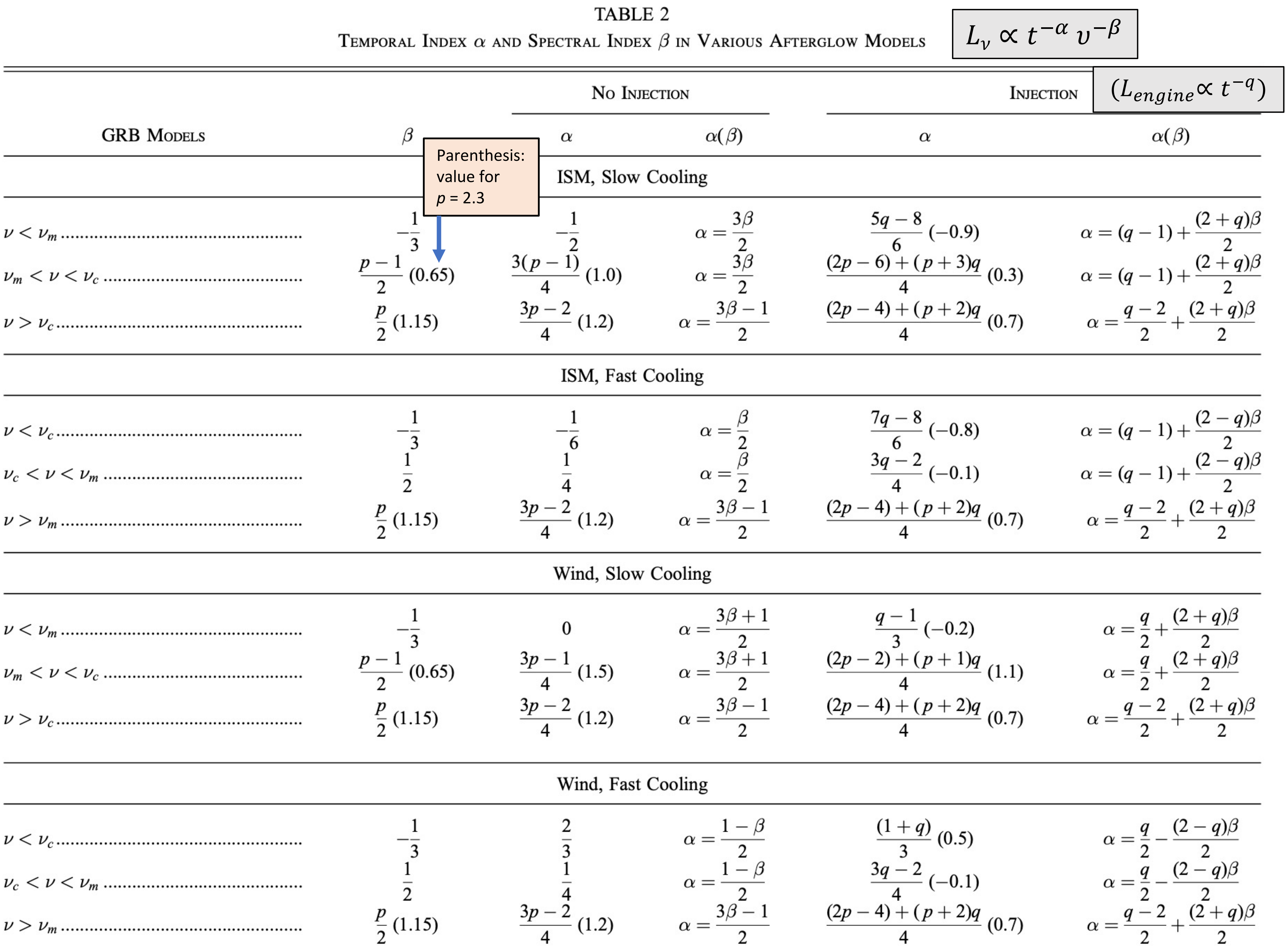

TABLE 2

TEMPORAL INDEX α AND SPECTRAL INDEX β IN VARIOUS AFTERGLOW MODELS

$L_\nu \propto t^{-\alpha}\, \upsilon^{-\beta}$

$(L_{engine} \propto t^{-q})$

Parenthesis: value for p = 2.3

GRB MODELS	β	NO INJECTION α	NO INJECTION $\alpha(\beta)$	INJECTION α	INJECTION $\alpha(\beta)$
		ISM, Slow Cooling			
$\nu < \nu_m$	$-\frac{1}{3}$	$-\frac{1}{2}$	$\alpha = \frac{3\beta}{2}$	$\frac{5q-8}{6}$ (−0.9)	$\alpha = (q-1) + \frac{(2+q)\beta}{2}$
$\nu_m < \nu < \nu_c$	$\frac{p-1}{2}$ (0.65)	$\frac{3(p-1)}{4}$ (1.0)	$\alpha = \frac{3\beta}{2}$	$\frac{(2p-6)+(p+3)q}{4}$ (0.3)	$\alpha = (q-1) + \frac{(2+q)\beta}{2}$
$\nu > \nu_c$	$\frac{p}{2}$ (1.15)	$\frac{3p-2}{4}$ (1.2)	$\alpha = \frac{3\beta-1}{2}$	$\frac{(2p-4)+(p+2)q}{4}$ (0.7)	$\alpha = \frac{q-2}{2} + \frac{(2+q)\beta}{2}$
		ISM, Fast Cooling			
$\nu < \nu_c$	$-\frac{1}{3}$	$-\frac{1}{6}$	$\alpha = \frac{\beta}{2}$	$\frac{7q-8}{6}$ (−0.8)	$\alpha = (q-1) + \frac{(2-q)\beta}{2}$
$\nu_c < \nu < \nu_m$	$\frac{1}{2}$	$\frac{1}{4}$	$\alpha = \frac{\beta}{2}$	$\frac{3q-2}{4}$ (−0.1)	$\alpha = (q-1) + \frac{(2-q)\beta}{2}$
$\nu > \nu_m$	$\frac{p}{2}$ (1.15)	$\frac{3p-2}{4}$ (1.2)	$\alpha = \frac{3\beta-1}{2}$	$\frac{(2p-4)+(p+2)q}{4}$ (0.7)	$\alpha = \frac{q-2}{2} + \frac{(2+q)\beta}{2}$
		Wind, Slow Cooling			
$\nu < \nu_m$	$-\frac{1}{3}$	0	$\alpha = \frac{3\beta+1}{2}$	$\frac{q-1}{3}$ (−0.2)	$\alpha = \frac{q}{2} + \frac{(2+q)\beta}{2}$
$\nu_m < \nu < \nu_c$	$\frac{p-1}{2}$ (0.65)	$\frac{3p-1}{4}$ (1.5)	$\alpha = \frac{3\beta+1}{2}$	$\frac{(2p-2)+(p+1)q}{4}$ (1.1)	$\alpha = \frac{q}{2} + \frac{(2+q)\beta}{2}$
$\nu > \nu_c$	$\frac{p}{2}$ (1.15)	$\frac{3p-2}{4}$ (1.2)	$\alpha = \frac{3\beta-1}{2}$	$\frac{(2p-4)+(p+2)q}{4}$ (0.7)	$\alpha = \frac{q-2}{2} + \frac{(2+q)\beta}{2}$
		Wind, Fast Cooling			
$\nu < \nu_c$	$-\frac{1}{3}$	$\frac{2}{3}$	$\alpha = \frac{1-\beta}{2}$	$\frac{(1+q)}{3}$ (0.5)	$\alpha = \frac{q}{2} - \frac{(2-q)\beta}{2}$
$\nu_c < \nu < \nu_m$	$\frac{1}{2}$	$\frac{1}{4}$	$\alpha = \frac{1-\beta}{2}$	$\frac{3q-2}{4}$ (−0.1)	$\alpha = \frac{q}{2} - \frac{(2-q)\beta}{2}$
$\nu > \nu_m$	$\frac{p}{2}$ (1.15)	$\frac{3p-2}{4}$ (1.2)	$\alpha = \frac{3\beta-1}{2}$	$\frac{(2p-4)+(p+2)q}{4}$ (0.7)	$\alpha = \frac{q-2}{2} + \frac{(2+q)\beta}{2}$

Afterglows

In radio the flux may initially increase with time (α negative).

At higher energies (>= optical), **the flux decreases already within hours**.

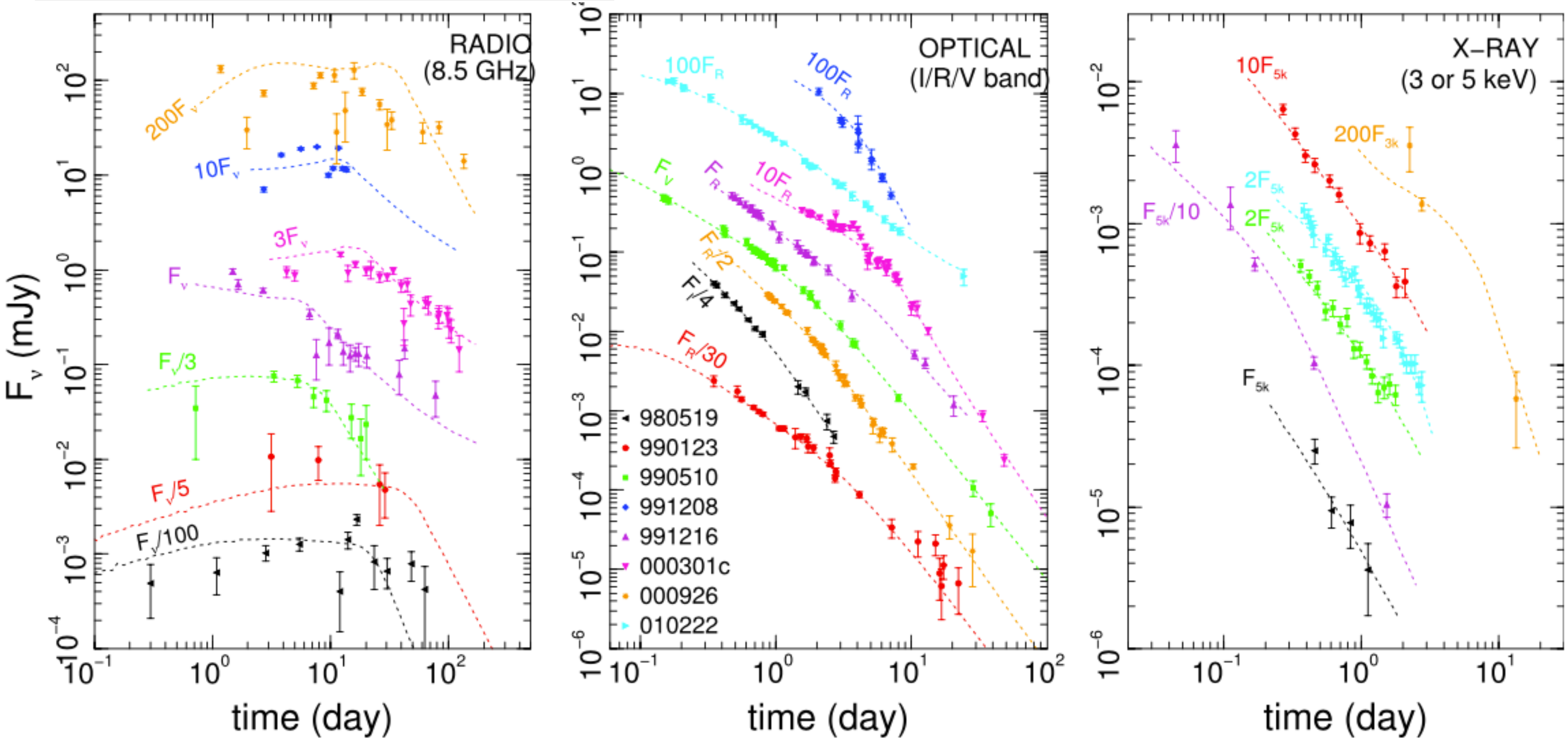

Dashed lines : best-fit synchrotron models (more details later).

Panaitescu 2001

More luminous prompt emission → more luminous afterglow

Afterglow power

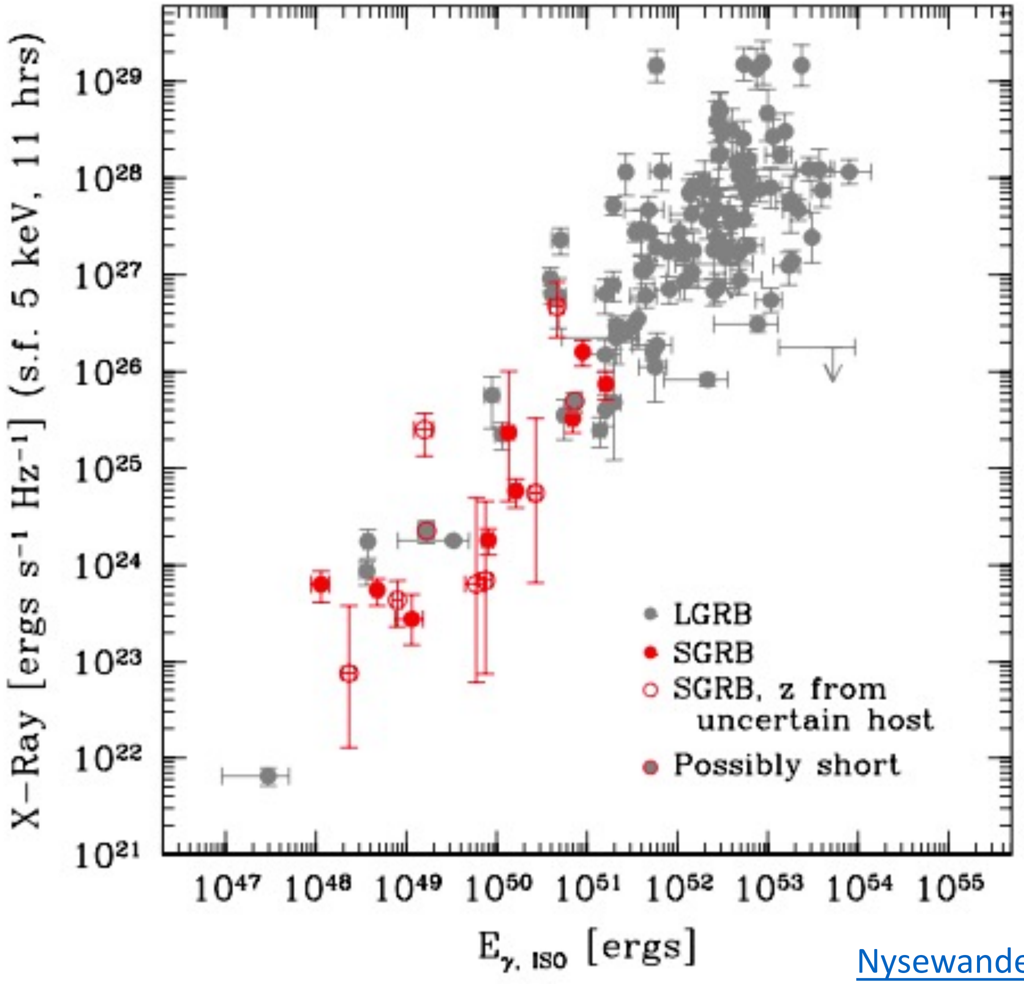

Prompt emission energy

Nysewander 2009

Short GRBs have typically ~100 times weaker emission in both components compared to **long GRBs**.

This has led to a situation where short GRBs are much less well studied than long GRBs.

Fundamental constraints on the prompt emission source

Assume the emission would come from a non-relativistic flow. Then the observed variability on $\Delta t = \mathrm{ms}$ time-scales means the source would have size $R \ \leq c \cdot \Delta t \sim 300 \text{ km}$.

Luminosity $L \ \leq n_{photons} 4\pi R^2 ch\upsilon$, where $n_{photons}$ is the number density of photons.

For a non-relativistic flow the rest-frame photon energy must also be in gamma-ray regime. Take $h\nu{\sim}1 \text{ MeV}$, and typical observed $L \sim 10^{50}$ erg s^{-1},

$$\rightarrow n_{photons} \geq \frac{10^{50}\mathrm{erg\ s}^{-1}}{4\pi R^2 c{\cdot}1\ \mathrm{MeV}} \geq 10^{29}\mathrm{cm}^{-3}.$$

But then $\tau_{pair-production} \ = \ \sigma_{pair-production} \cdot n_{photons} \cdot \Delta R \geq 10^{12} (\sigma_{pair-production}{\sim}10^{-25}\mathrm{cm}^2)$ and the gamma rays would be trapped and convert to electron-positron pairs. A thermal equilibrium with such pairs would be set up and the spectrum would become thermal, whereas observed spectra are highly non-thermal. Also, the formed pairs would provide Thomson scattering opacity also for lower energy photons. "Compactness problem".

Conclusion: The source must be relativistic. For a relativistic source:

1. $\nu_{\mathrm{obs}} = \Gamma * \nu_{\mathrm{emiss},}$ so if $\Gamma >> 1$ the rest-frame photons are X-rays rather than gamma rays. X-rays cannot pair produce (a total photon energy > 1.022 MeV is needed).
2. The source size is much larger than 300 km (next slide).

Lithwick & Sari 2001 : **Lorentz factors $\boldsymbol{\Gamma = \frac{1}{\sqrt{1-\left(\frac{v}{c}\right)^2}} \gtrsim 200}$ needed → Largest relativistic motions known** (AGN: Γ ~few). Time evolution of radio scintillations (which stop when the emitting source has grown large enough) supports this conclusion.

Time intervals for source and observer in a relativistic flow

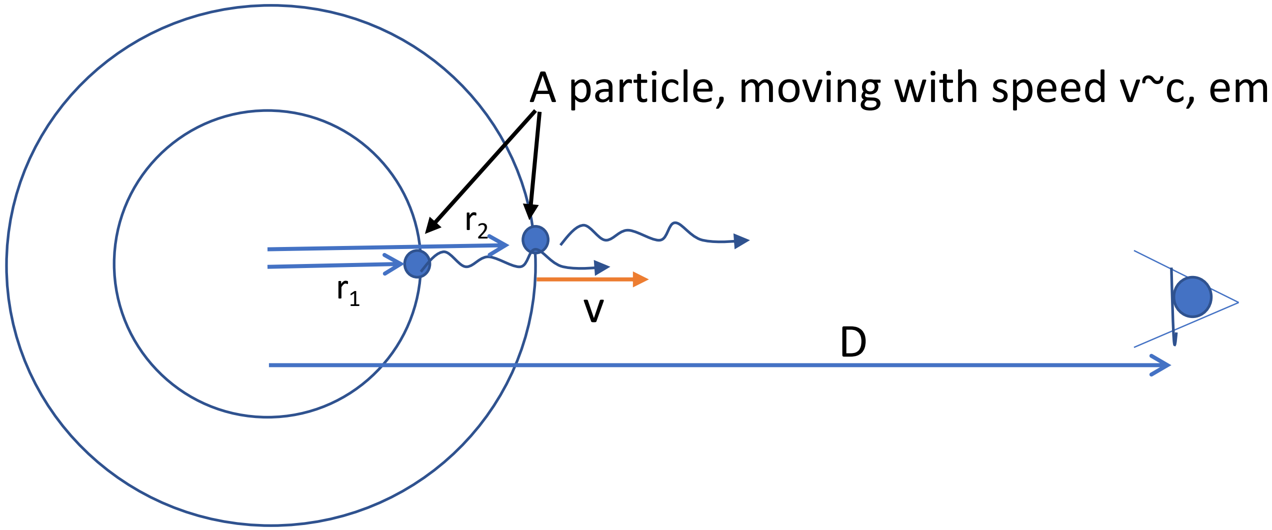
A particle, moving with speed v~c, emits first at r_1, then at r_2.

$t_1^{obs} = t_1^{emiss} + (D-r_1)/c$
$t_2^{obs} = t_2^{emiss} + (D-r_2)/c$

$dt^{obs} = dt^{emiss} - (r_2-r_1)/c = dt^{emiss} - v\, dt^{emiss}/c = dt^{emiss}*(1 - v/c)$

$\Gamma^2 = 1/(1-\beta^2) \quad = \quad 1/(1+\beta)(1-\beta) \quad \sim \quad 1/(2*(1-\beta))$

So

$$\boxed{dt^{obs} = \frac{dt^{emiss}}{2\Gamma^2}}$$

Size of emitting region is then not $R \lesssim c*dt^{obs}$ but $R \lesssim 2*\Gamma^2*c*dt^{obs}$. For Γ=200, $R \lesssim$ **$2*10^{12}$ cm ~ 0.1 AU.**

Beaming

From a relativistic outflow, **relativistic beaming** will focus the emission in a narrow cone along the flow direction.

Thus, what we see comes only from gas moving quite aligned with the line of sight. If the source would expand with spherical symmetry → Would only see a **segment.** Half the radiation is received within angle $\boldsymbol{\theta_{90}}$.

In a simplified picture, beaming gives uniform radiation within a cone of solid angle $d\Omega = 4\pi \sin^2(\theta_{90}/2) \sim \pi\theta_{90}^2$, and none outside. It means we would be able to see a chunk $d\Omega$ of the outflow.

Aberration formula:

$$\cos\theta = \frac{\cos\theta' + \beta}{1 + \beta\cos\theta'}$$

observer frame angle

comoving frame angle

θ'	θ for β=0.99
120	14
90	**8.1(=** θ_{90})
45	3.4
10	0.7

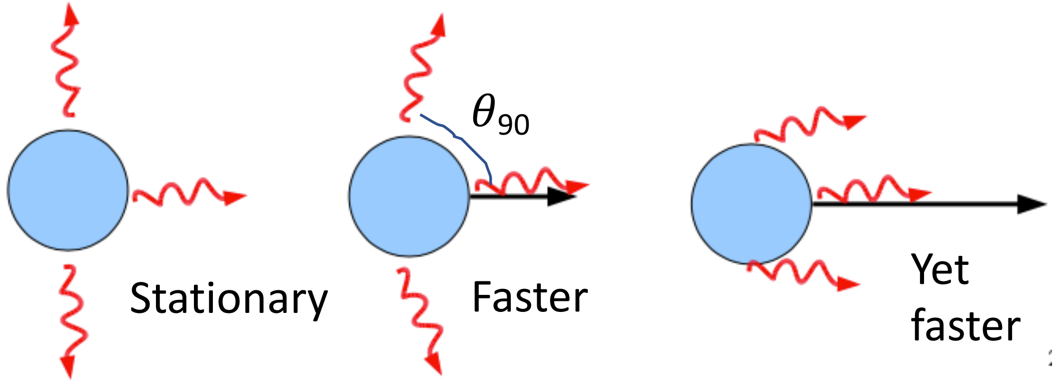

Emission from **the shell** except the **blue segment** is beamed away from observer.

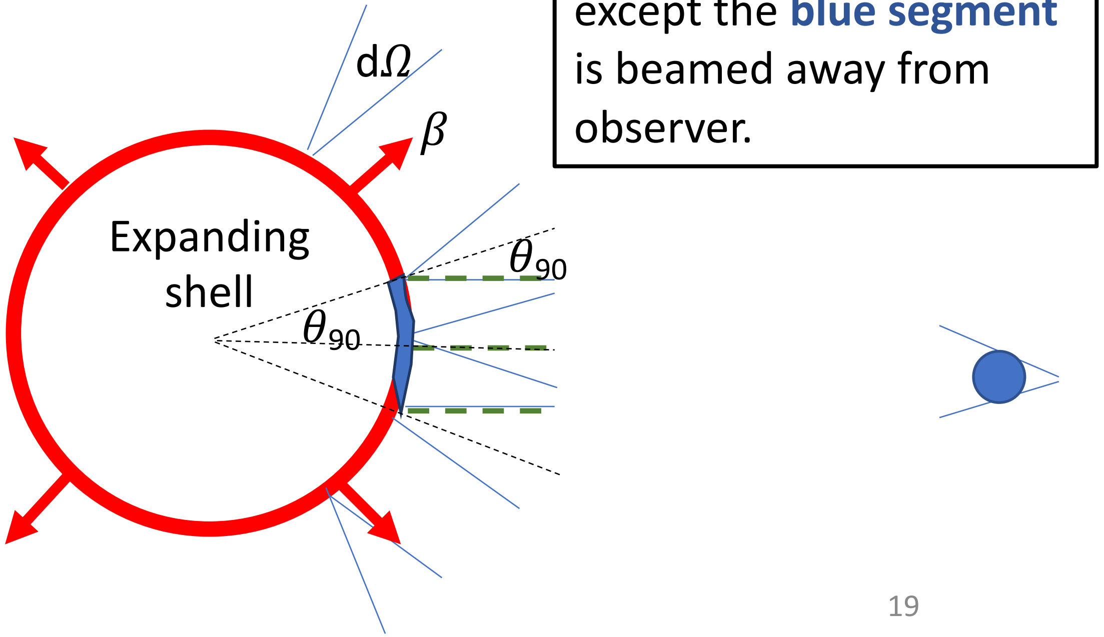

Beaming

$\theta_{jet} = 10^\circ, \theta_{90} = 5^\circ$

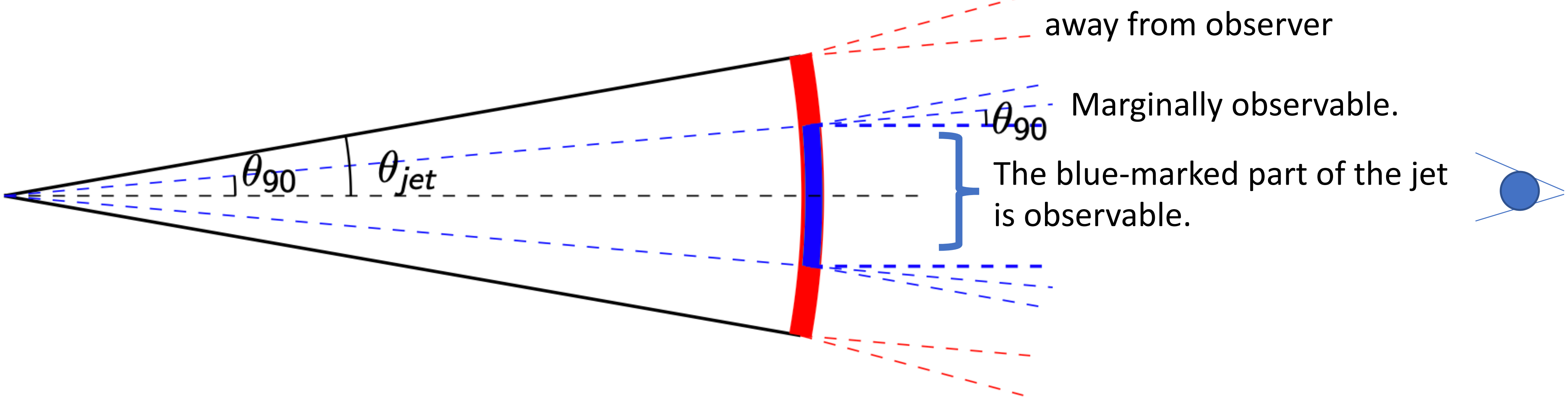

Jet edge emission beamed away from observer

Marginally observable.

The blue-marked part of the jet is observable.

Beaming

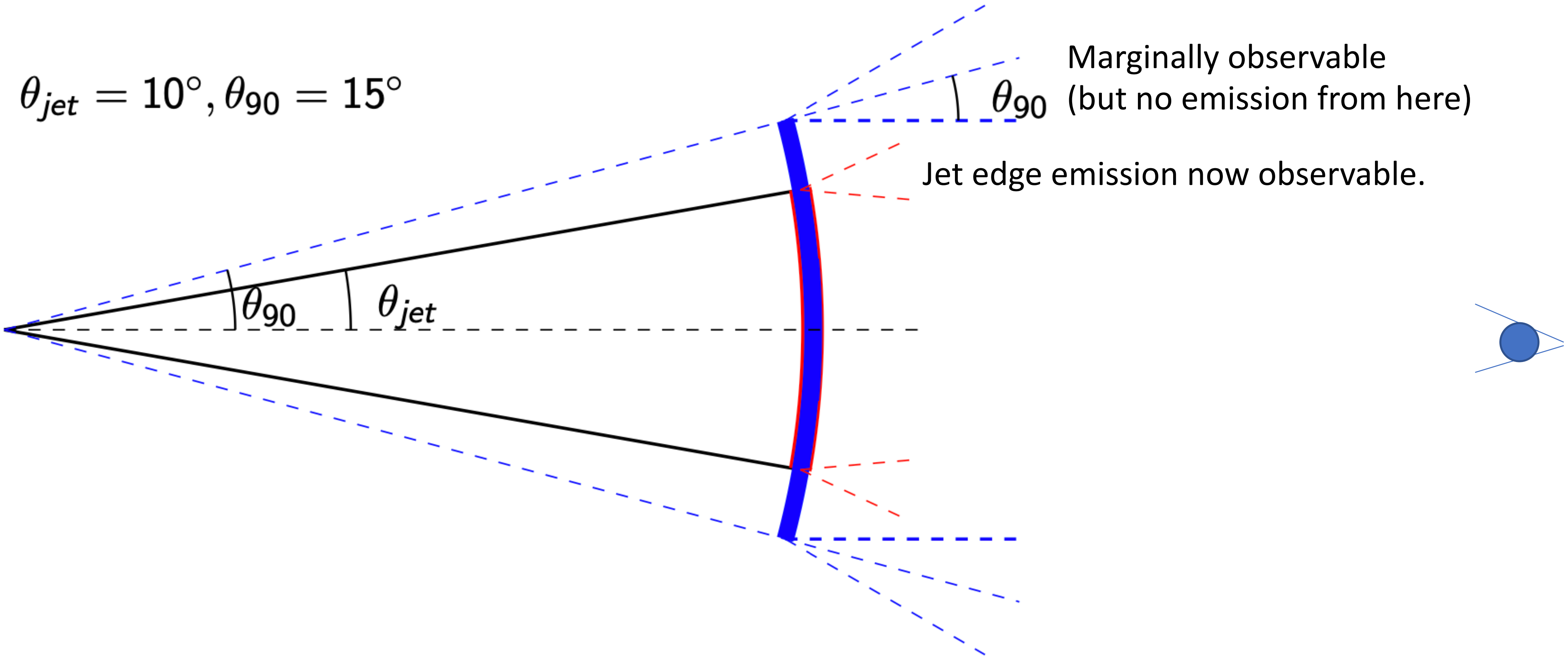

When θ_{90} reaches θ_{jet} (it grows in time as β is reduced when the jet decelerates), the observer becomes aware that the emitting layer has an edge (is jet shaped). Get **a jet break when** $\theta_{90}(\beta) = \theta_{\text{jet}}$. In practise determine the β evolution from data of the whole afterglow.

Jet angle from afterglow breaks

Since θ_{90}~$1/\Gamma$, if Γ can be determined at the break point, the jet angle can be determined from equating $\theta_{\text{jet}} = 1/\Gamma_{\text{break}}$.

Typical results: θ_{jet} ~ 10 degrees.

Consequence: We see the (prompt) emission from only about 1 in 100 GRBs (π*(10/180*π)^2 / (4π) = 1 / 130).

The intrinsic GRB/SN(Ibc) rate ratio is the observed one (~$1/10^5$) times the beaming correction (~100) → ~1 in 1000.

A second effect of **lateral spreading** of the jet, which occurs around a similar epoch as the jet break, can lead to a yet steeper decline.

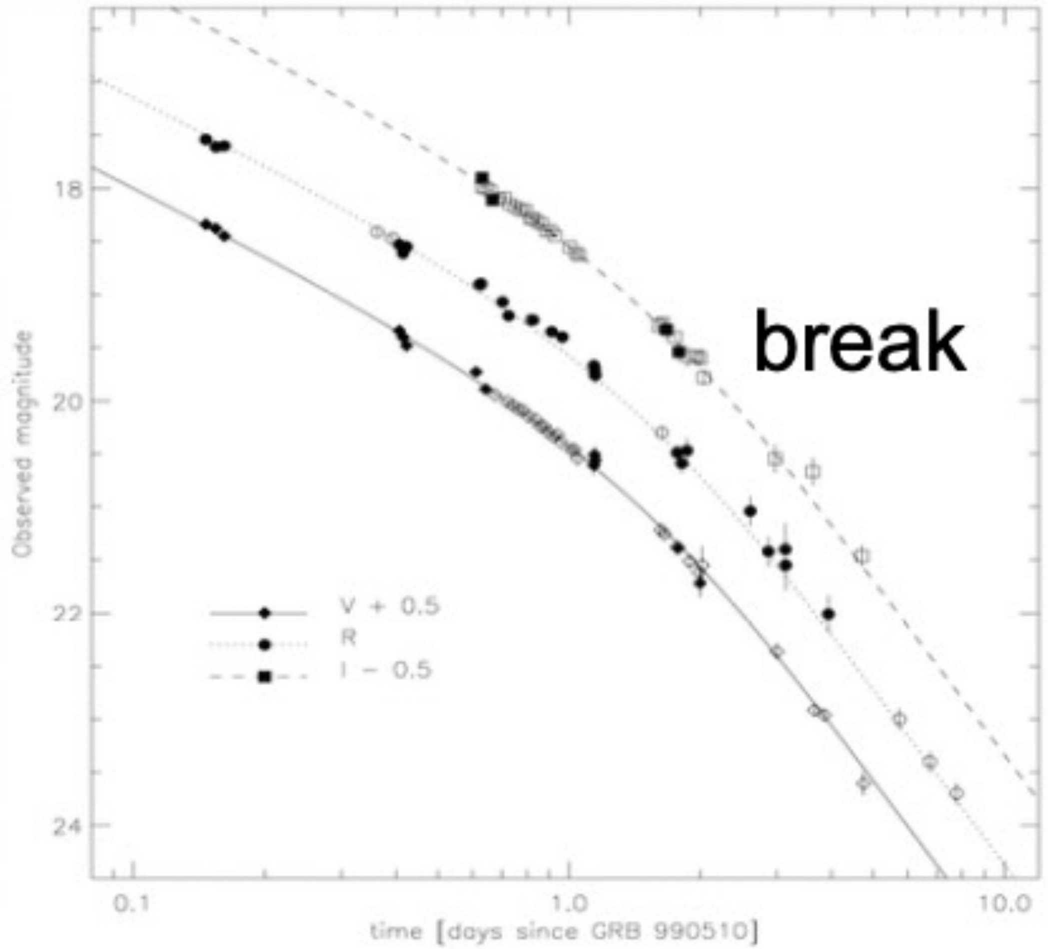

Jet breaks are (typically) **achromatic**: an important observational property to interpret them as due to a relativistic beaming effect.

Jet angles determined from afterglow breaks

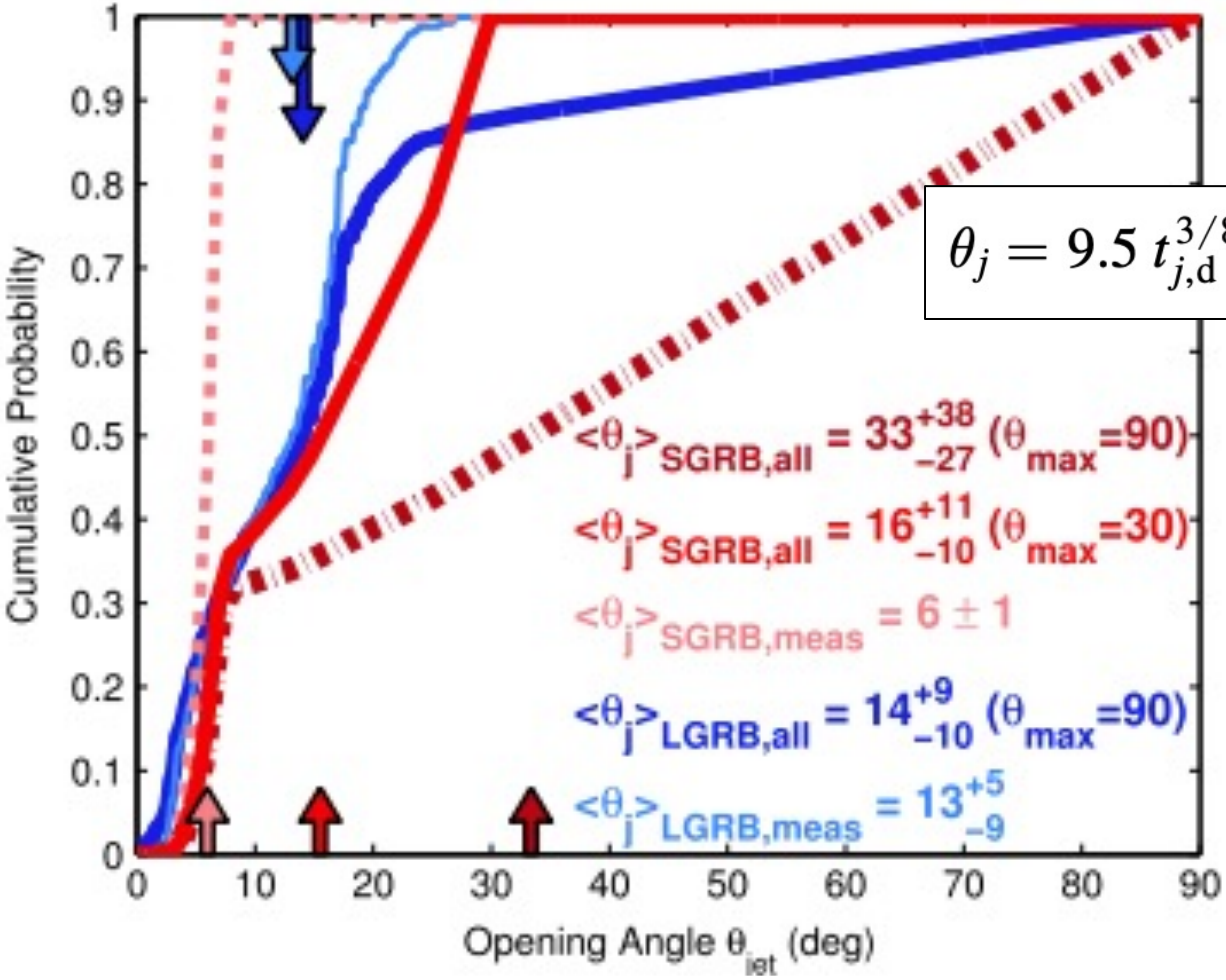

$$\theta_j = 9.5\, t_{j,\mathrm{d}}^{3/8}(1 + z)^{-3/8}E_{\mathrm{K,iso,52}}^{-1/8}n_0^{1/8} \text{ deg,}$$

“all” includes lower limits, “meas” only GRBs with observed breaks. (248 long, 4 short).

Arrows: Median values.

[Fong 2015]

Jets in cosmos : quite common

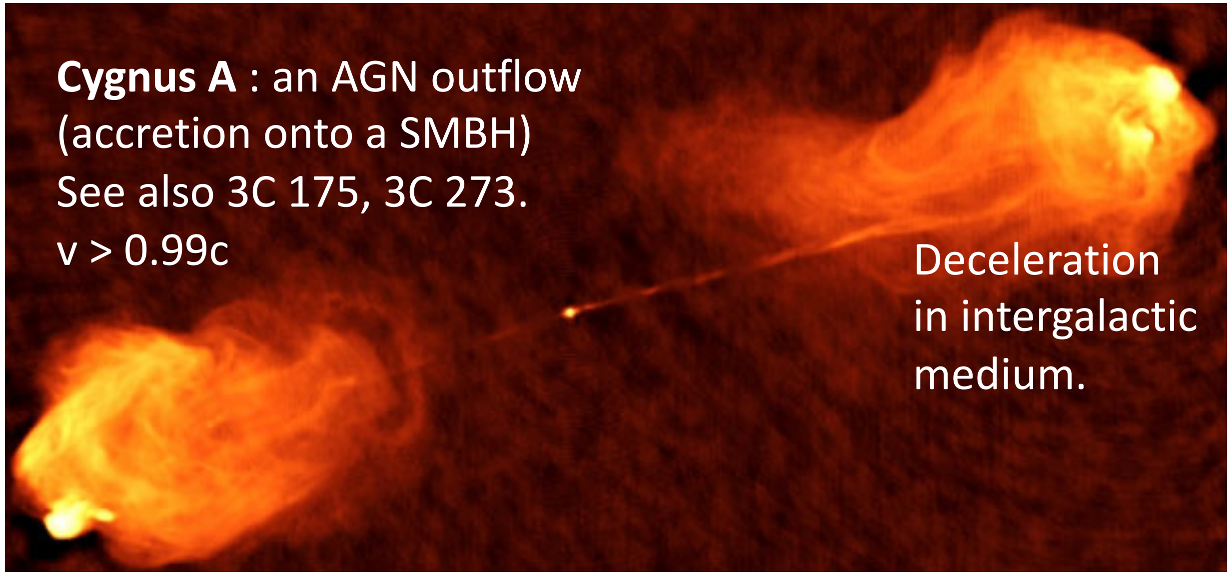

Cygnus A : an AGN outflow
(accretion onto a SMBH)
See also 3C 175, 3C 273.
v > 0.99c

Deceleration
in intergalactic
medium.

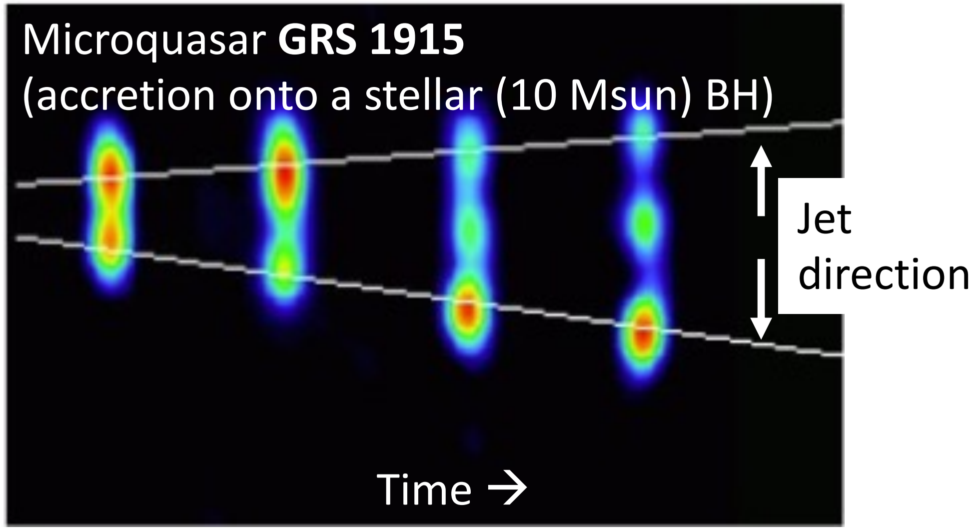

Microquasar **GRS 1915**
(accretion onto a stellar (10 Msun) BH)

Jet
direction

Time →

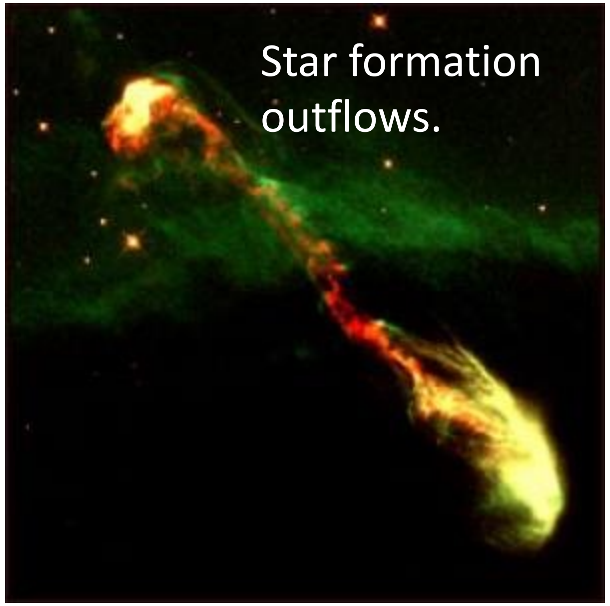

Star formation
outflows.

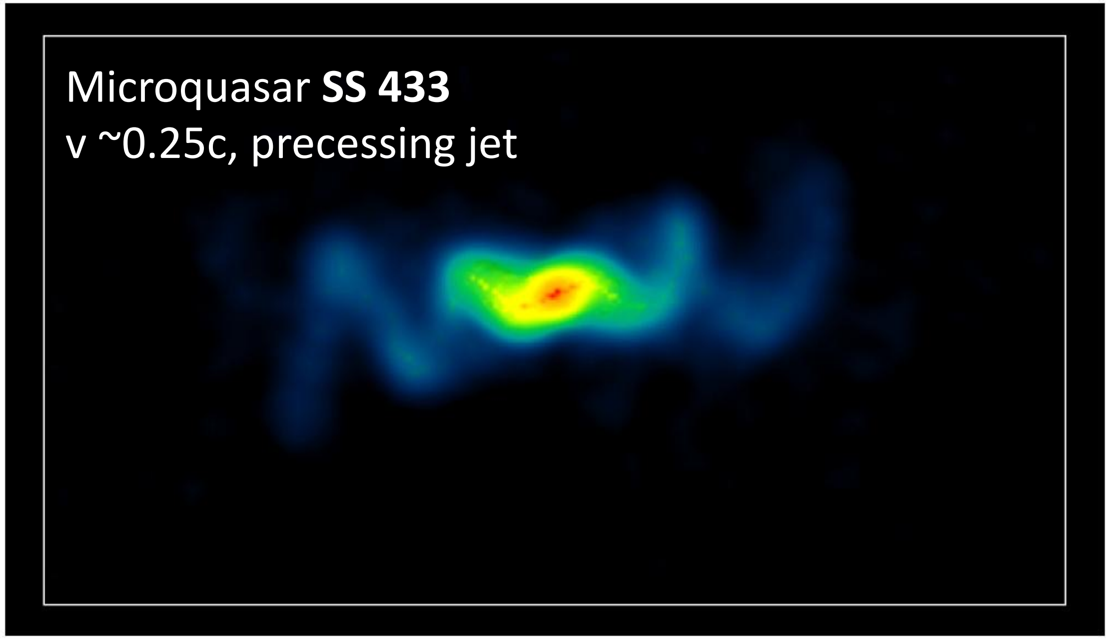

Microquasar **SS 433**
v ~0.25c, precessing jet

The afterglows can constrain the density of the circumburst medium (CBM)

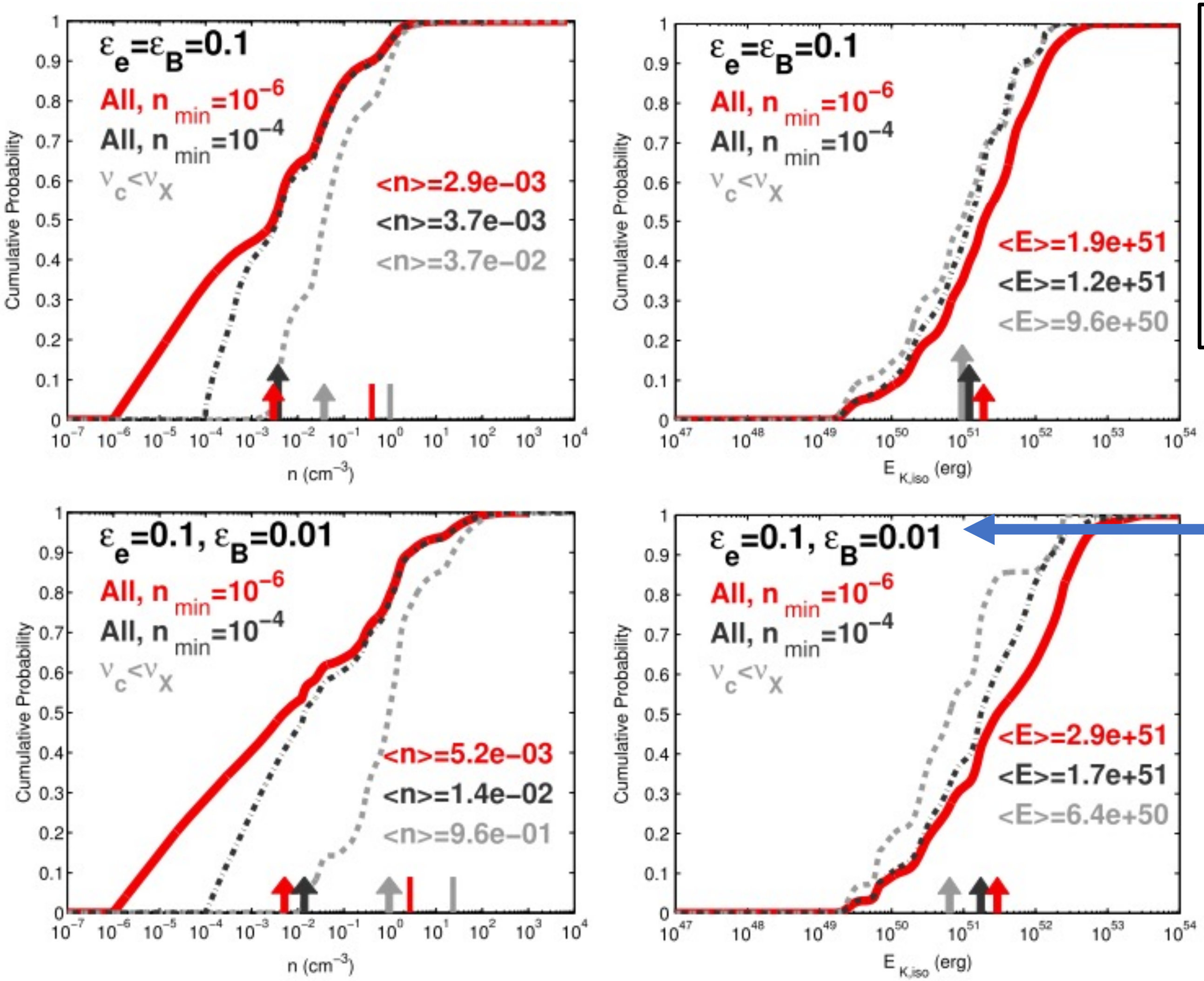

Short GRBs: circumburst densities are low, <~ 1 cm^{-3}.

In general,a **constant density CBM** is favoured over a **wind density** one ($\rho \propto r^{-2}$) (~0.1 pc scales probed).

→ Consistent with ISM rather than CSM interaction.

$\boldsymbol{\varepsilon_e}$ (fraction of internal energy in rel. electrons) and $\boldsymbol{\varepsilon_B}$ (fraction of internal energy in magnetic fields) are two free parameters that influence the inferred CBM density (and jet energy).

$$F_{\nu,i} \propto \begin{cases} n_0^{1/2} E_{\mathrm{K,iso},52}^{5/6}\, \epsilon_{e,-1}^{-2/3}\, \epsilon_{B,-1}^{1/3} & \nu_a < \nu_i < \nu_{\mathrm{m}} \\ n_0^{1/2} E_{\mathrm{K,iso},52}^{\frac{3+p}{4}}\, \epsilon_{e,-1}^{p-1} \epsilon_{B,-1}^{\frac{1+p}{4}} & \nu_{\mathrm{m}} < \nu_i < \nu_{\mathrm{c}}\,, \\ E_{\mathrm{K,iso},52}^{\frac{2+p}{4}}\, \epsilon_{e,-1}^{p-1} \epsilon_{B,-1}^{\frac{p-2}{4}} & \nu_i > \nu_{\mathrm{c}} \end{cases}$$

Fong 2015 (short GRBs exclusively)

The afterglows can constrain the density of the circumburst medium (CBM)

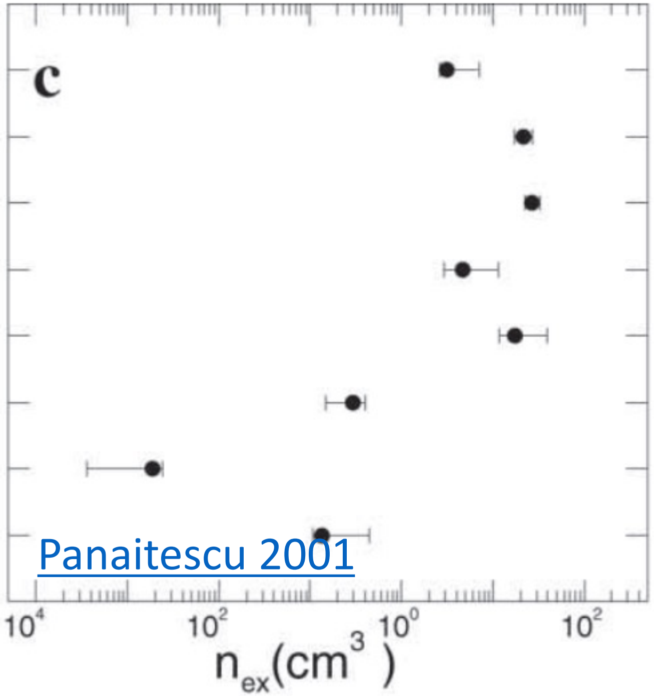

Panaitescu 2001

Long GRBs: Complex picture : sometimes constant density favoured, sometimes wind profile.

- Constant density cases
  - ISM (low mass loss from progenitor)?
  - Shocked winds? Wijers 2001, Chevalier 2004

A* ~ 1 for normal WR star wind ($\dot{M}\sim10^{-5}M_{\odot}/$ yr, $v_w\sim10^3$km/s).

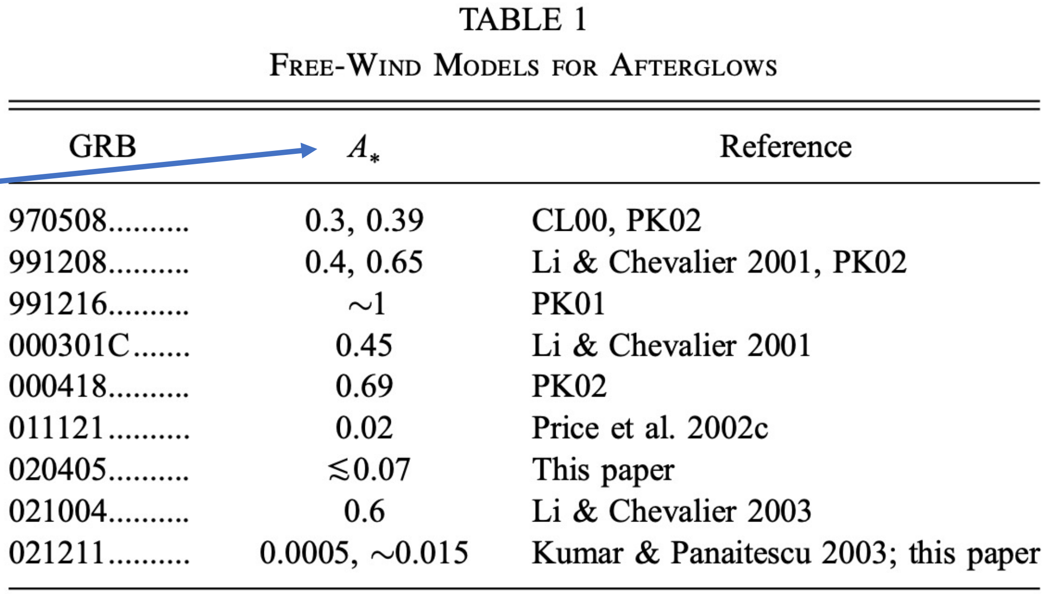

TABLE 1

Free-Wind Models for Afterglows

GRB	A_*	Reference
970508..........	0.3, 0.39	CL00, PK02
991208..........	0.4, 0.65	Li & Chevalier 2001, PK02
991216..........	$\sim$1	PK01
000301C.......	0.45	Li & Chevalier 2001
000418..........	0.69	PK02
011121..........	0.02	Price et al. 2002c
020405..........	$\lesssim$0.07	This paper
021004..........	0.6	Li & Chevalier 2003
021211..........	0.0005, $\sim$0.015	Kumar & Panaitescu 2003; this paper

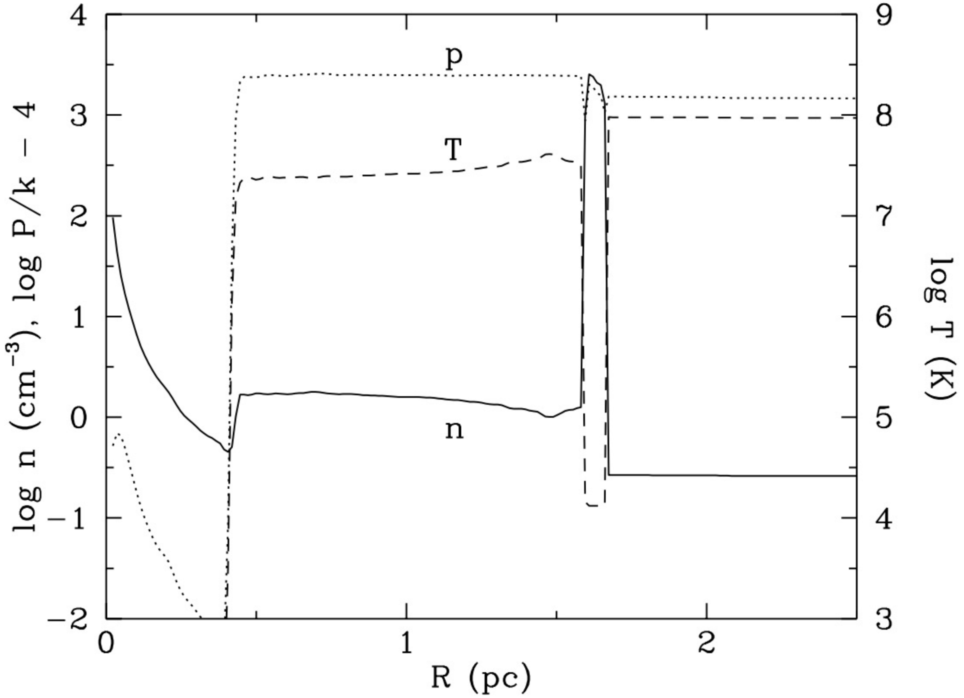

Fig. 1.—Wind bubble structure at the end of the Wolf-Rayet stage for the case of an ISM pressure and density typical of the hot, low-density phase of a starburst galaxy, with $P/k = 2\times10^7$ K cm^{-3} and a density of 0.2 cm^{-3}. The solid line gives the number density, the dashed line the temperature, and the dotted line the pressure. The wind termination shock is at 0.4 pc, and the red supergiant shell at 1.7 pc. The region outside the red supergiant shell is the remains of the bubble from the main-sequence phase. [*See the electronic edition of the Journal for a color version of this figure.*]

Chevalier 2004

With jet angle determined, one can determine the energy radiated

Total radiated energy $E_{tot} = E_{iso} * \frac{d\Omega}{4\pi} = E_{iso} * \frac{\theta_{jet}^2}{4}$ --> typically **around 10^{51} erg** for prompt emission in long GRBS.

~0.01 for $\theta_{\rm jet}$=10 degrees = 0.17 rad

Both the **scale** of this energy, and the **quite small spread,** are important constraints.

The afterglow energy is comparable : typically a few times 10^{50} erg. (e.g. Panaitescu 2001).

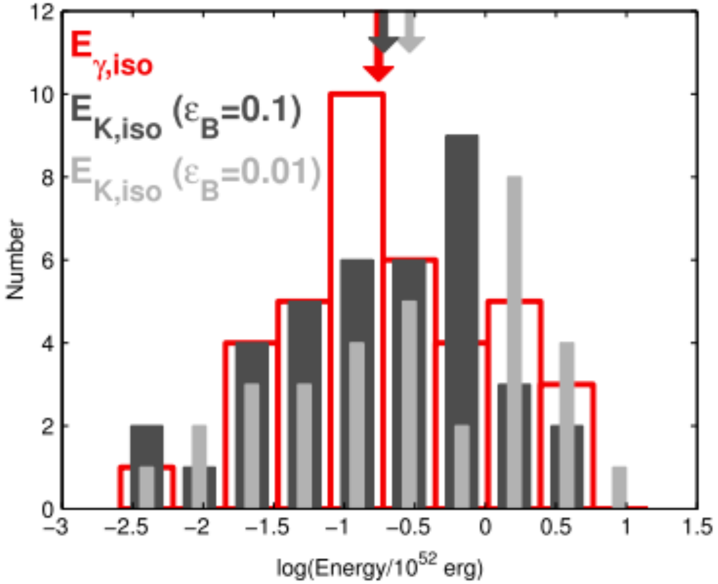

Fong 2015

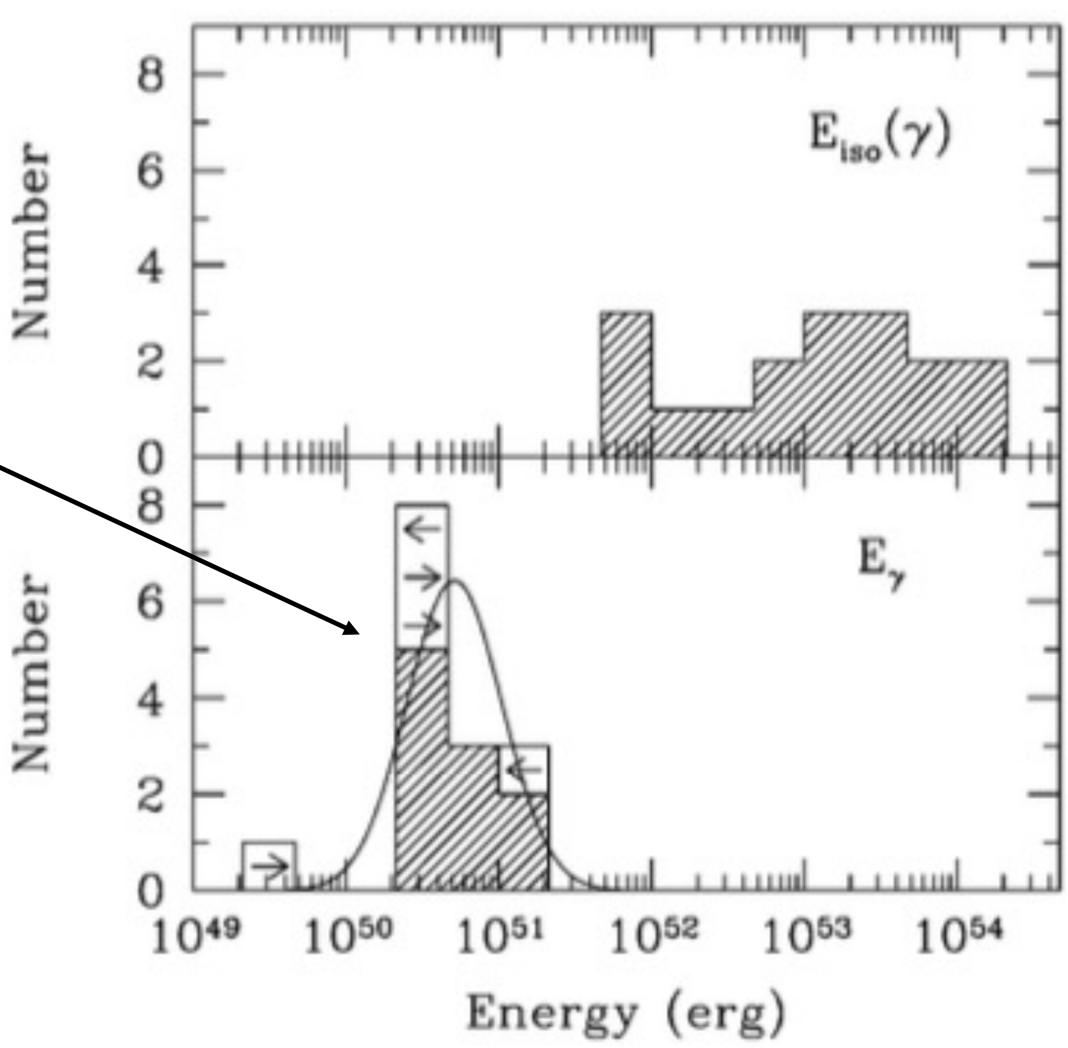

Frail 2001

The standard model for Gamma Ray Bursts

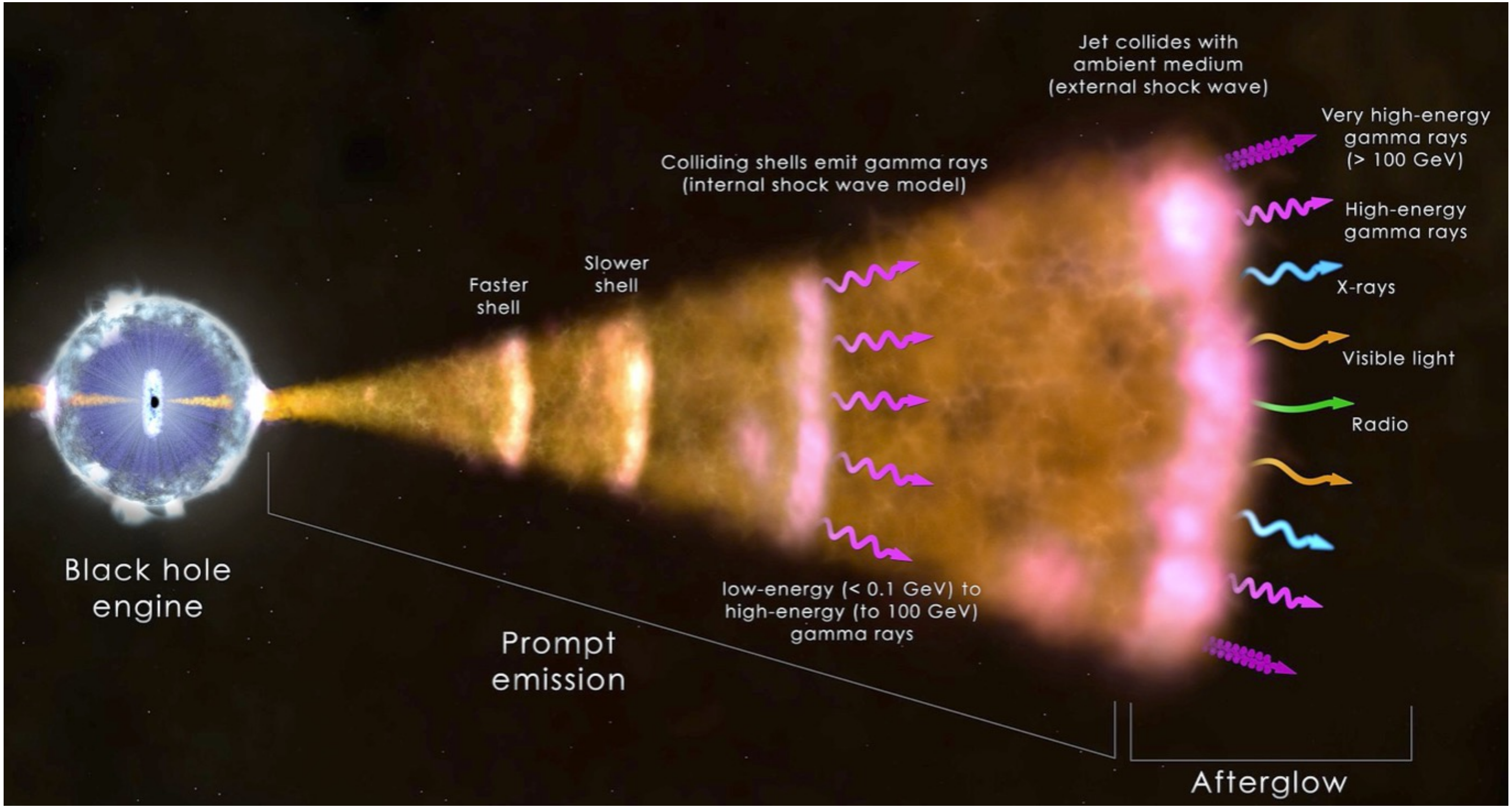

10^8 cm $10^{13\text{-}14}$ cm 10^{16} cm

The standard model for Gamma Ray Bursts

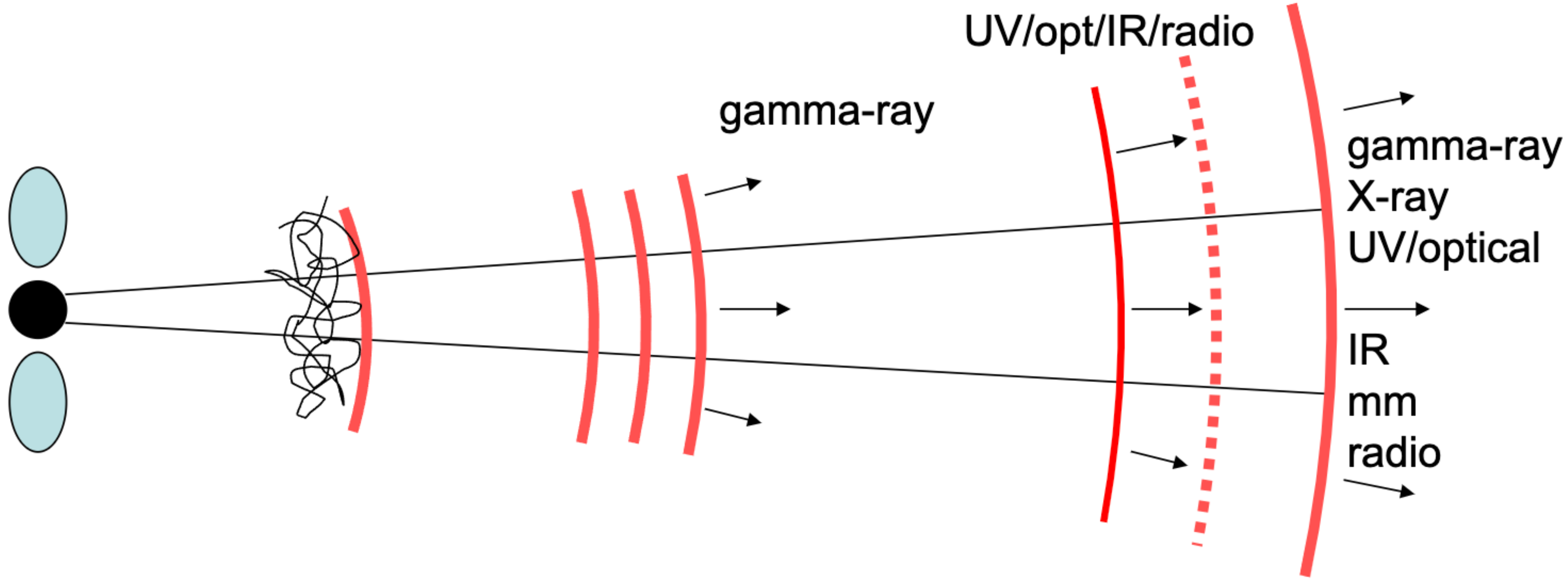

central engine	**photosphere**	**internal (shocks)**	**external shocks (reverse) (forward)**
1E6cm	**1E9cm**	**1E12-1E14cm**	**1E17cm for ISM** **1E15cm for wind**

Creating the prompt emission

Standard model: ***Internal shocks*** develop in the outflow as it is launched with time-varying Γ factors.

For two outflow segements with Lorentz factors Γ_1 and Γ_2, launched a time dt apart, internal shocks will develop at radius R ~ $\Gamma_1 * \Gamma_2 * c$ dt (Rees & Meszaros 1994) ~ 10^{13} cm ($\Gamma_1 * \Gamma_2 / 10^4$) (dt/0.1 s).

In the internal shocks, **synhrotron emission** and **inverse Compton scattering** produce high-energy radiation.

Can show that $dt_{obs} = dt_{source} * \Gamma_1 / \Gamma_2 \sim dt_{source}$ → the engine variability roughly reflected in the observed variability ($\Gamma_1 \sim \Gamma_2$) – a strength of the internal shock model because simulations of accretion flow give ms time-scales as observed.

Model calculations show between 1-10% of the shell kinetic energies can be radiated, so $E_\gamma << E_{kin}$. This is in some tension with observational results that indicate $E_\gamma \sim E_{kin}$.

Other candidate processes for the prompt emission exist, e.g. (See Kumar 2015 Section 7.)

- n-p collisions that give pions that decay to gamma rays
- Proton synchrotron emission
- Photo-pion
- Bethe-Heitler processes.

For magnetic jets (Poynting-flux dominates), dissipation and emission processes give further possibilities (e.g. “hotspot magnetic reconnection”).

Creating the prompt emission

A model in which *N* shells are ejected with random Lorentz factors and then collide.

L : shell separation
l : shell width
η : a density parameter

Main results:

1. Number of observed peaks ~ *N*.
2. Peak duration (~variability) ~ T*1/*N*.
3. Radiation efficiency ~10% (but varies 1-40% depending on details).

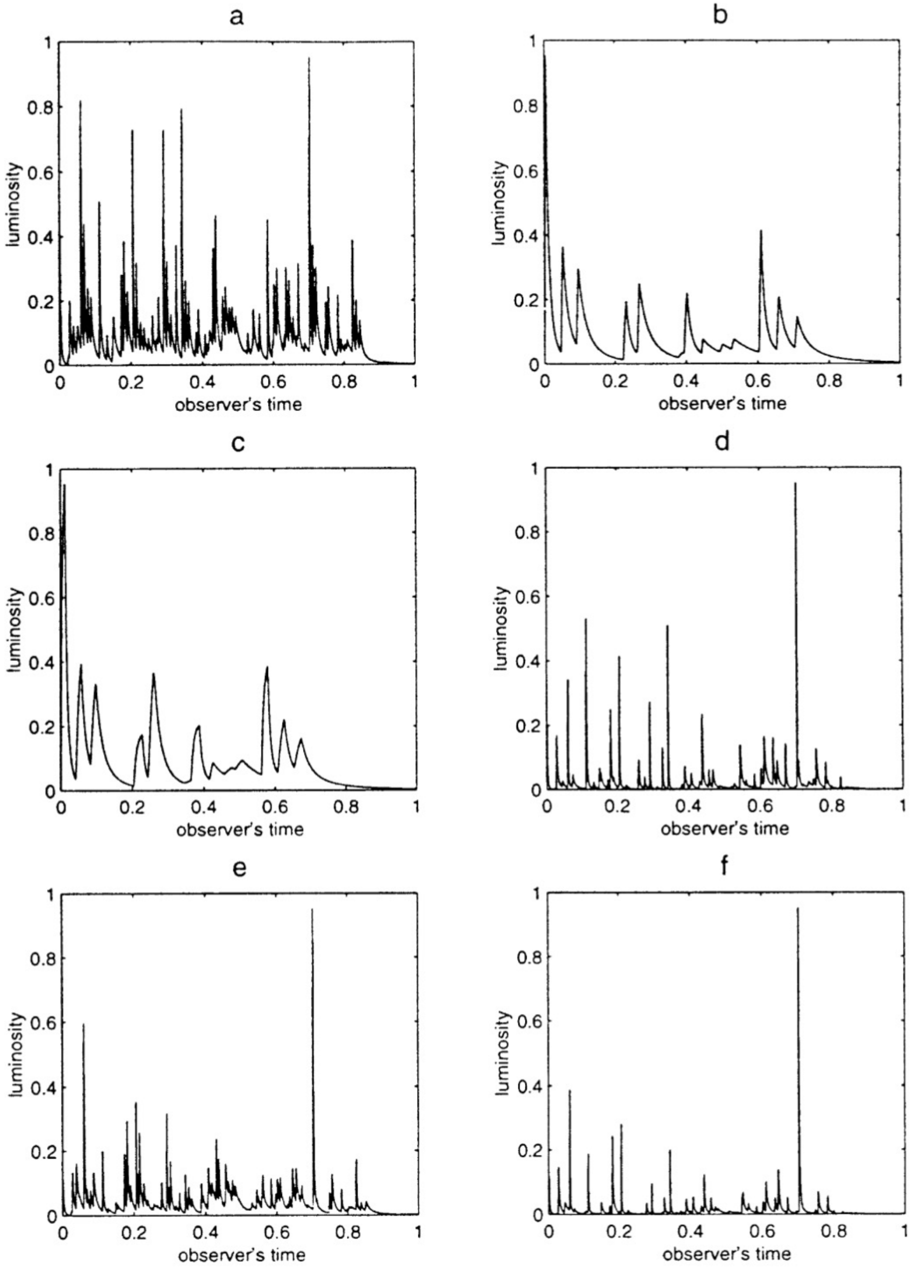

Fig. 20. Luminosity vs. observer time, for different synthetic models: (a) $\gamma_{\rm min} = 100$, $\gamma_{\rm max} = 1000$, $N = 100$, $\eta = -1$ and $L/l = 5$; (b) $\gamma_{\rm min} = 100$, $\gamma_{\rm max} = 1000$, $N = 100$, $\eta = 1$ and $L/l = 5$; (c) $\gamma_{\rm min} = 100$, $\gamma_{\rm max} = 1000$, $N = 20$, $\eta = -1$ and $L/l = 5$; (d) $\gamma_{\rm min} = 100$, $\gamma_{\rm max} = 1000$, $N = 20$, $\eta = -1$ and $L/l = 1$; (e) $\gamma_{\rm min} = 100$, $\gamma_{\rm max} = 1000$, $N = 100$, random energy with $E_{\rm max} = 1000$ and $L/l = 5$; (f) $\gamma_{\rm min} = 100$, $\gamma_{\rm max} = 1000$, $N = 100$, random density with $\rho_{\rm max} = 1000$ and $L/l = 5$. From

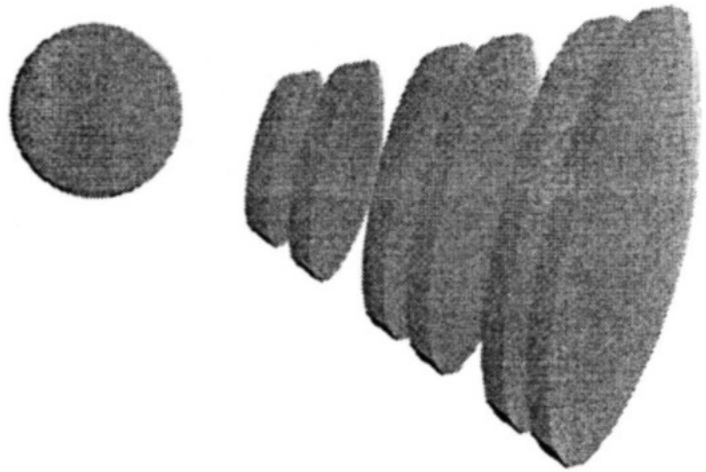

Kobayashi 1997

Creating the prompt emission

Somewhat surprisingly

- The observed duration of the whole display ~ duration of central source activity.
- The time sequence of observed pulses, with few exceptions, follows that of shell ejections.

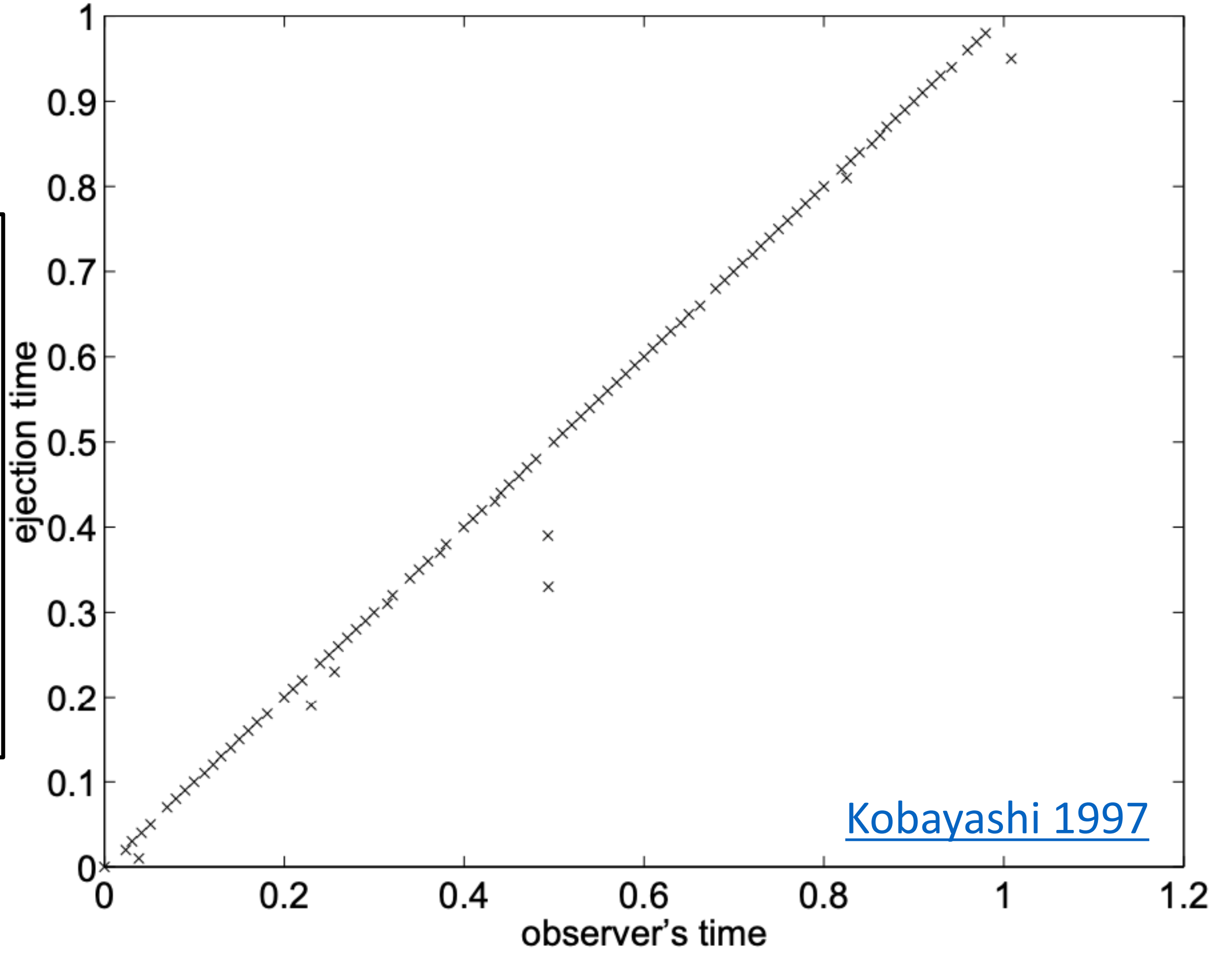

Kobayashi 1997

FIG. 3.—Time of ejection of a shell by the inner engine, $\tilde{t}_j$ vs. observed time of the photon produced in that shell, $t_{\mathrm{obs},j}$, for $N = 100$, $\gamma_{\min} = 10$, $\gamma_{\max} = 1000$, $\eta = -1$, and $L/l = 5$. The initial positions 0 and 100 correspond to the inner and outer edge of the wind.

GRB supernovae

SN 1998bw was discovered in association with GRB980425: the first time a GRB was shown to be associated with a SN.

Detecting SNe associated with GRBs is often not possible because the afterglow is much brighter than a SN (compare energy release of 0.5 M_{sun} of ^{56}Ni, ~10^{49} erg, to the kinetic energy of GRB jets, >~ 10^{51} erg).

Also, most GRBs are at redshift z >~1 and then

1. The dominant SN emission (=optical) redshifts into the harder-to-observe near-infrared range.
2. It’s hard to get spectra at those distances → have to rely on light curve bumps to infer the SN.

But SN 1998bw had a very weak afterglow, so detection was quite easily made.

Galama 1998

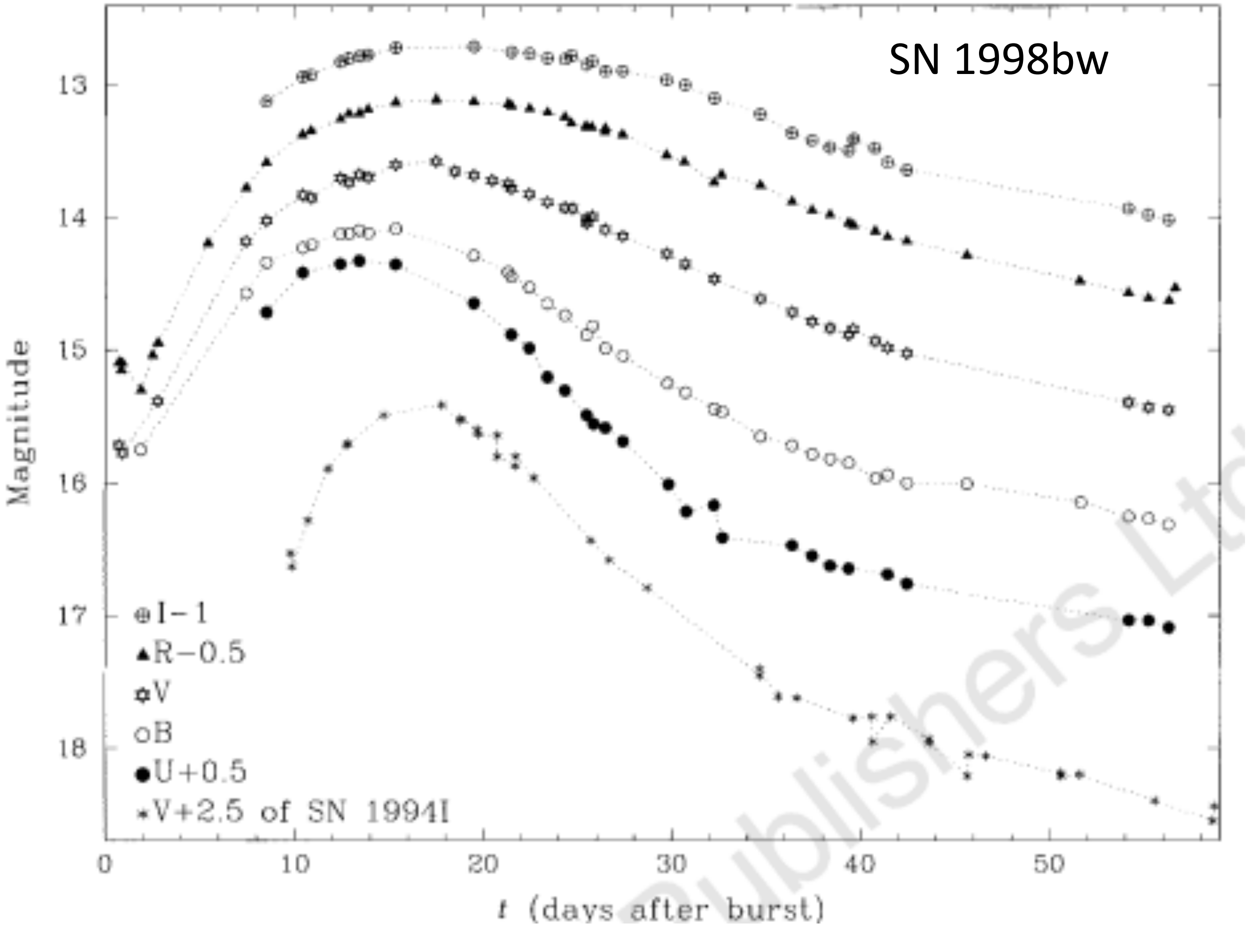

SN 1998bw

z = 0.0085 (40 MPc).

Type Ic-BL. (BL = Broad Lined).

No traditional afterglow seen (and this helped to detect the SN, Hjorth 2012).

Most luminous radio SN ever recorded.

Nebular spectra: large mass of oxygen (>~ 5 M_{sun}) inferred → a very massive star.

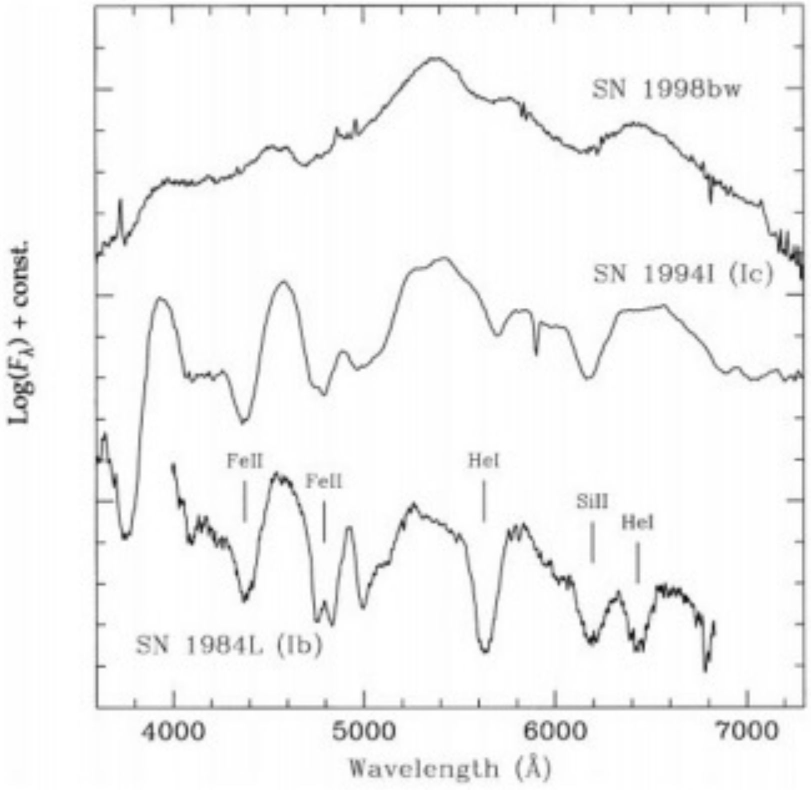

Ic-BL

Ic

Ib

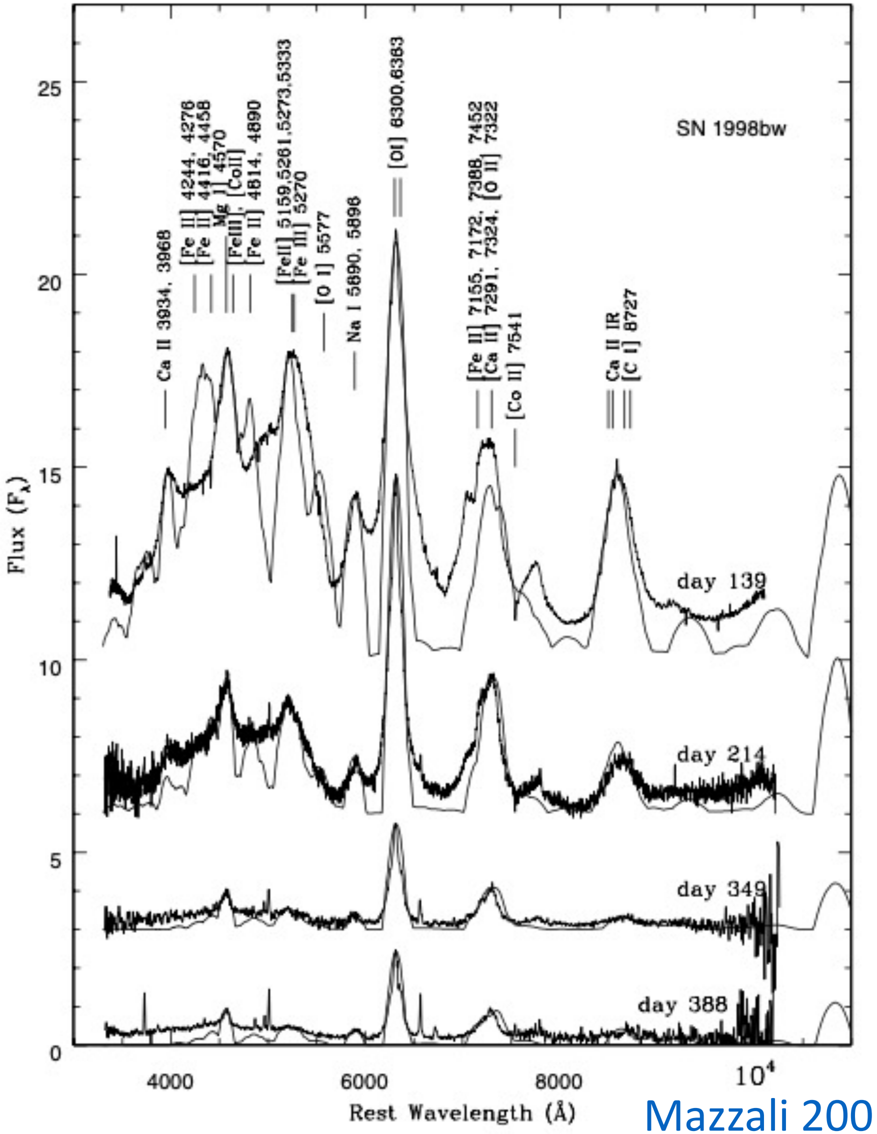

Mazzali 2001

The second GRB SN : **SN 2003dh**/GRB030329

Hjorth 2003

Between 1998-2003 it remained a possibility that GRB980425/SN1998bw was an oddball, not actually a ”normal” GRB similar to the standard cosmological ones.

Then **GRB 030329** / **SN2003dh** came along : its GRB did have a normal E_{iso} , and the SN looked similar to SN 1998bw in every way, removing that doubt.

The SN luminosity was ~5% of afterflow flux → the light curve and SED of the SN dependend to some extent on certain assumptions in the afterglow subtraction process.

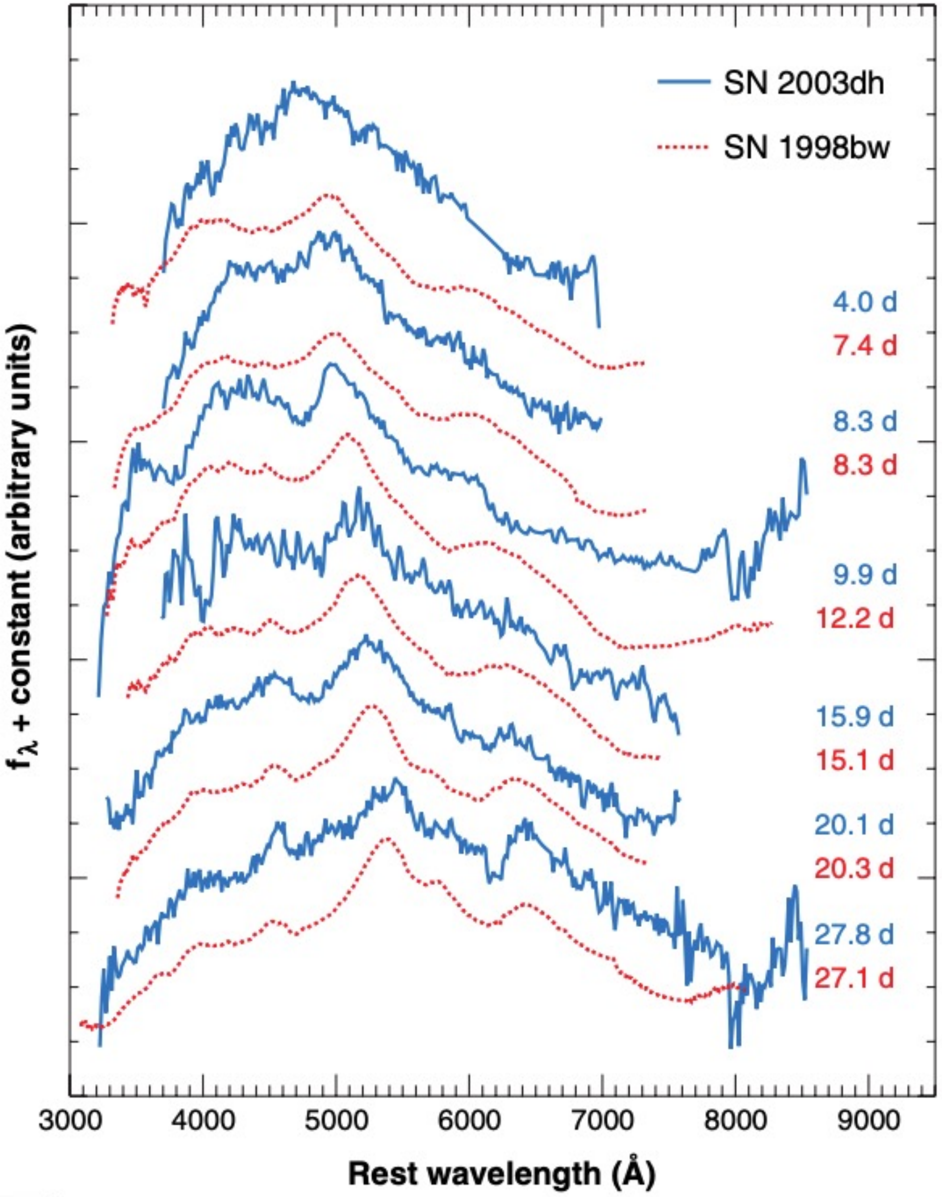

GRB supernovae, general properties

- Always Type Ic-BL.

- However, not all Ic-BL Sne seem to host GRBs (inferred from non-beamed afterglow constraints, next slide).

- Somewhat controversially, some (formally long) GRBs don’t seem to produce SNe (limits of ~0.01*SN1998bw established). However, some of these GRBs share some properties with short bursts so the picture is still somewhat unclear whether all long GRBs make SNe or not. Fynbo 2006, Della Valle 2006.

- At high redshift cannot get spectra, so have to identify SNe just from small bumps in photometric light curves → more uncertainty.

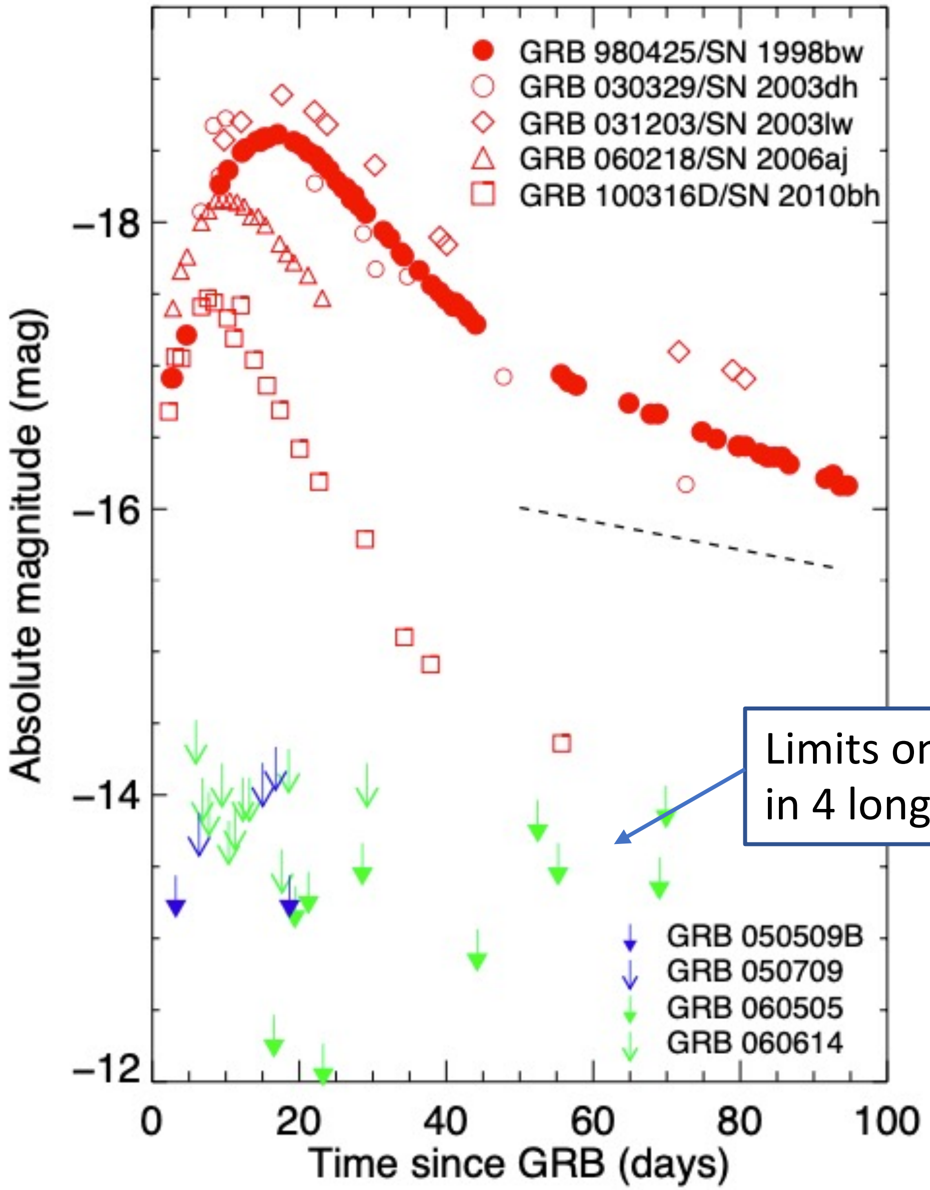

Limits on SNe in 4 long* GRBs.

GRB SNe:
1998bw
2003lw
2006aj
2008hw
2009nz
2010bh
2011kl
2012bz
2013cq
2013dx
2013ez

Do all Ic-BL SNe harbour GRBs?

We would only see the (beamed) GRB prompt emission in ~1% of them.

But the late, less weakly beamed afterglow should be more generally detectable.

Soderberg 2006: No such (radio) emission in most Ic-BL SNe → ***Most Ic-BL SNe don't harbor a GRB*** (max 3%).

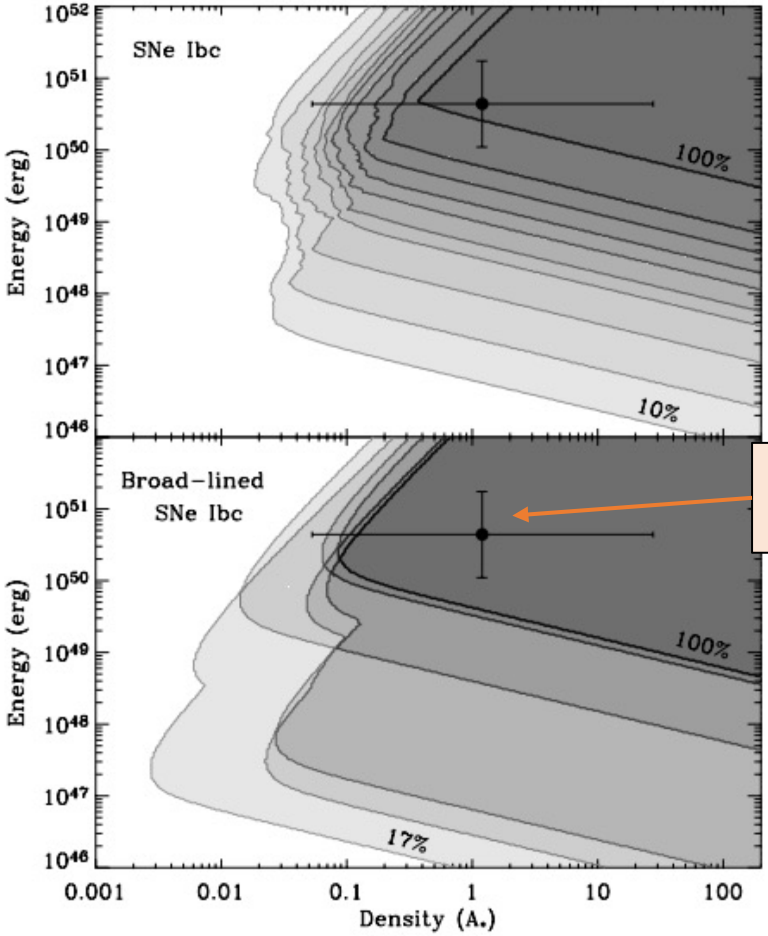

Mean GRB energy and CBN density

Soderberg 2006

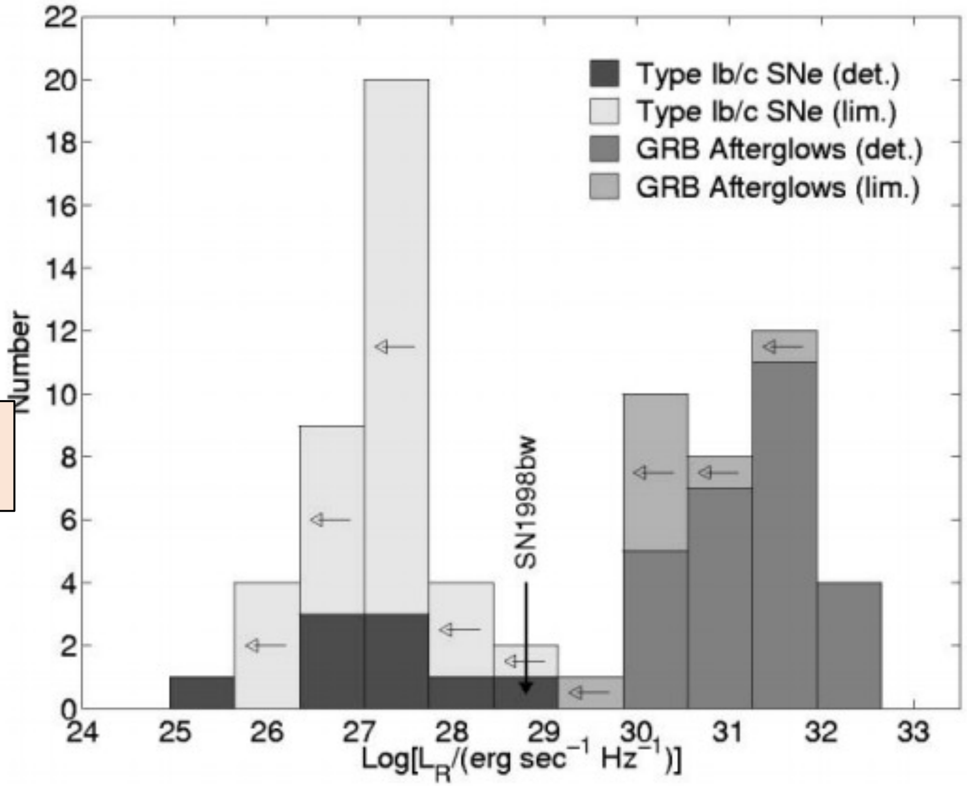

Berger 2003

Central engine: what launches the jet?

Two main model classes:

1. **Accreting BH.** Woosley 1993: "Collapsar"
2. **Spinning down millisecond NS.** Metzger 2011

$$E_{rot} = 2*10^{52} \text{ erg } P_{ms}^{-2}$$

Consensus on two points:

1. It's a signal from a stellar death (a massive star either collapses or merges with a compact object).
2. Lots of angular momentum is needed.

Note the origin of the rotation energy of the NS is gravitational binding energy, not rotation energy of the progenitor.

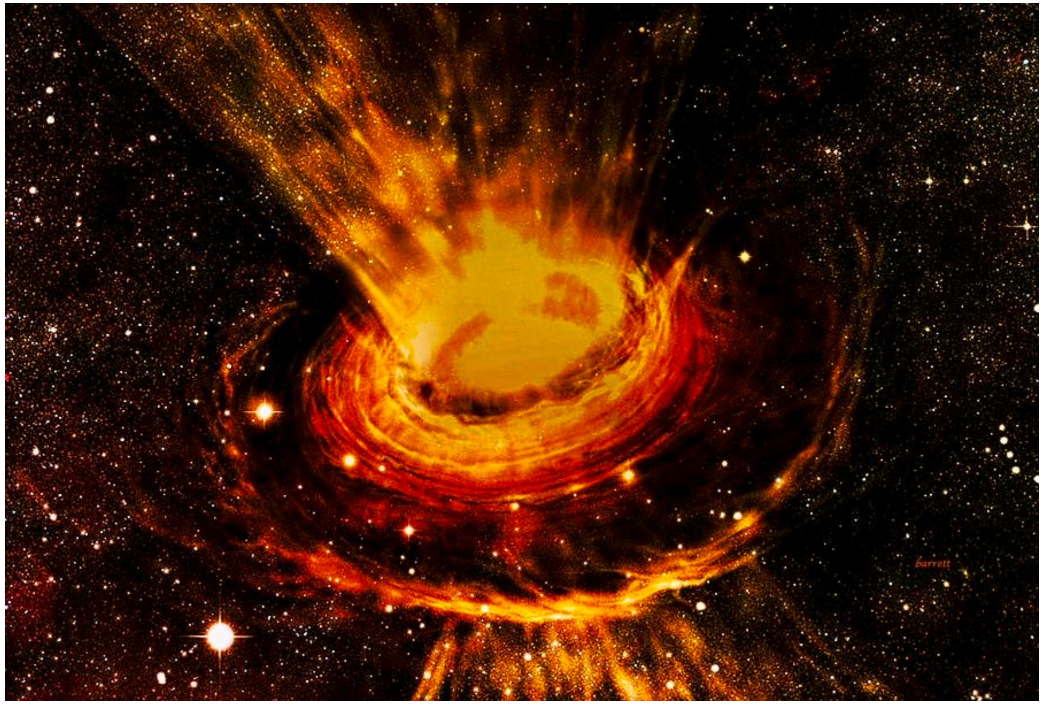

The collapsar model

In 1993, before it was known whether GRBs even came from cosmological distances, Stan Woosley presented a semi-quantitative model for how collapsing stellar cores (“collapsars”) may produce them.

The fundamental idea is that for massive enough cores, the infall cannot be halted by the neutrino emission from the proto-neutron star (as happens in SN explosions). Accretion onto the proto-NS therefore continues beyond the Tolman-Oppenheimer-Volkov limit and a BH forms.

If there is no or little rotation, the whole star falls into the BH with no strong electromagnetic display.

However, if there is sufficient angular momentum (j >~ $3*10^{16}$ cm^2 s^{-1}), the outer infalling layers will form an **accretion disk**. The initial disk forms on hydrodynamic timescale 446 s/sqrt(ρ) ~ 1s, but growth continues by slower free-fall from larger radii.

An energy budget of x*Mc^2 is available for material that falls in the gravitational potential to the last stable orbit, where x=0.06 for a non-rotating BH and 0.29 for a maximally rotating one. This translates to up to 10^{54} erg for M_{BH}=3 M_{sun} and M=1 M_{sun}. However only a fraction of this can realistically be radiated as electromagnetic emission.

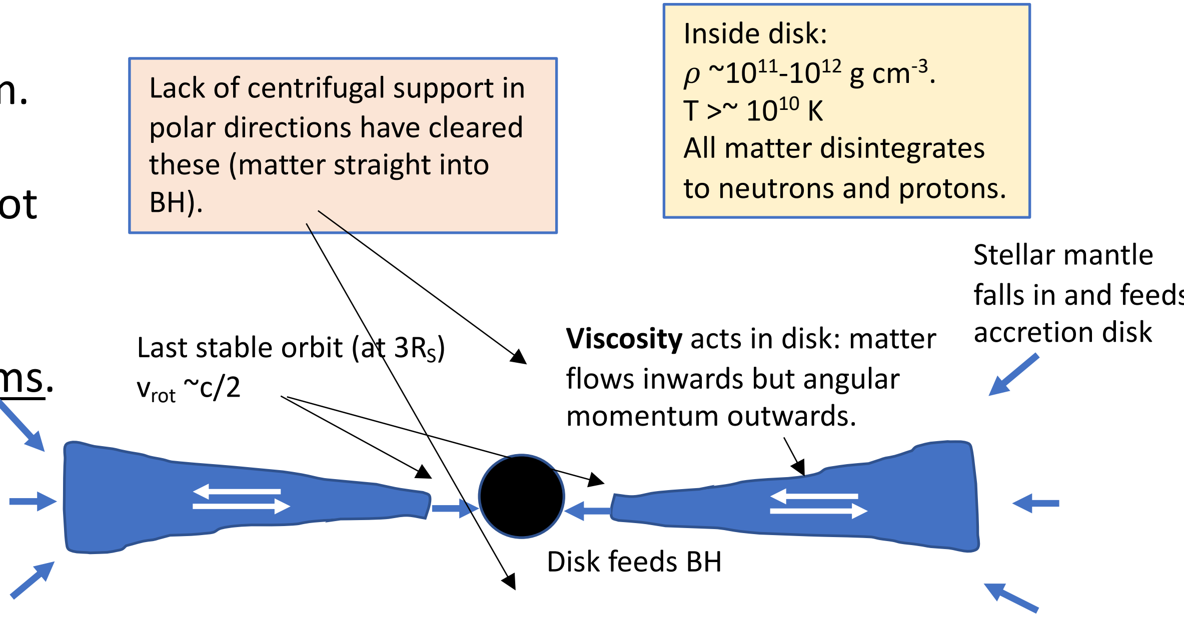

Lack of centrifugal support in polar directions have cleared these (matter straight into BH).

Inside disk:
ρ ~10^{11}-10^{12} g cm^{-3}.
T >~ 10^{10} K
All matter disintegrates to neutrons and protons.

Stellar mantle falls in and feeds accretion disk

Last stable orbit (at $3R_S$)
v_{rot} ~c/2

Viscosity acts in disk: matter flows inwards but angular momentum outwards.

Disk feeds BH

Flows of ~0.1 M_{sun}/s established, similar into and out of disk. Infall factor ~10 slower than free-fall estimate as pressure decelerates.

α

Angular frequency

Diffusion timescale $\tau = r^2/\nu$, $\nu \sim 0.01 * c_s^2/\boldsymbol{\Omega}$
$\boldsymbol{\Omega}$ ~3000 s^{-1} --> τ ~3s

Viscosity

Sound speed
c_s~10^9 cm/s

For Keplarian motion at ~30 km

$M_{dot} = M / \tau$ --> few tenths of M_{sun} per second.

Viscosity physics: Pringle 1981

The collapsar model

Neutrino emission processes:

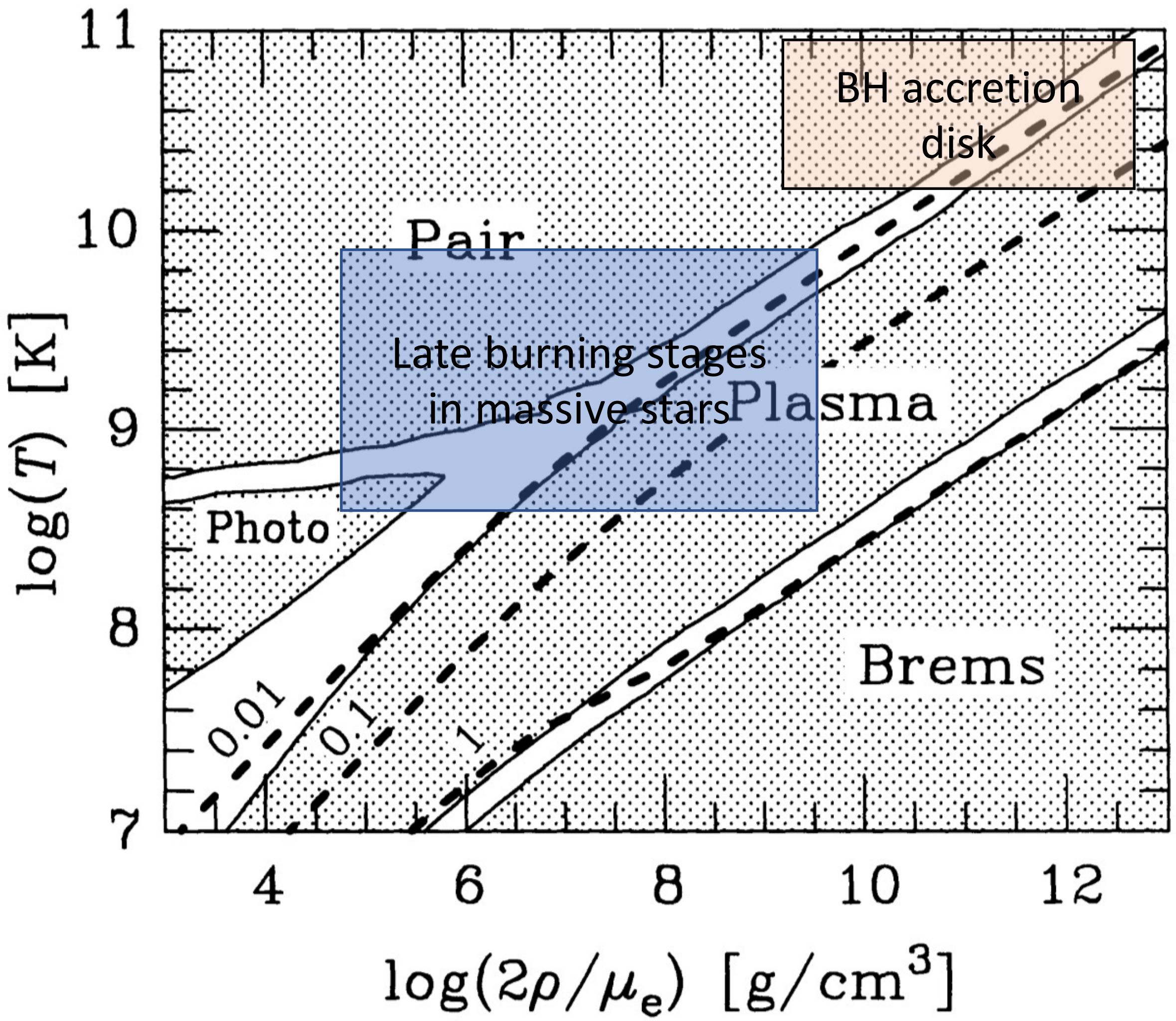

In addition to pair annihilations, now also **e-/e+ captures on nucleons** an important process.

Haft 1994

The collapsar model

Two possible pathways for transferring energy to the jet:

1) Neutrino pair production.

~20

collision angle

Neutrino annihilation cross section σ ~$10^{-44}<\varepsilon_{\mathrm{MeV}}>^2\cos(\phi)^2$ cm^2.
Neutrino number density $n_\nu \sim L_\nu / (4\pi R^2 * \varepsilon * c) \sim 10^{33}$ cm^{-3}
$\boldsymbol{\tau}$ **=** $\sigma * n_\nu * R \sim 0.01$ for R = 30 km → order 1% efficiency for converting neutrinos to pairs.

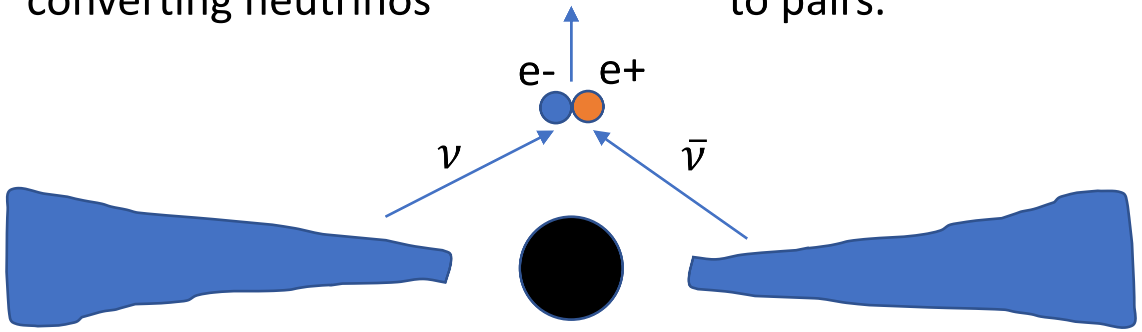

q = specific energy of last stable orbit

Energy dissipation $\dot{M} * \mathrm{q} \sim 10^{53}$ erg/s,
radiates as neutrinos (inner disk is optically thick to these, compare to SN explosion process). Pair annihilation and pair capture on free nucleons dominate neutrino creation.

Neutrinos moving towards central region can meet and annihilate (~1% of power → ~1E51 erg/s)
Note ok to make gammas here – this is not the emitting region.

2) Black hole rotation energy extracted by the Blandford-Zjanek mechanism (MHD process).

$\dot{E}$ = $4*10^{52}\ \mathrm{B}_{15}^2\ \mathrm{M}_{10}^2$ erg/s

Magnetic field lines thread and semi-corotate with the BH → induction.

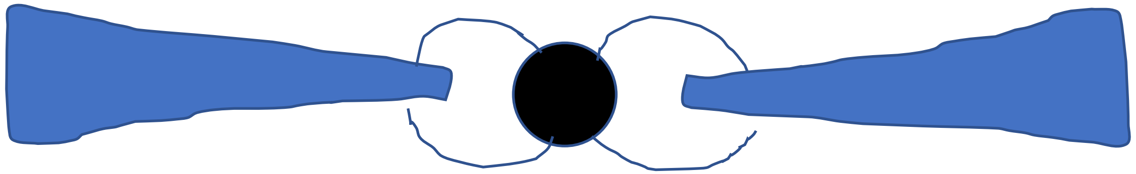

Charged particles supplied from accretion disk maintain currents in magnetosphere.

Simulations of collapsar disks

First works by MacFadyen & Woosley 1999 (2D Eulerian hydrodynamics).

Quite a lot of parametrizations/assumptions:

- **Angular momentum** of progenitor arbitrarily distributed
  - Woosley 1993: Assume $F_{centr} = 0.01 F_{grav}$ → disk forms at ~100 km.
- **Viscosity**
  - α-viscosity : $\boldsymbol{v} = \alpha * c_s * H$

    Free parameter

    Characteristic length scale

    Sound speed
- **Boundary conditions**
  - Absorbing inner boundary at 50 km (in reality last stable orbit evolves with time).
- **Photon and neutrino radiation fields**
  - Neutrino cooling in optically thin limit.
- **Nuclear energy**
  - Burning ignored, but energy release by photodisintegrations to *n* and *p* included (but note this can yield only ~1% of mc^2 compared to (6-40)% released by accretion.)

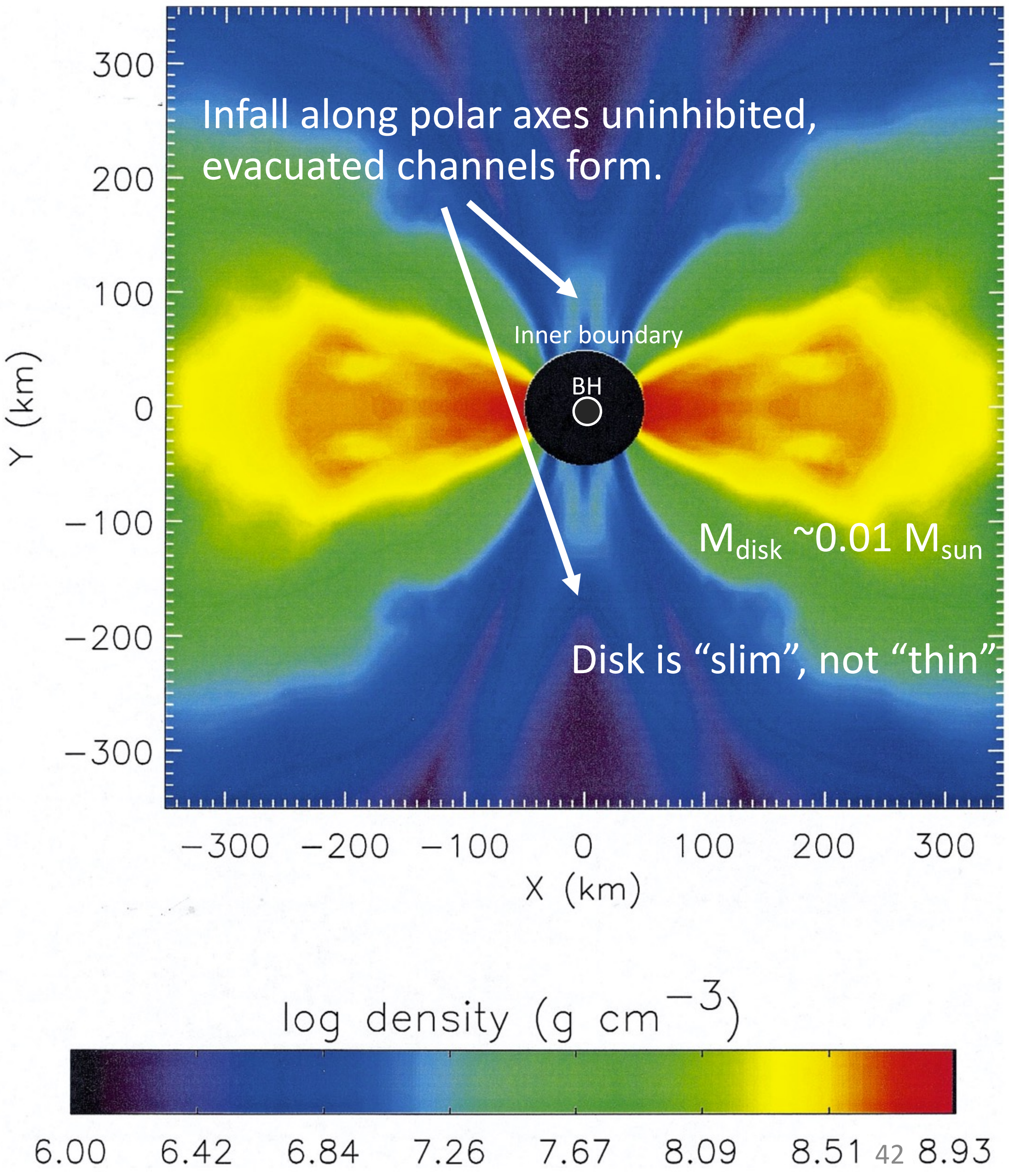

Infall along polar axes uninhibited, evacuated channels form.

Inner boundary

BH

M_{disk} ~0.01 M_{sun}

Disk is “slim”, not “thin”.

Simulations of collapsar disks

Accretion rate shown to vary on timescales of tens of milliseconds
→ Could explain GRB prompt emission variability observed on similar timescales.

However, it is not certain that the observed GRB variability is linked to such engine variability, it may also be due to relativistic turbulence in emission region, instabilities in the jet-stellar matter interactions, or current-driven kink instabilities (magnetic jets).

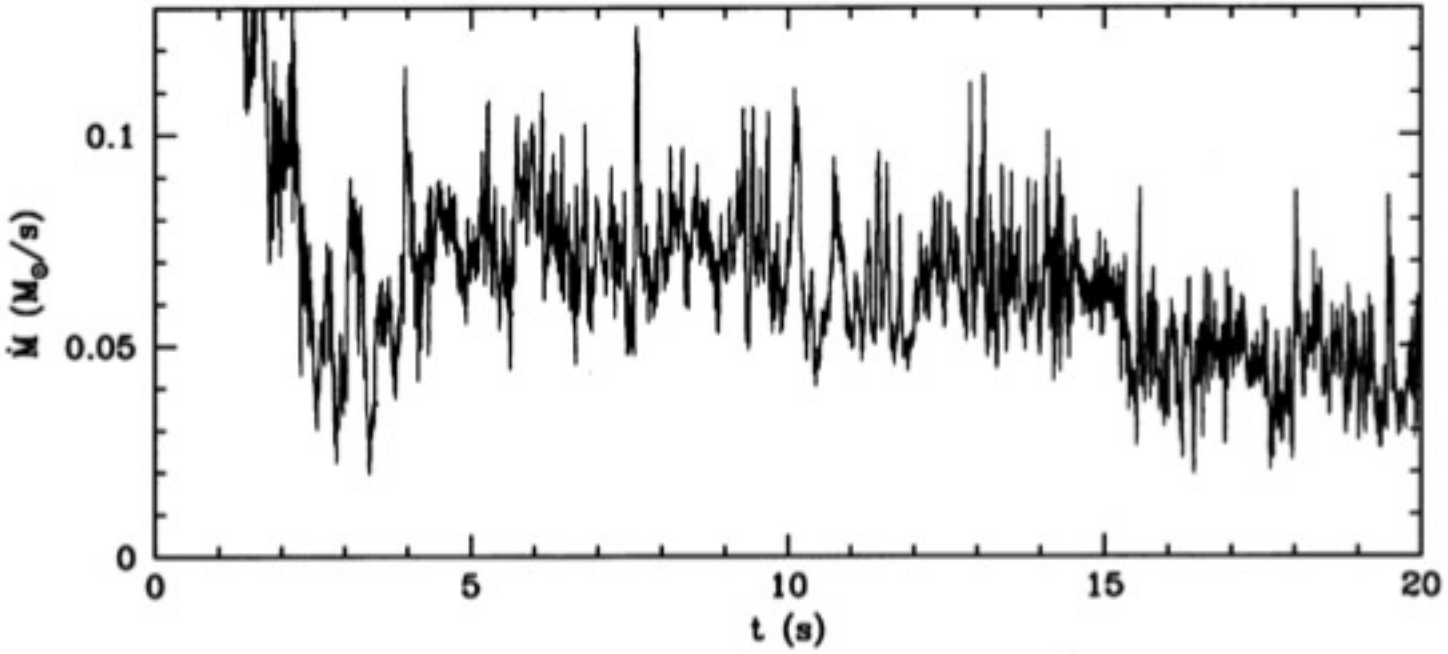

MacFadyen & Woosley 1999

Simulation of collapsar disks

$10^{51} – 10^{52}$ erg
shown to be deposited by
neutrino annihilations
in the polar regions.

Jet pushes material
to the side and may
produce a **supernova**.

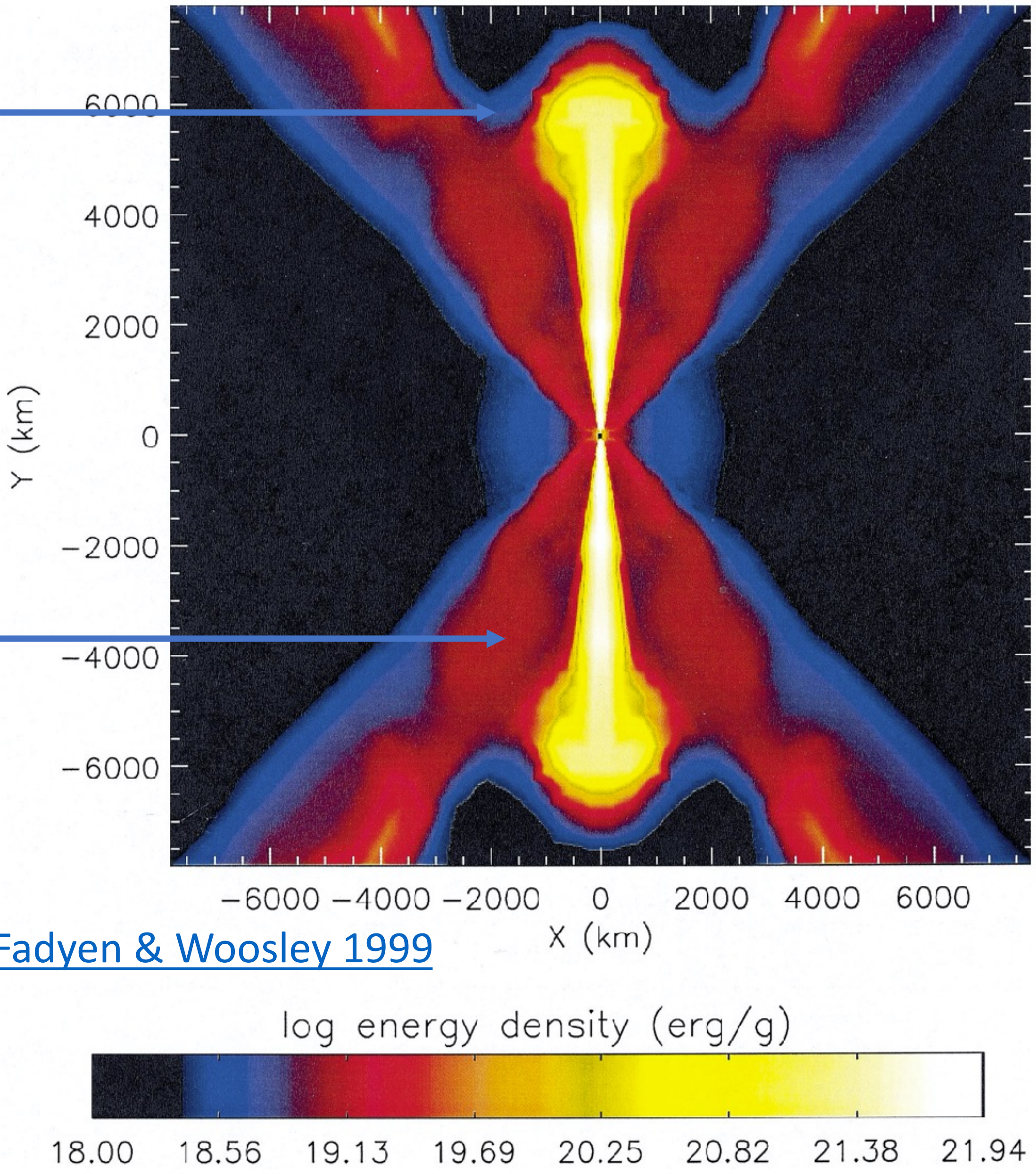

MacFadyen & Woosley 1999

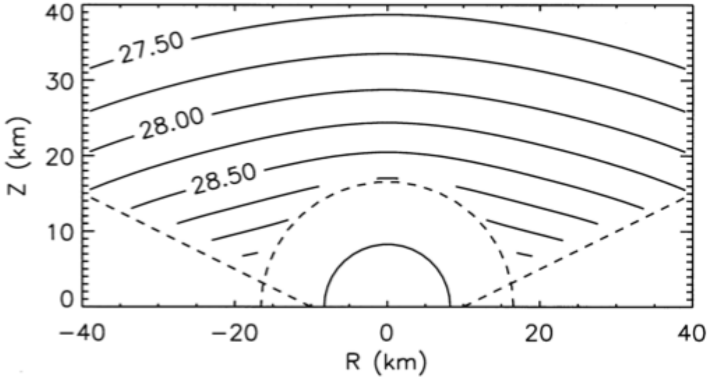

FIG. 20.—Energy deposition by neutrino annihilation for the "conservative" (see text) $\dot{M} = 0.1\ M_\odot\ s^{-1}$, $a = 0.5$, $M_{bh} = 3\ M_\odot$ case. Contours of the logarithm of the energy deposition rate in ergs $cm^{-3}\ s^{-1}$ are shown with an equal spacing of 0.25 dex between contour lines. The energy deposition rate is peaked along the pole. The dashed diagonal lines approximately represent the disk scale height below which annihilation energy was neglected (the ratio of scale height to radius is not constant in the PWF model as it appears here). The dashed semicircle represents twice the event horizon radius within which all neutrino emission and absorption is neglected. The solid semicircle represents the event horizon.

Not a very realistic jet simulation (neutrino transport and annihilations done analytically, and not a relativistic code for the jet propagation) – but first indication that

1. **Jet formation does occur by the neutrino annihilation mechanism.**
2. **The jet accelerates and starts to punch a hole through the star.**

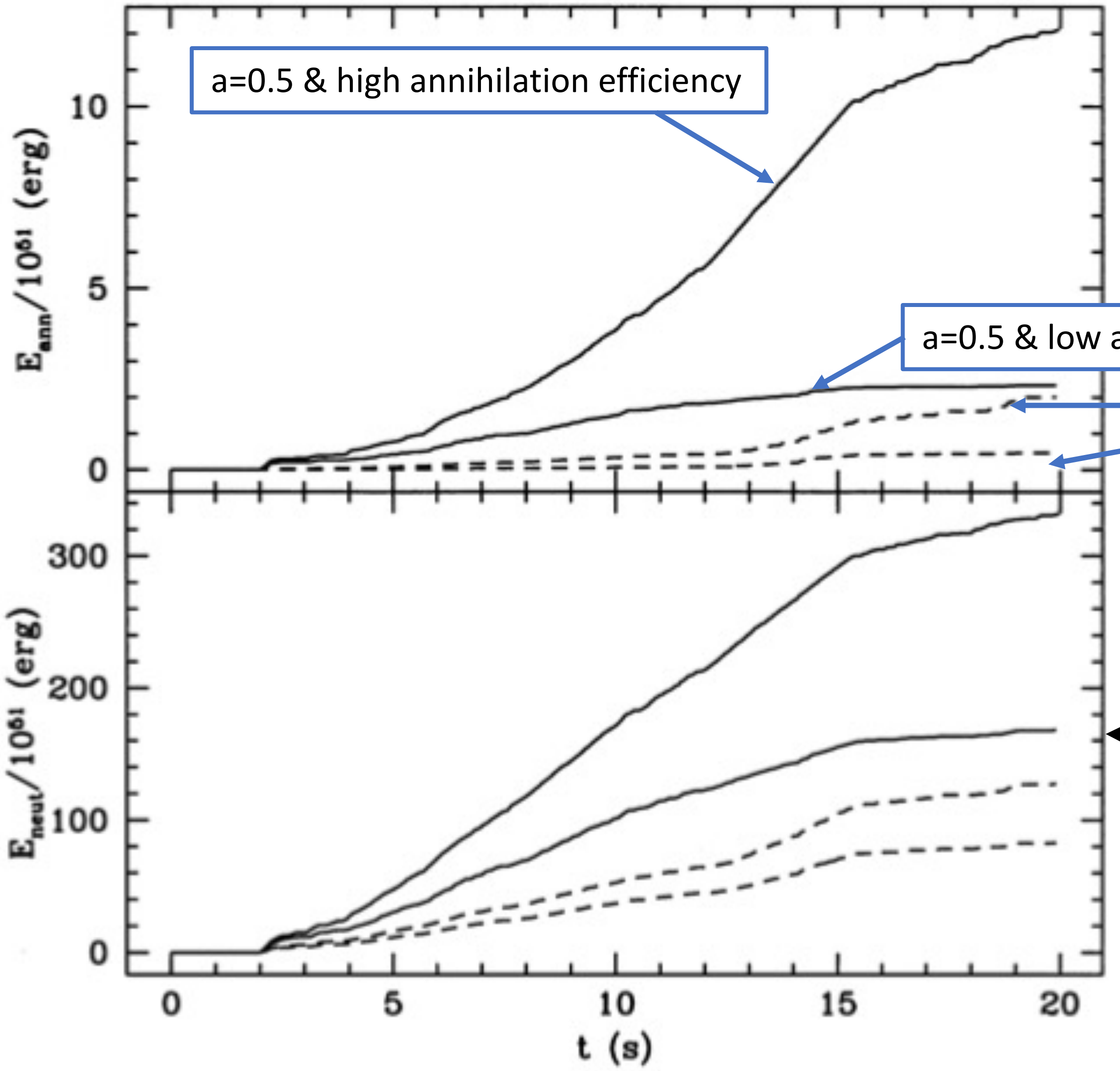

Accumulative neutrino annihilation power can reach over 10^{52} erg.

Accumulative neutrino energy radiated from disk can reach over $3*10^{53}$ erg.

Mechanism more efficient for higher BH rotation.

[MacFadyen & Woosley 1999]

FIG. 22.—Time-integrated neutrino annihilation energy. The top panel shows the running integral of the energy deposited for two choices of initial Kerr parameter ($a_{\mathrm{init}} = 0$: *dashed lines*; $a_{\mathrm{init}} = 0.5$: solid lines) and for two assumptions regarding the efficiency of neutrino annihilation (§ 4.1.7). The higher lines for each case use the "optimistic" neutrino rates. The bottom panel gives the *total* neutrino energy radiated from the disk for the same assumptions.

Simulations of collapsar disks

SN-like ejection also possible by a second mechanism: **a disk wind**.

MacFadyen 1999 simulation:

- E_{wind} ~10^{51} erg.
- M_{wind} ~1 $M_{sun.}$
- Outflow angles 30-45 degrees.
- Initially nucleons in wind but assemble to ^{56}Ni (although Y_e is not computed so only if it stays close to 0.5)

Disk wind nucleosynthesis: e.g. Pruet 2004, Surman & MacLoughlin 2005.

Wind velocity will be of order escape velocity from disk, ~0.1c. Could explain the “BL” in Ic-BL.

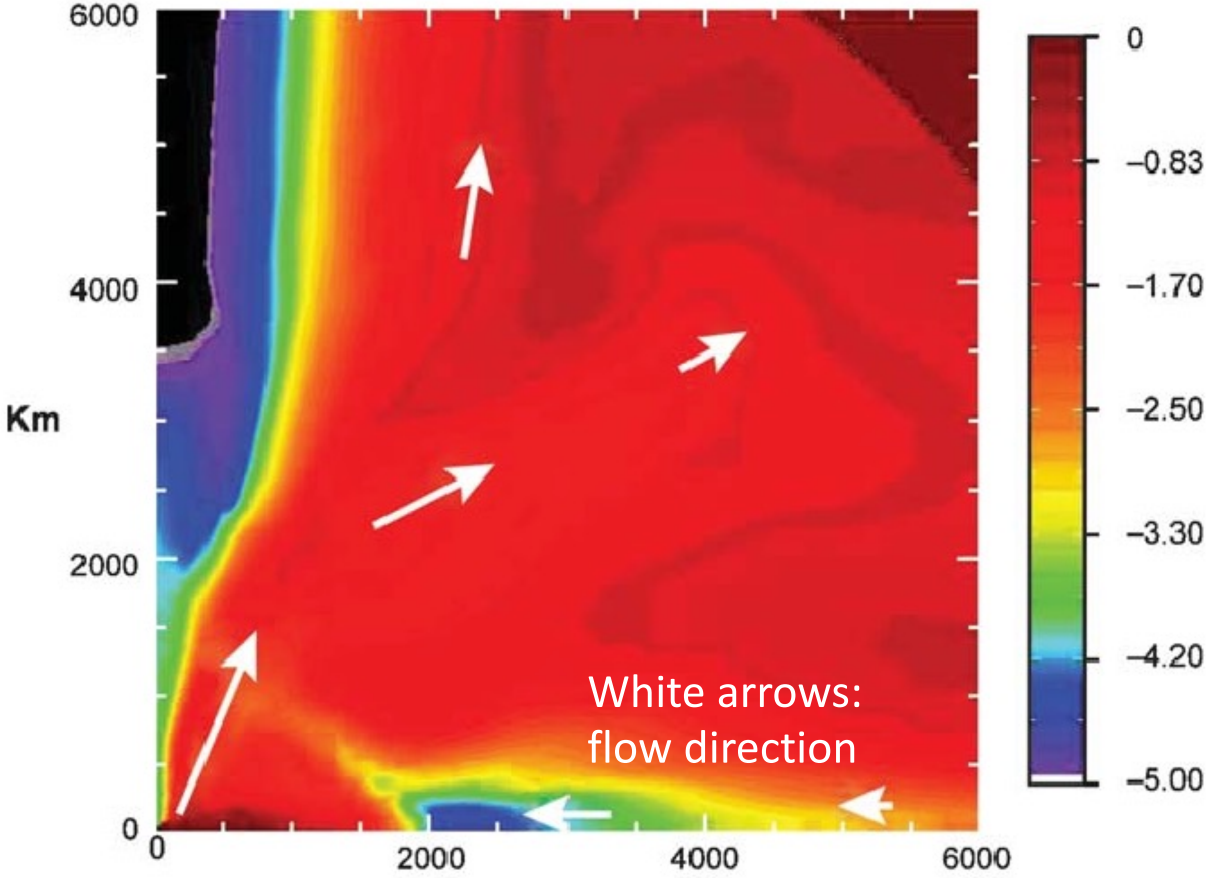

White arrows: flow direction

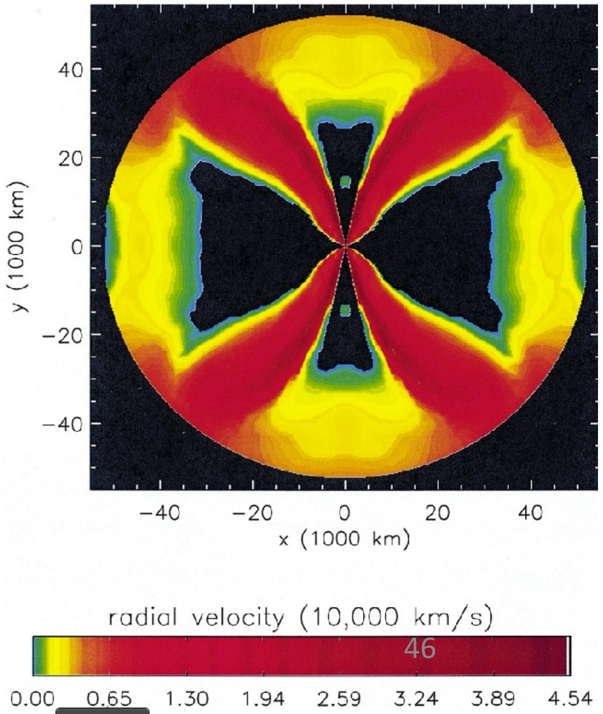

The Blandford-Znajek mechanism

Spin parameter
a = Ω / Ω_{max}

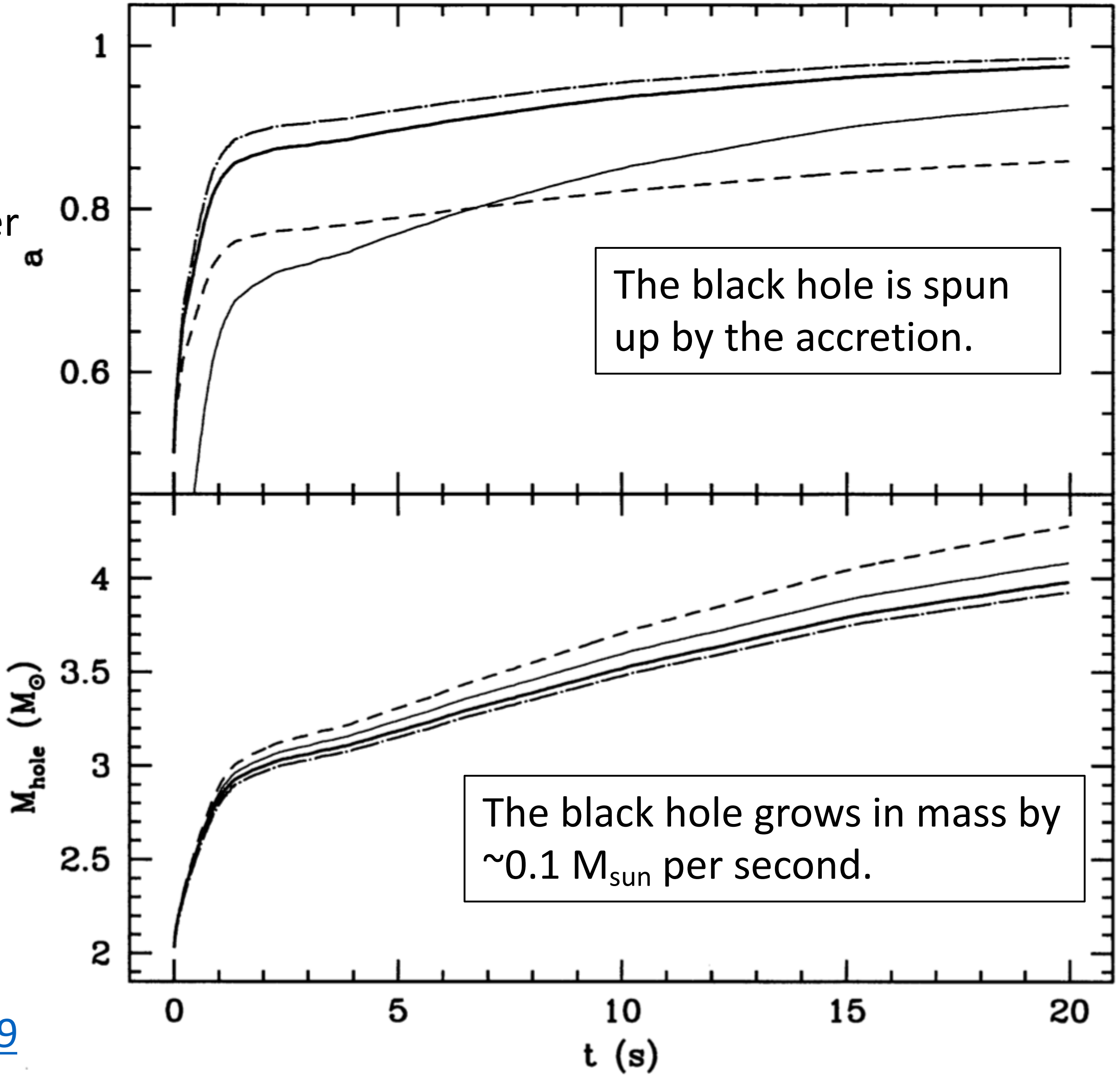

The black hole is spun up by the accretion.

The black hole grows in mass by ~0.1 M_{sun} per second.

Maximal spin, here E_{rot} ~10^{54} erg.

If even a small fraction of this BH rotation energy could be extracted it would dominate neutrino annihilations.

But, note also that higher spin parameter means that the disk moves in, get a more compact geometry, higher *T* and *L*, and stronger neutrino emission.

MacFadyen & Woosley 1999

The Blandford-Znajek mechanism

Nagataki 2009, 2011: Evidence for the BZ mechanism becoming operational, even though insufficient Lorentz factors (~10) reached.

High BZ power still needs a significant accretion rate, and so the neutrino process would also operate to some extent – GRBs may have contribution by both processes.

BZ gives a “**cold, Poynting-flux jet**” (dominated by large-scale magnetic fields) compared to “**hot fireball jet**” for the neutrino case. The Poynting flux cannot be efficiently reradiated unless re-randomized. Impact on external medium could help do this.

29% of the mass-energy of maximally rotating BH is associated with rotation. The BZ power is of order

$$\dot{E} = 4 * 10^{52} B_{15}^{2} \left(\frac{M_{BH}}{10\ _{Msun}}\right)^{2} \text{erg s}^{-1}.$$

Lorentz factor

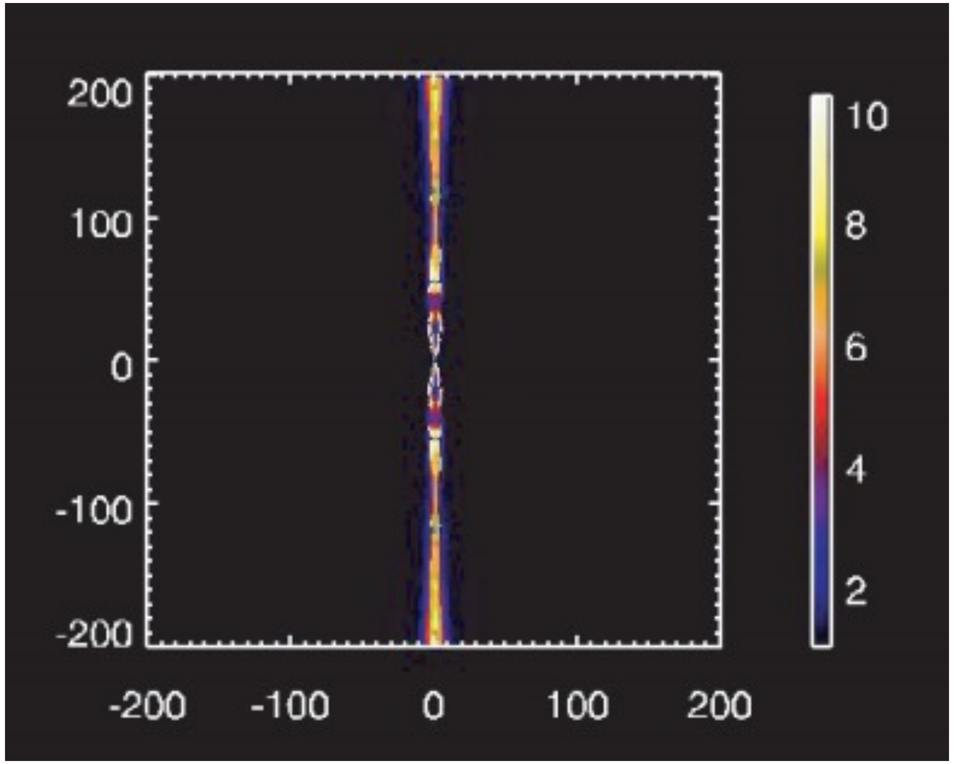

Nagataki 2011

Magnetic jet acceleration and prompt emission

In the rest frame (=comoving frame CMF) of a gas parcel (primed quantities):

Magnetic field energy density $e_B = B'^2/8\pi$. (Note $B'^2 = B^2/\Gamma^2$ but we are at base so Γ still ~ 1.)

Electric field energy density $e_E=0$ (vanishes in CMF, E = - v/c cross B, v=0 in CMF)

Particle energy density $e_p = \rho' c^2 + p' = 1E26\ \rho_5 + 2e25\ T_{10}^4$

Magnetization parameter $\sigma \equiv e_B/e_p >> 1$ (energy density dominated by magnetic fields) if $B' \gtrsim 10^{13}$ G.

From conservation laws, one can show that the jet accelerates by conversion of magnetic field energy to kinetic energy (just an adiabatic expansion in which any internal energy converts to bulk flow). Simulations demonstrate that it is possible to reach $\Gamma \gtrsim 100$ (e.g. Komissarov papers), but there are certain assumptions on boundary conditions in such work (e.g. funnel).

Once an ultrarelativistic jet is produced, gamma-rays may be produced by either

- Internal shocks (same as fireball jet).
- Hotspot magnetic reconnection events.

Numeric simulations of high σ, high Γ, magnetic dissipation/reconnection jets are yet not feasible (and far from being so)--> **magnetic jets remain as a sketch/possibility concept**.

The magnetar model

Bucciantini 2007, Metzger 2011

Two phases

1) Magnetar wind
2) Magnetically accelerated neutrino-powered wind with wound-up B fields.

Assumes an initial SN explosion (whereas in the collapsar model the GRB and SN mechanisms are separated).

Unclear whether ^{56}Ni can be produced.

Unclear whether focused jet can be produced, but some recent simulation results support (Aloy 2021, Obergaulinger 2020).

Has a maximum energy budget few*10^{52} erg, whereas the collapsar model can exceed this significantly.

Late-time activity here due to magnetar glitches (in collapsar model due to fall-back).

Strengths: Relates to an object known to exist (the magnetar) and energy and time scales viable.

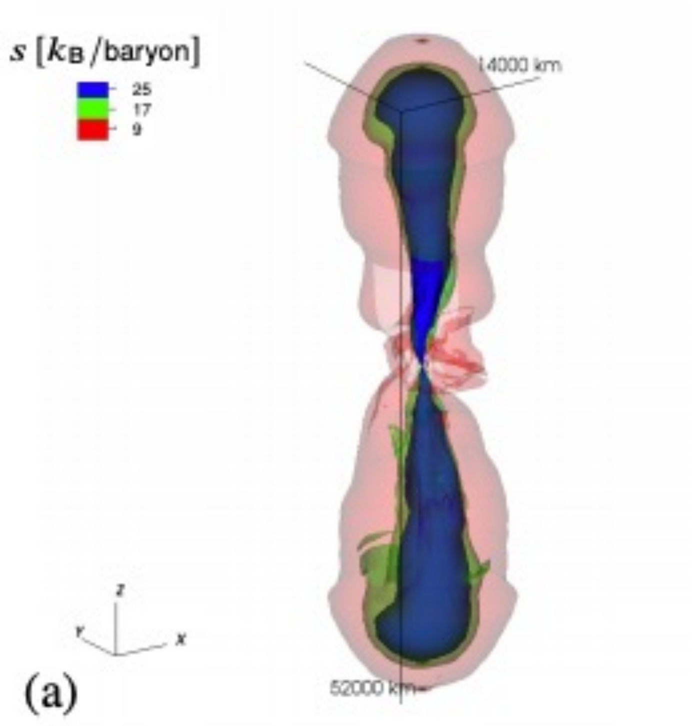

Obergaulinger 2020:
A collimated jet produced by a magnetar.

Simulations of jet propagation

Zhang 2004, Woosley & Zhang 2007

Jet takes 10-20s to break out through star. Simulations show it must be sustained over that period
→ constraint that **central engine must be active for 10-20s.**

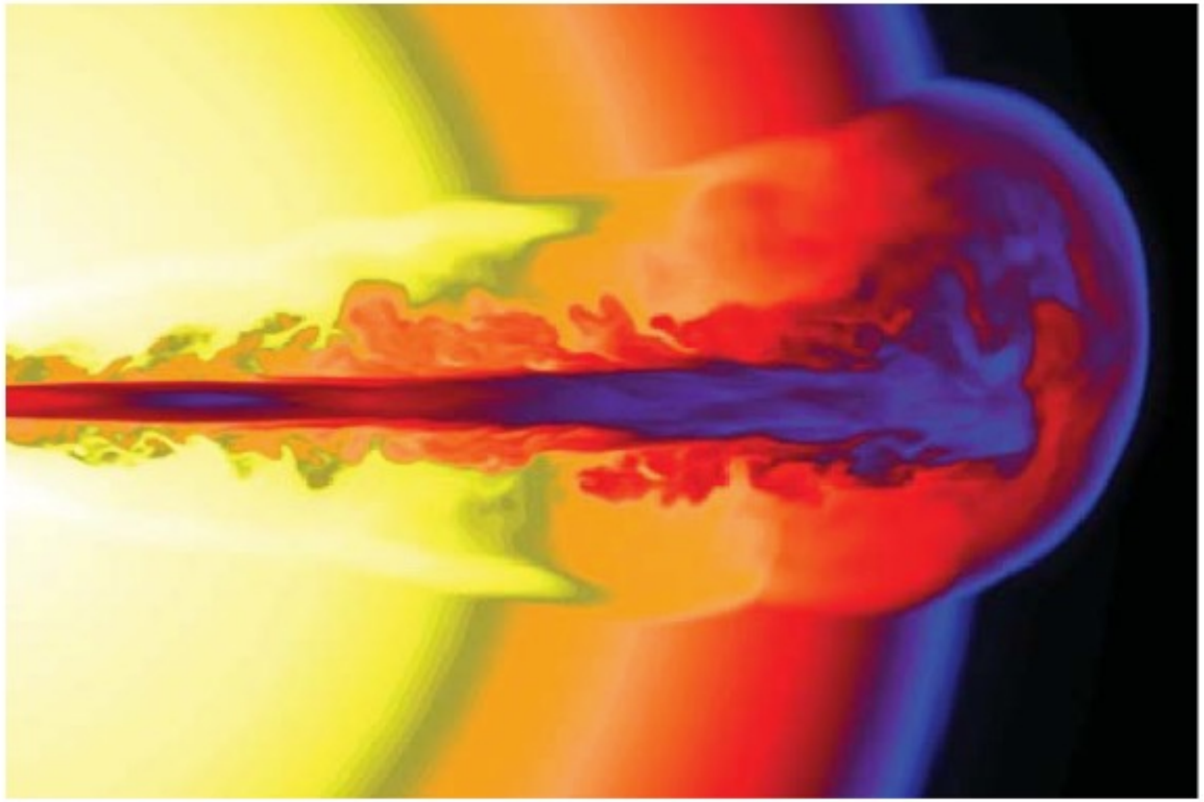

Figure 8

Break out of a relativistic γ-ray burst jet with energy 3×10^{50} erg s^{-1} 8 s after it is launched from the center of a 15 $M_\odot$ WR star. The radius of the star is 8.9×10^{10} cm and the core jet, at infinity, will have a Lorentz factor $\Gamma \sim 200$. Note the cocoon of mildly relativistic material that surrounds the jet and expands to larger angles. Once it has expanded and converted its internal energy this cocoon material will have Lorentz factor $\Gamma \sim 15$–30. An off-axis observer may see a softer display dominated by this cocoon ejecta. If the star were larger or the jet stayed on a shorter time, the relativistic core would not emerge, though there would still be a very energetic, highly asymmetric explosion. (Zhang, Woosley & Heger 2004.)

Jets can be of type
1) "Fireball"
2) Poynting flux (large-scale magnetic fields)

Only the first type can be quasi-realistically simulated.

Simulations of jet propagation

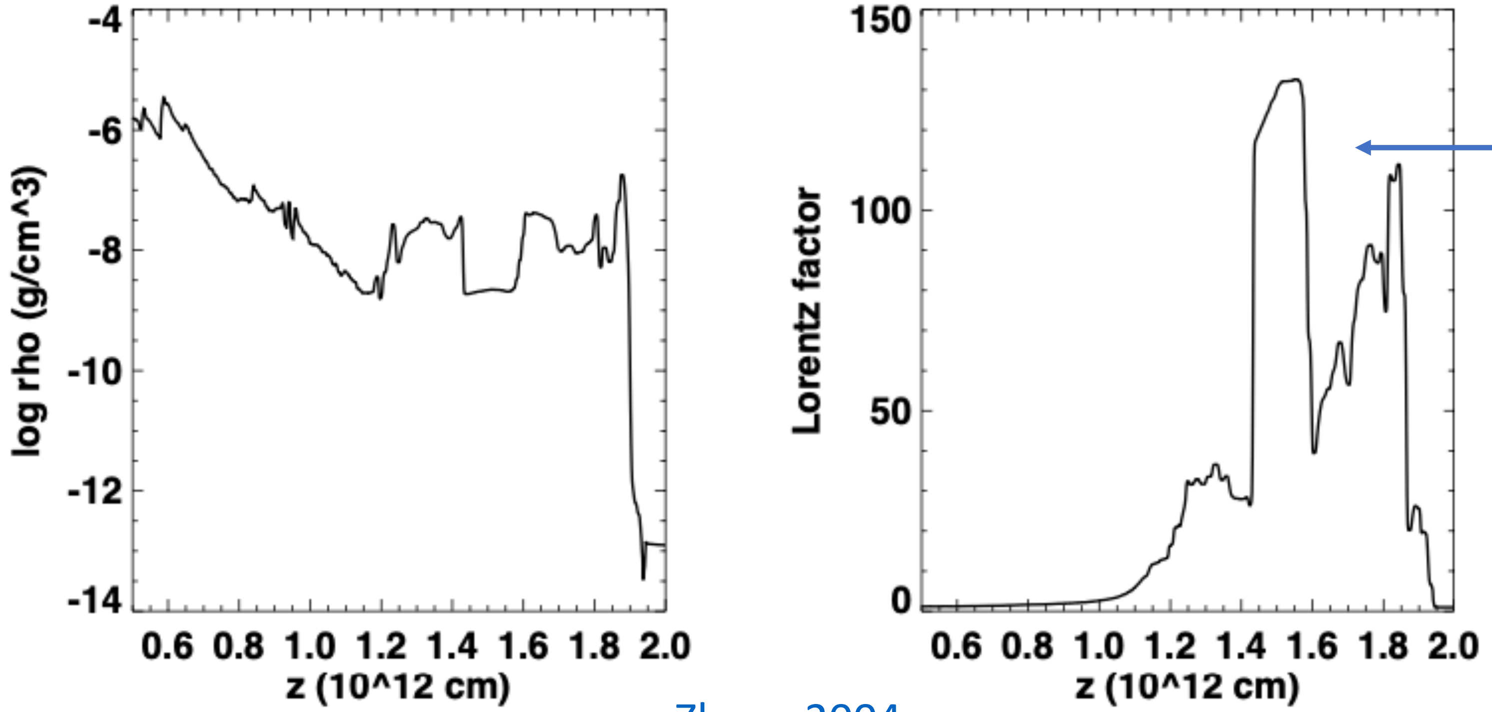

Variable Lorentz factors achieved (a requisite for internal shock models for GRB prompt emission).

Zhang 2004

Figure 109: Density and Lorentz factor in the jet in Fig. 108 at 70 s. Note the highly variable density and especially Lorentz factor (Zhang, and Woosley 2002).

SN 1998bw revisited: light curves and spectral modelling

No 1D ^{56}Ni-powered model fits the whole light curve well.

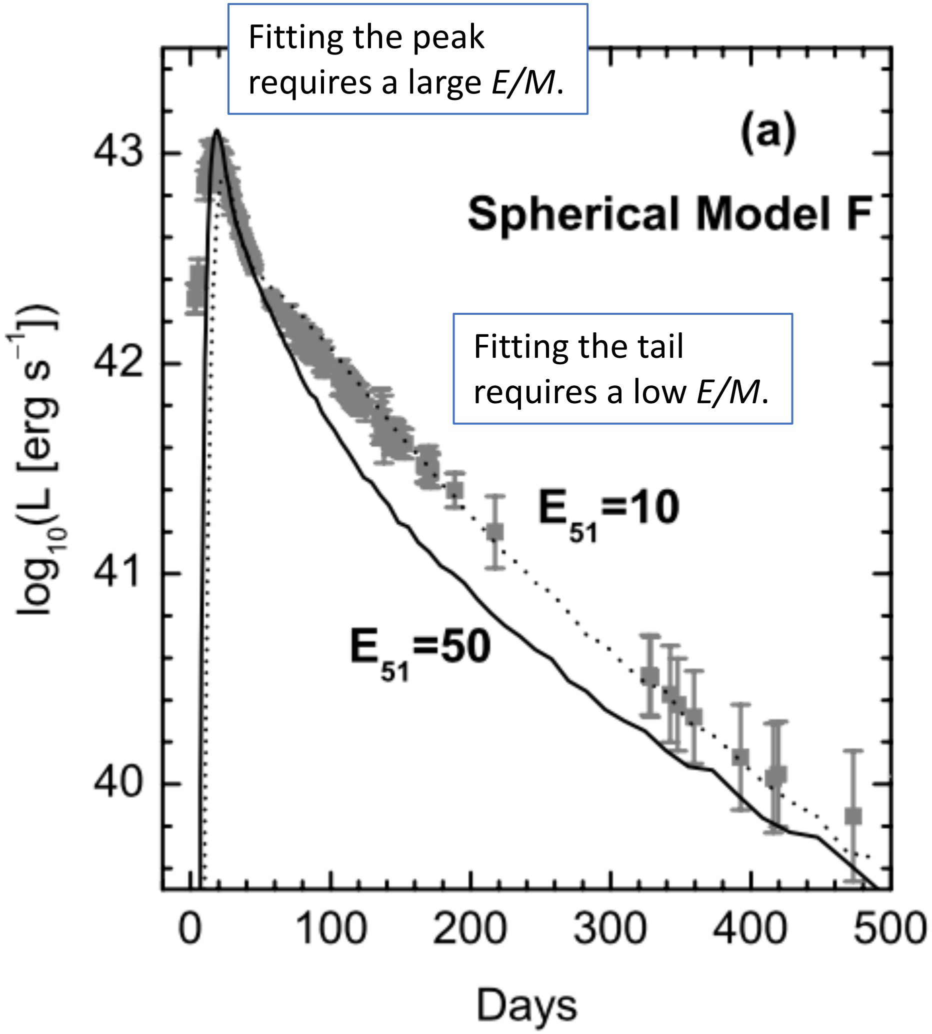

Fitting the peak requires a large *E/M*.

Fitting the tail requires a low *E/M*.

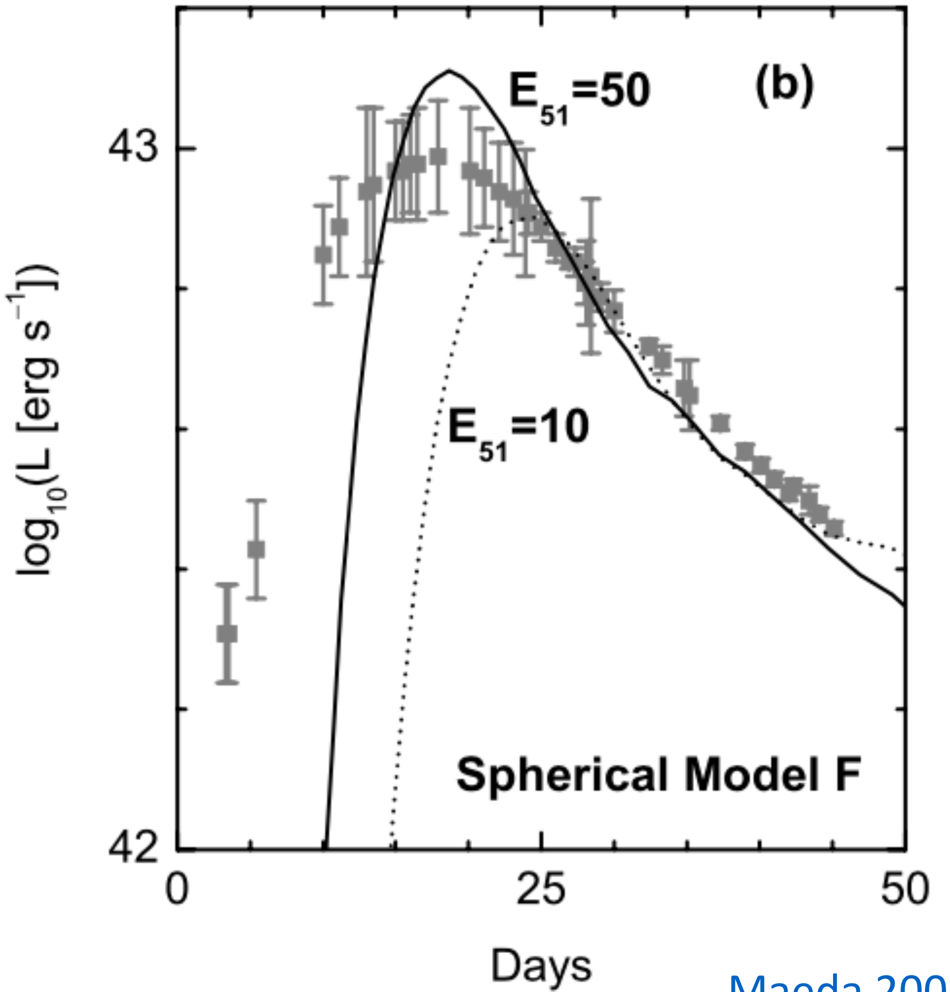

Maeda 2006

SN 1998bw revisited: light curves and spectral modelling

2D ^{56}Ni-powered models do better, however need quite extreme parameters.

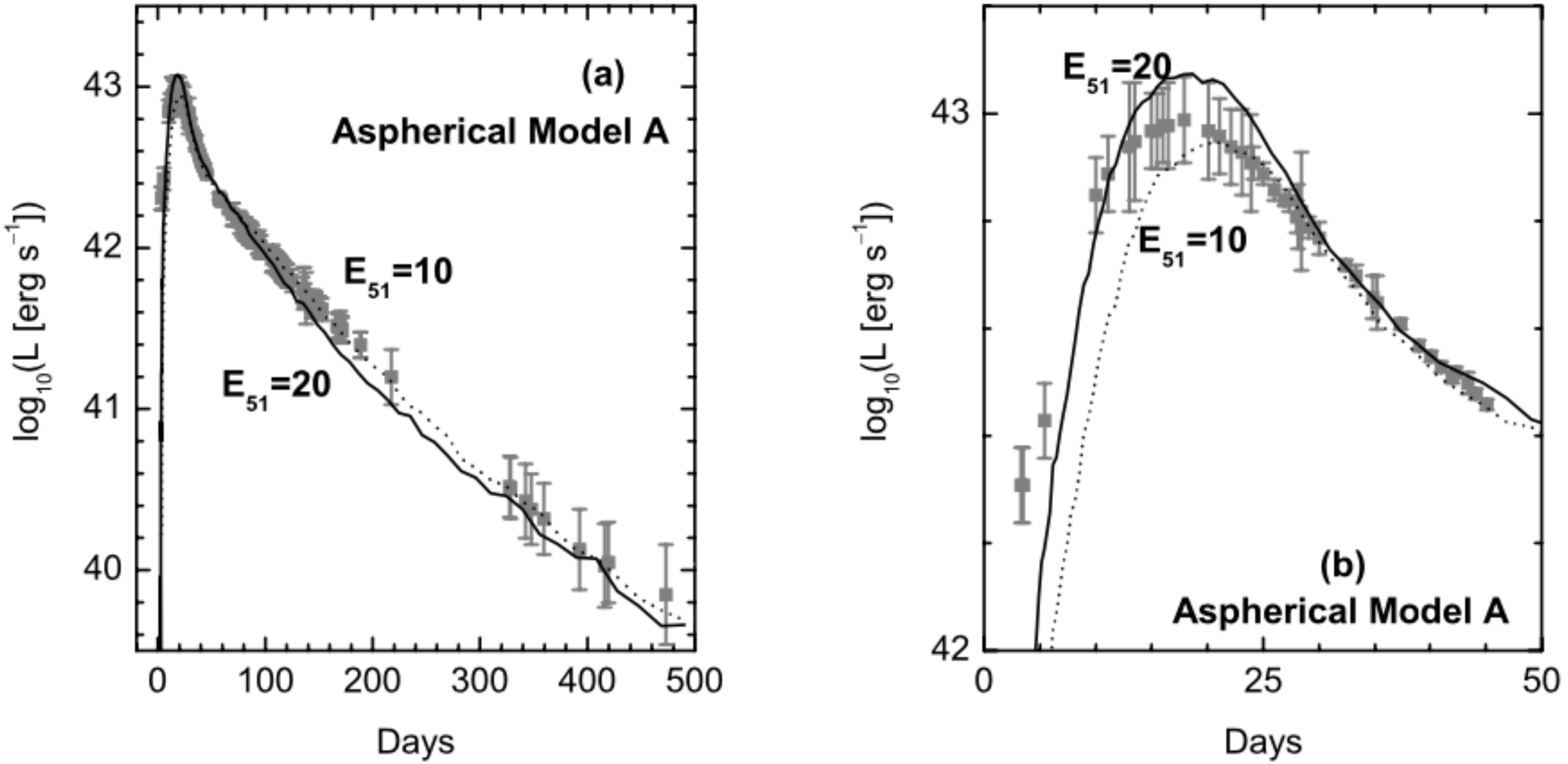

Model A: Explosion simulated by injecting energy asymmetrically : factor 16 times more power along polar directions.

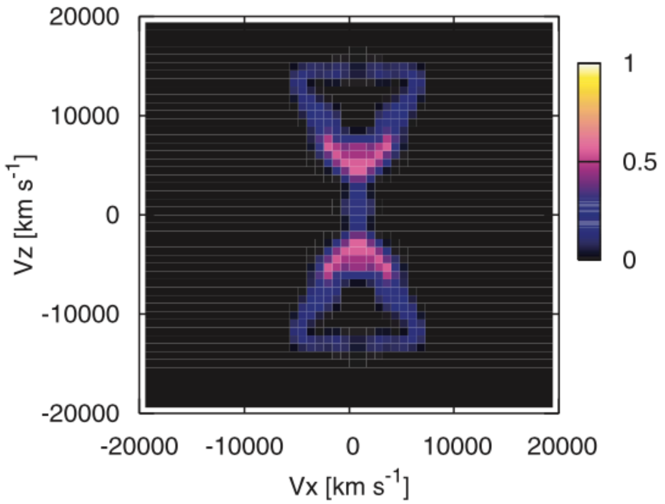

Maeda 2006

SN 1998bw revisited: light curves and spectral modelling

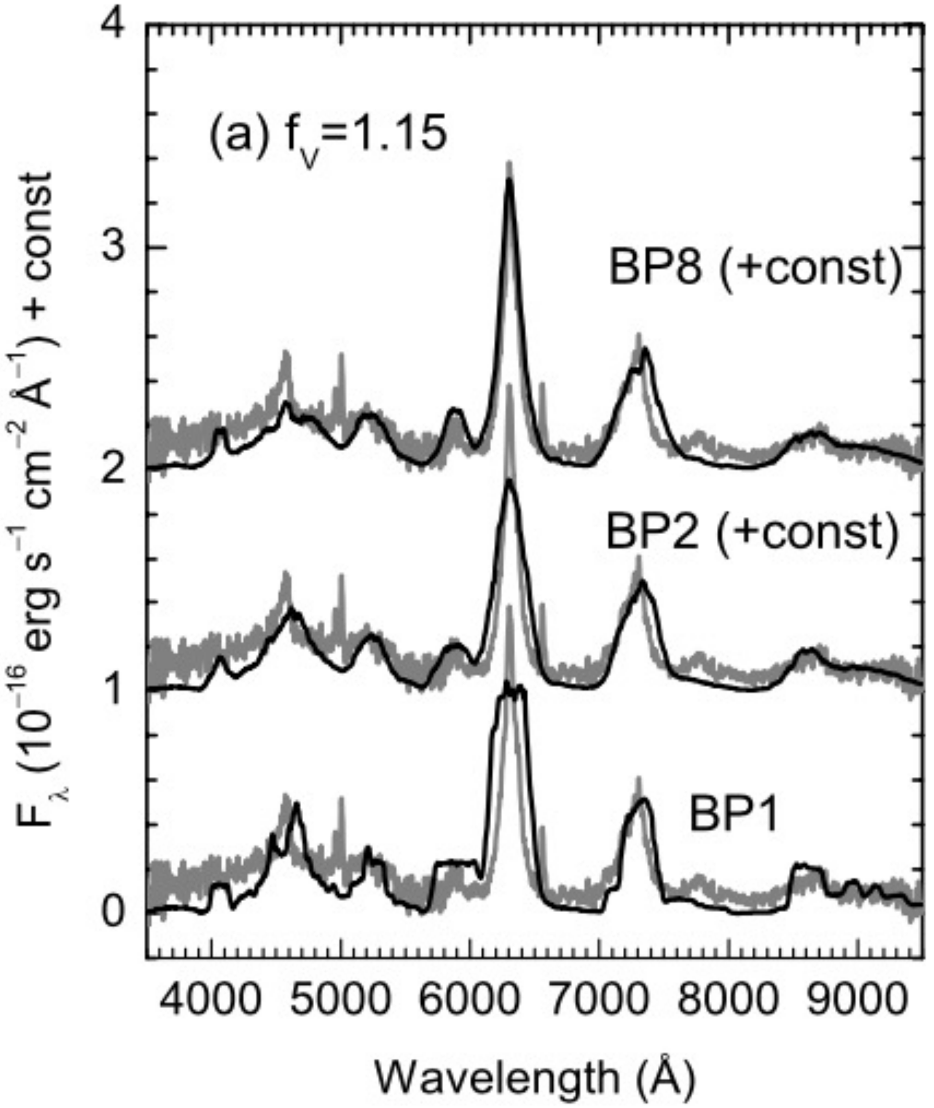

Also nebular spectra fit better with asymmetric models.

More asymmetry

Maeda 2006

Stellar progenitors of long GRBs

Long GRBs occur in star-forming regions and **clear association with the most massive stars**.

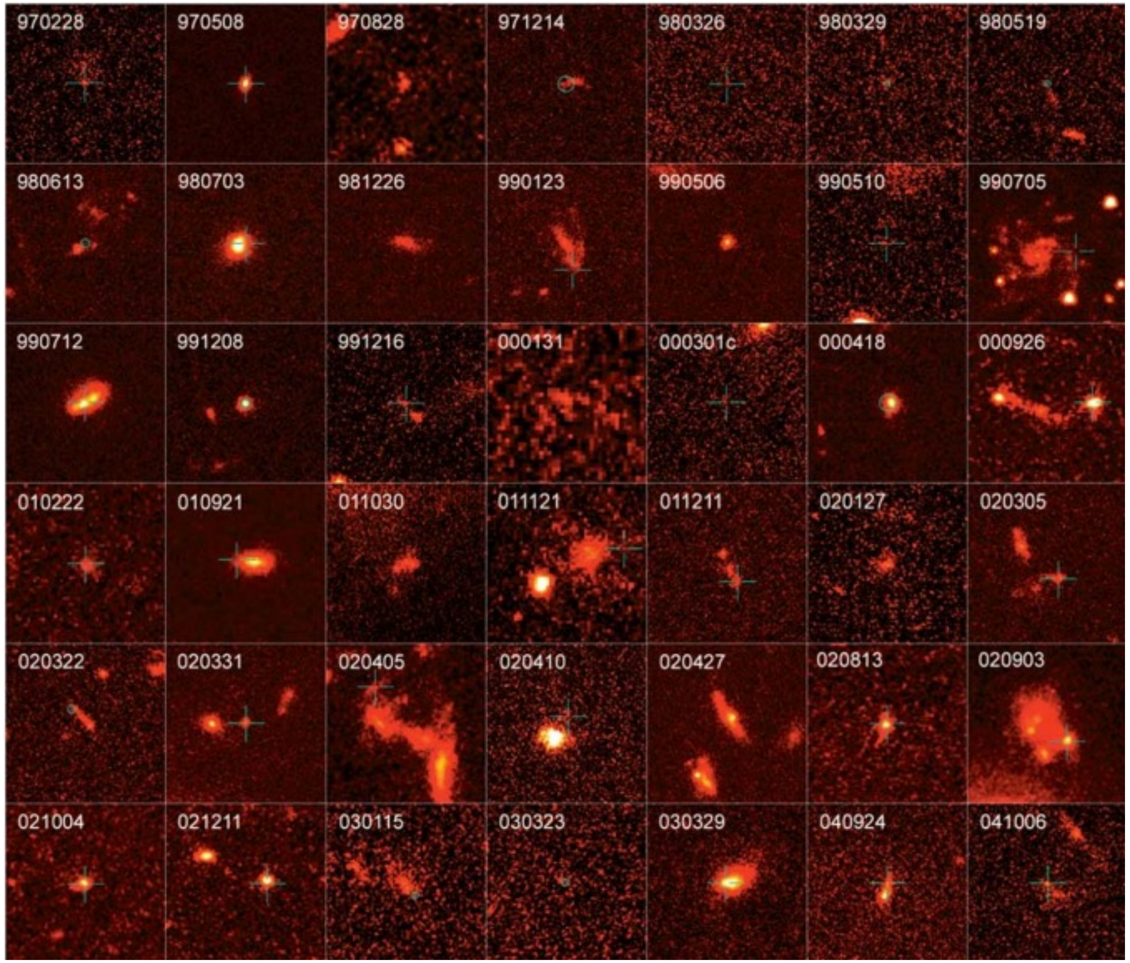

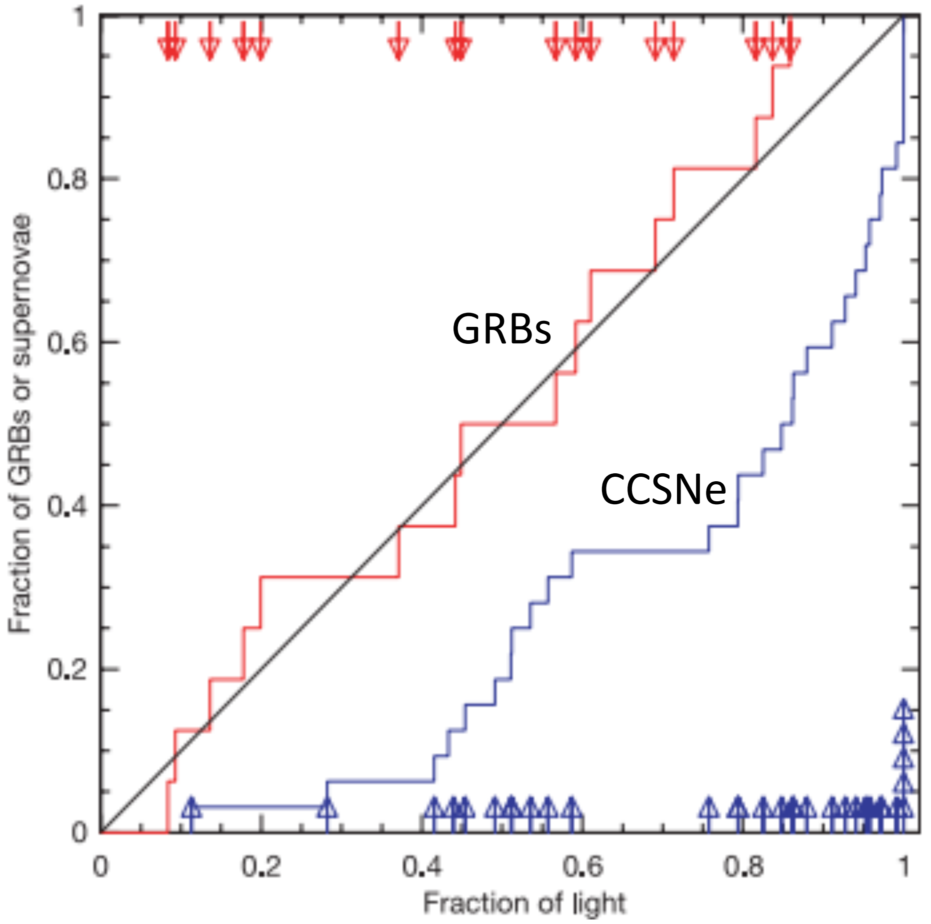

Fruchter 2006

Galaxies are often faint, blue (not intrinsic color in figure above), irregular.

Stellar progenitors of long GRBs

Woosley & Heger 2006,
Yoon, Langer &Norman 2006.

Main challenge : how to retain enough angular momentum in the core during a massive star's evolution?

High initial rotation the starting point.

But stars, and in particular their cores, tend to lose their angular momentum by

1. Wind mass loss (whole star)
2. Magnetic braking (core)

Important clue: GRBs seem to be more easily produced at **low metallicity**. Low metallicity reduces wind mass loss, and also keeps the star more compact which reduces both wind mass loss and magnetic braking.

But still need to get rid of the H envelope, and probably most of the He envelope (jets don't easily penetrate these while also retaining a structure necessary to make GRBs, Zhang 2004). Ideas:

1. H envelope removed by a companion instead of by winds (compare to the inferred binary stripping of most SE-SNe)?
2. Massive star at quite low metallicity?
3. Angular momentum comes instead from a merger event?

Magnetic fields remove angular momentum from stellar cores

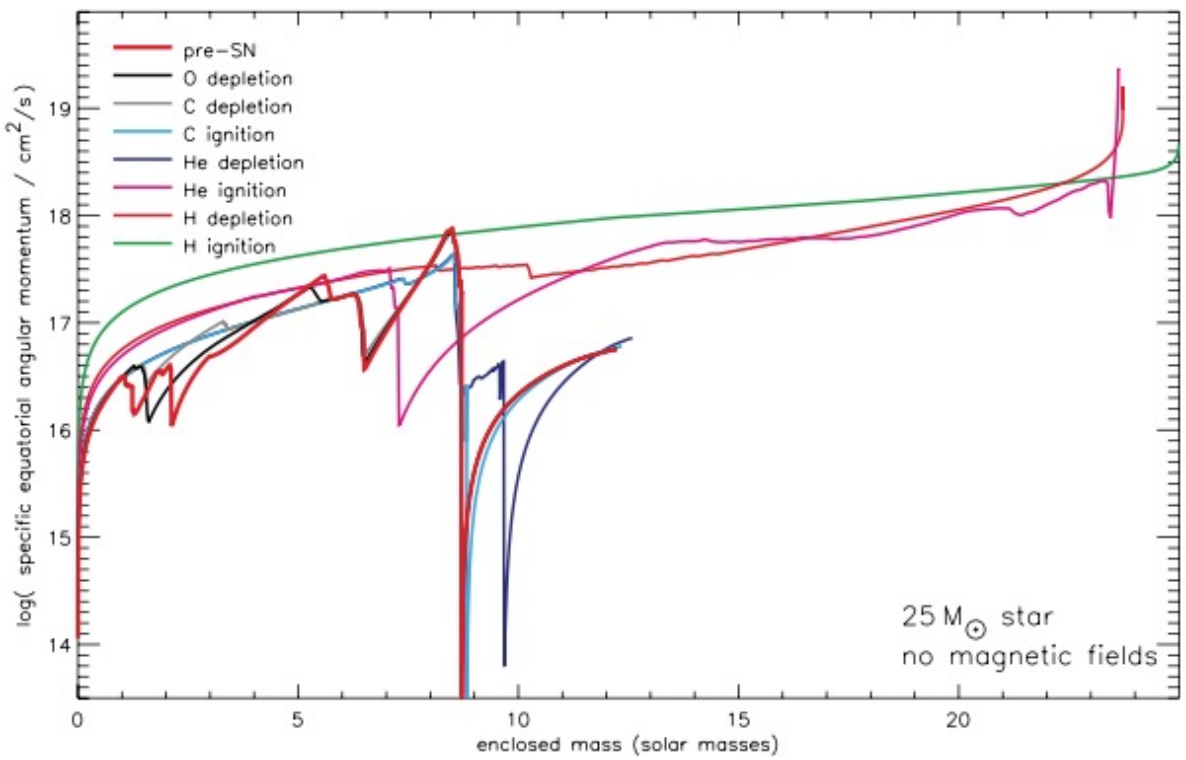

No B fields

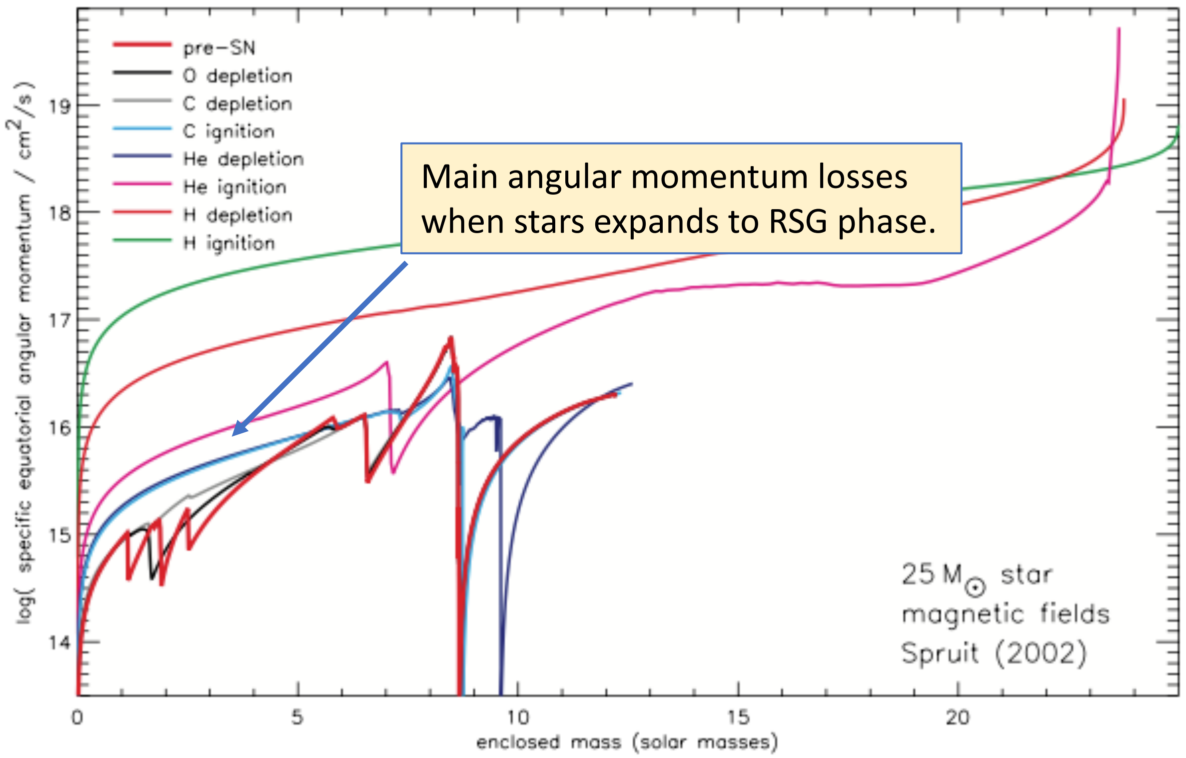

With B fields

Main angular momentum losses when stars expands to RSG phase.

Heger, Woosley & Spruit 2005

Magnetic torques usually included with prescription of Spruit 2002.
Successfully explains birth periods of “normal pulsars” from “normal stars” (Heger 2005).

Note that angular momentum can be transferred between different parts of the star
also by other processes: Eddington-Sweet circulation, shear instability, Goldreich instability, etc.
But the Spruit dynamo typically strongest effect. Implemented with a diffusion equation.

Rotation of stars

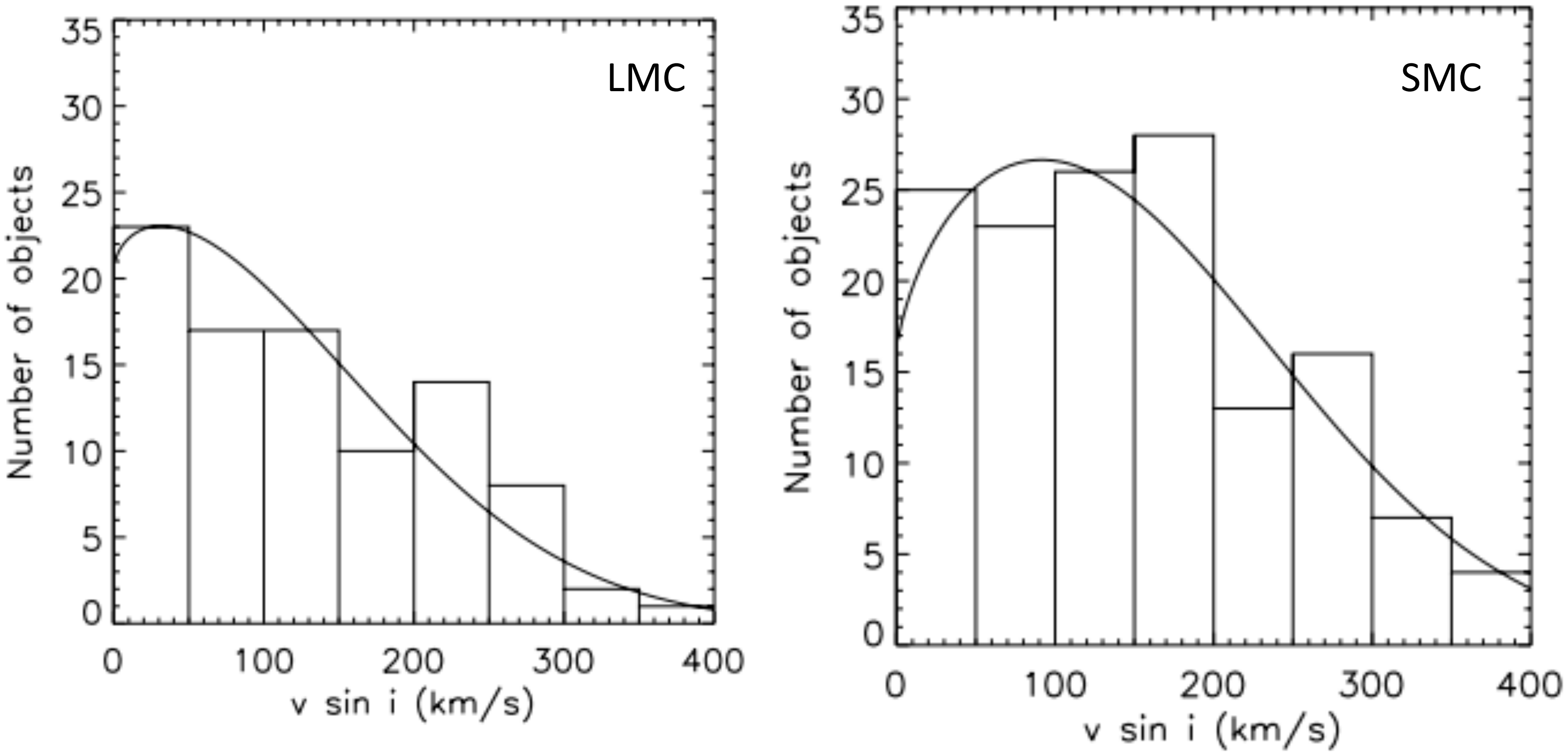

Average rotation speed of O & B stars is moderate, ~100-200 km/s (~20% of breakup).

About 1 in 300 stars rotate faster than 2/3 of breakup speed.

Lower-metallicity star rotate faster.

Rotation of Wolf-Rayet stars not well determined observationally.

Hunter 2008 : Measured rotation of O & B stars in LMC and SMC.

Rotation of stars

[Heger & Langer 2000](), [Heger et al. 2000]()

Centrifugal effects cause rotating stars to be hottest and most luminous along the poles ([von Zeipel 1924]()).

Rotation has an influence mainly in early burning stages (H, and sometimes He): the later stages transpire too quickly for rotational mixing effects to have an impact.

Initially, a rotating star is less luminous and colder (centrifugal support reduces burn rate). But, rotationally induced instabilities work to push the star's luminosity up. Strong chemical gradients established.

Over time the star therefore becomes more luminous. It then also develops a higher mass-loss rate and more easily evolves bluewards. It lives longer than a non-rotating one : more efficient mixing means an effectively larger fuel supply. This also leads to larger He cores, and larger CO cores. For example, a $M_{ZAMS} = 15\ M_{sun}$ star makes a $3\ M_{sun}$ He core with no rotation, but $4.5\ M_{sun}$ with fast rotation.

Compositional mixing occur by at least five different instabilities: the dominant one is typically **Eddington-Sweet circulation** which arises from thermal differences between poles and equator.

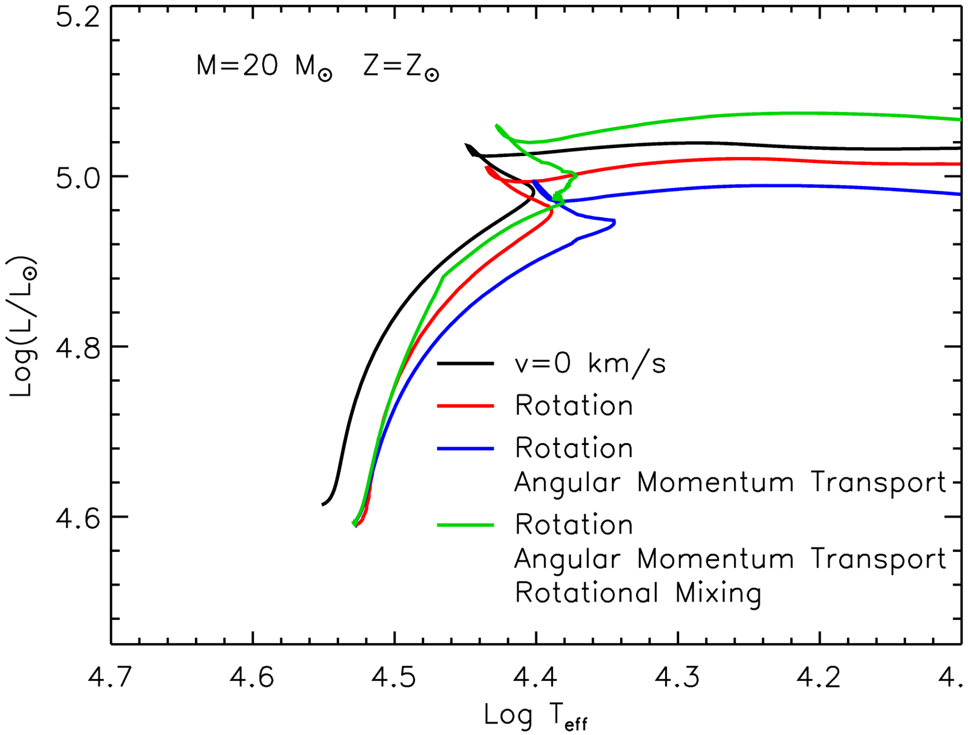

Credit: M. Limongi

Rotation of stars

Altair (2 M_{sun}, 2 R_{sun}, 16 ly distant) imaged by infrared interferometry : first resolved image if any main sequence star.

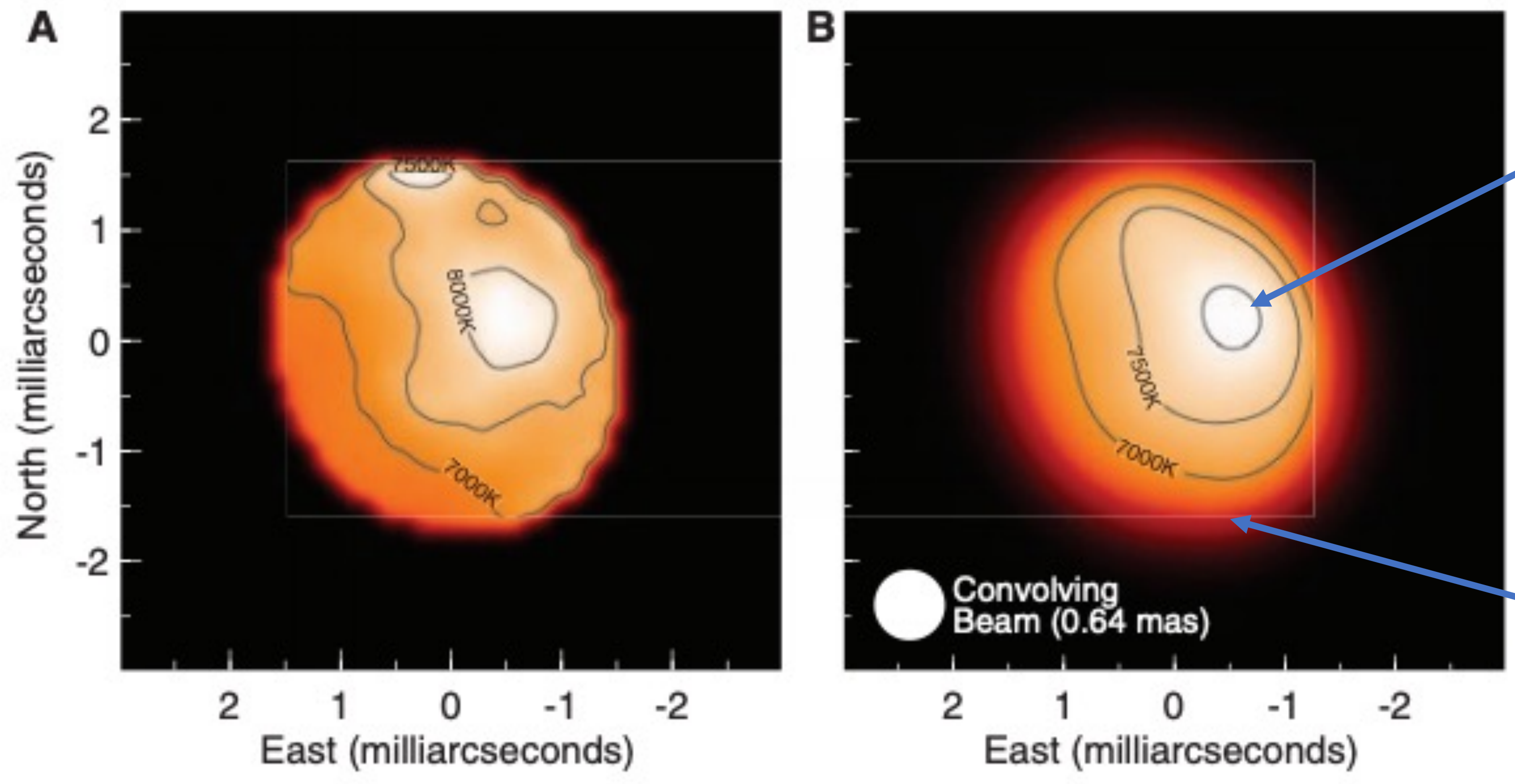

Hottest at the pole

Equatorial rotation 290 km/s

Monnier 2007

Rotation of stars

No rotation

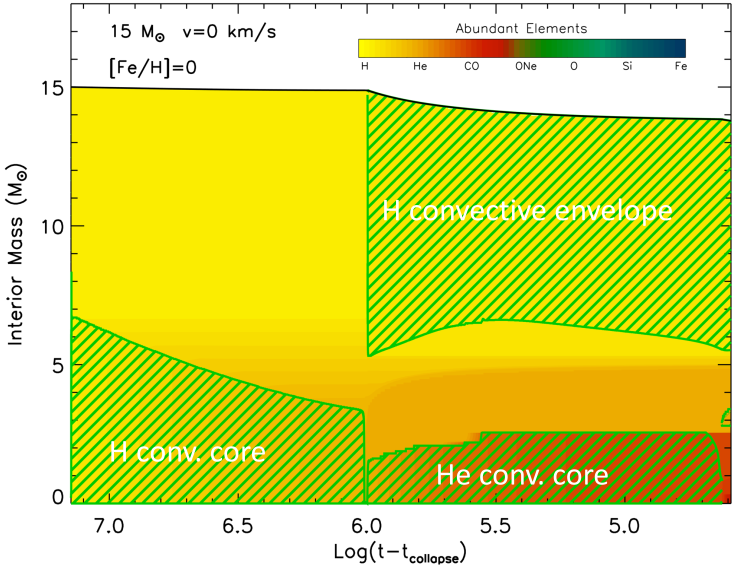

300 km/s rotation

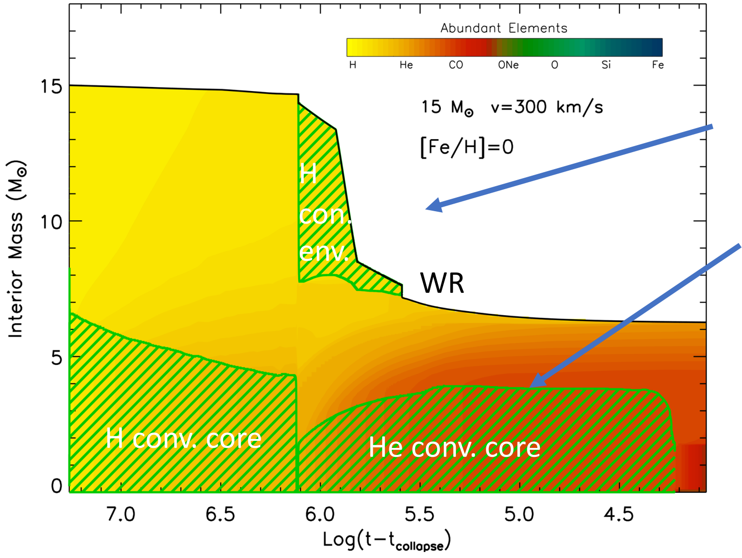

Stronger mass loss

Larger He core

Credit: M. Limongi

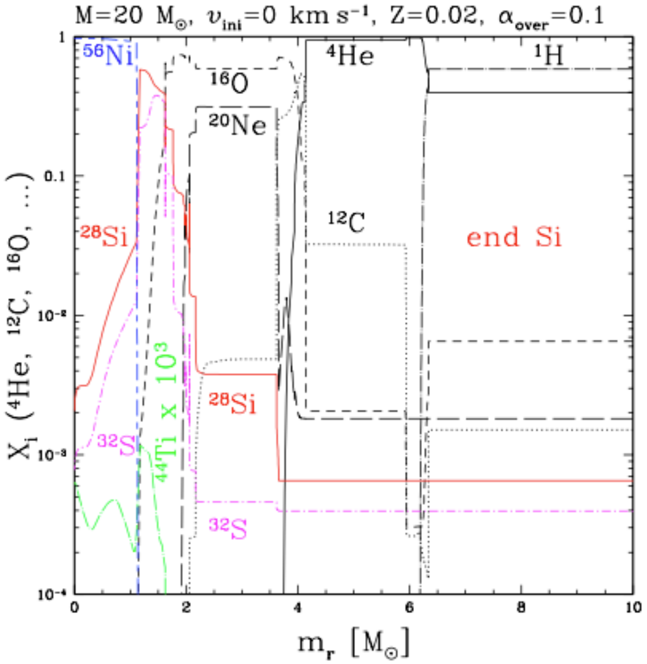

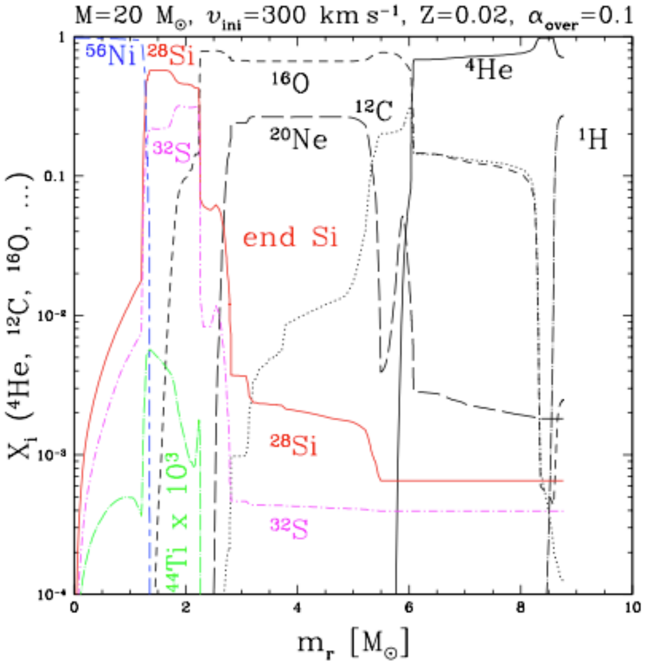

A rotating star “mimics” a higher mass non-rotating one.

Hirschi 2004

Chemically Homogenous Evolution (CHE)

At over ~50% of the critical rotation speed, the outer layers get efficiently mixed into the core → the whole star (or most of it) is processed by H burning and no large H envelope remains to make a supergiant. Instead O → WNha evolution, and the strong angular momentum losses associated with the supergiant stage (both by winds and magnetic braking) would be avoided.

This happens more easily at lower metallicity, and at higher mass.

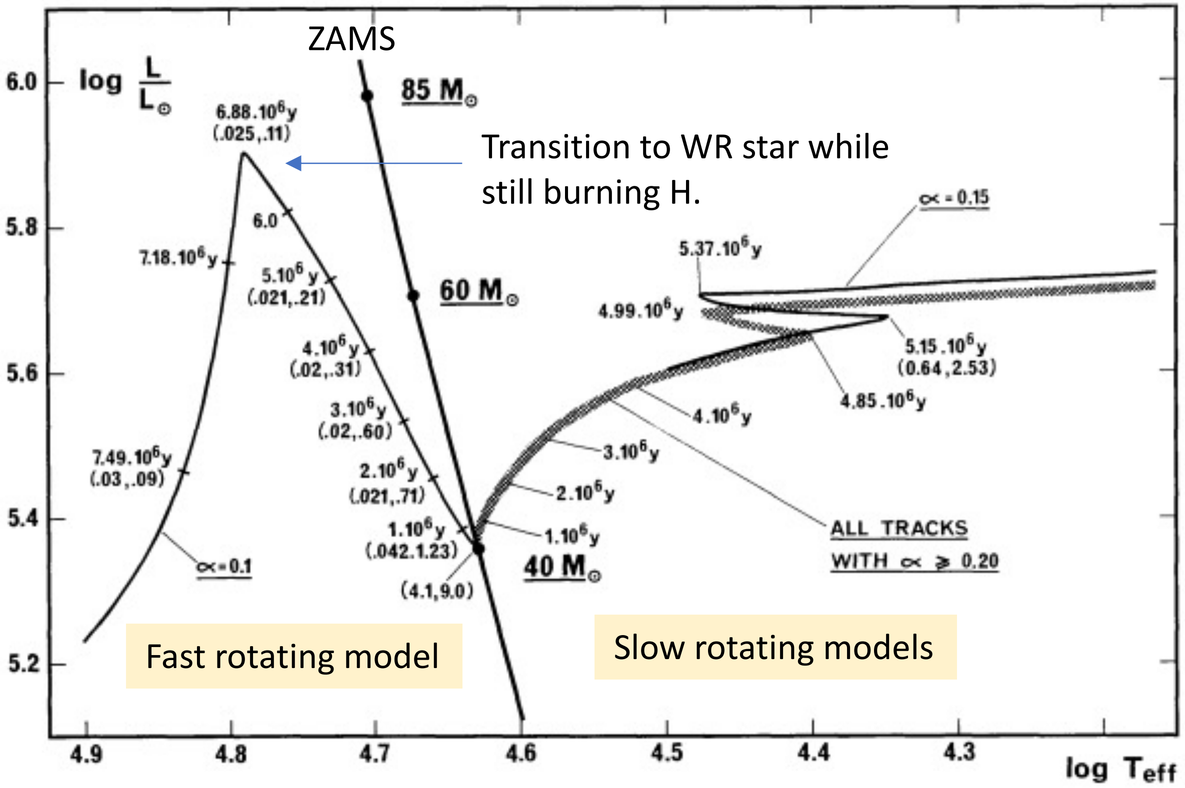

Transition to WR star while still burning H.

Fast rotating model

Slow rotating models

Maeder 1987

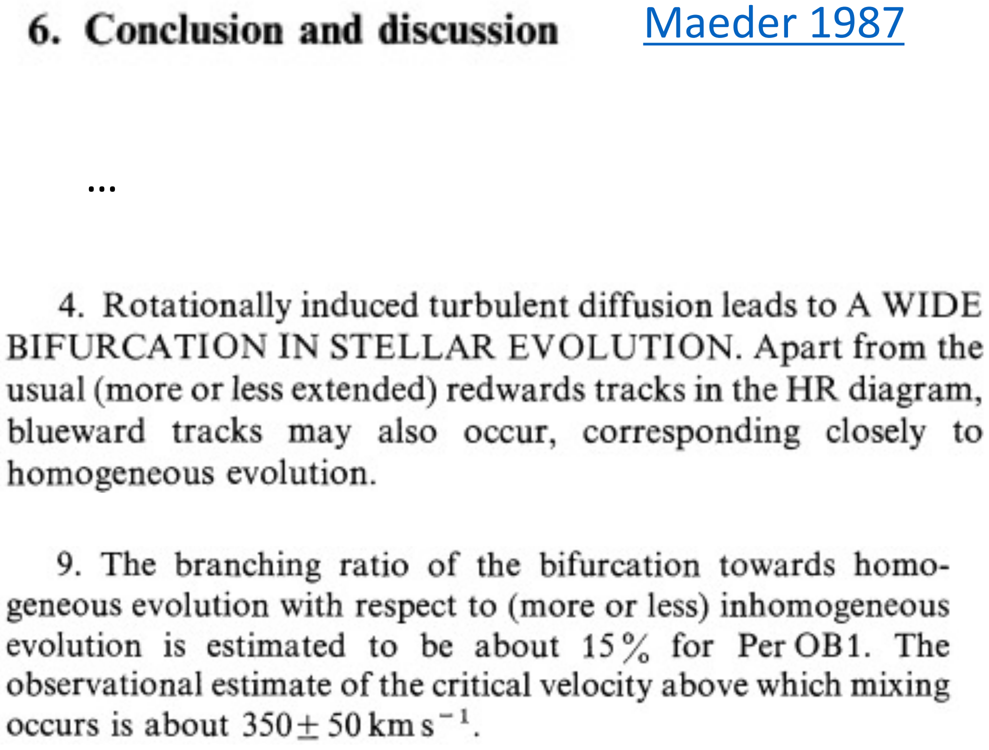

6. Conclusion and discussion

…

4. Rotationally induced turbulent diffusion leads to A WIDE BIFURCATION IN STELLAR EVOLUTION. Apart from the usual (more or less extended) redwards tracks in the HR diagram, blueward tracks may also occur, corresponding closely to homogeneous evolution.

9. The branching ratio of the bifurcation towards homogeneous evolution with respect to (more or less) inhomogeneous evolution is estimated to be about 15% for Per OB1. The observational estimate of the critical velocity above which mixing occurs is about 350 ± 50 km s^{-1}.

Angular momentum evolution in a star of M_{ZAMS}= 16 M_{sun}, v_{rot} = 400 km/s, Z = 1% of solar, WR mass loss rate suppressed by factor 3.

Almost no losses over H and He burning phases. Fast rotation → CHE and star never becomes a RSG, instead a WN star.

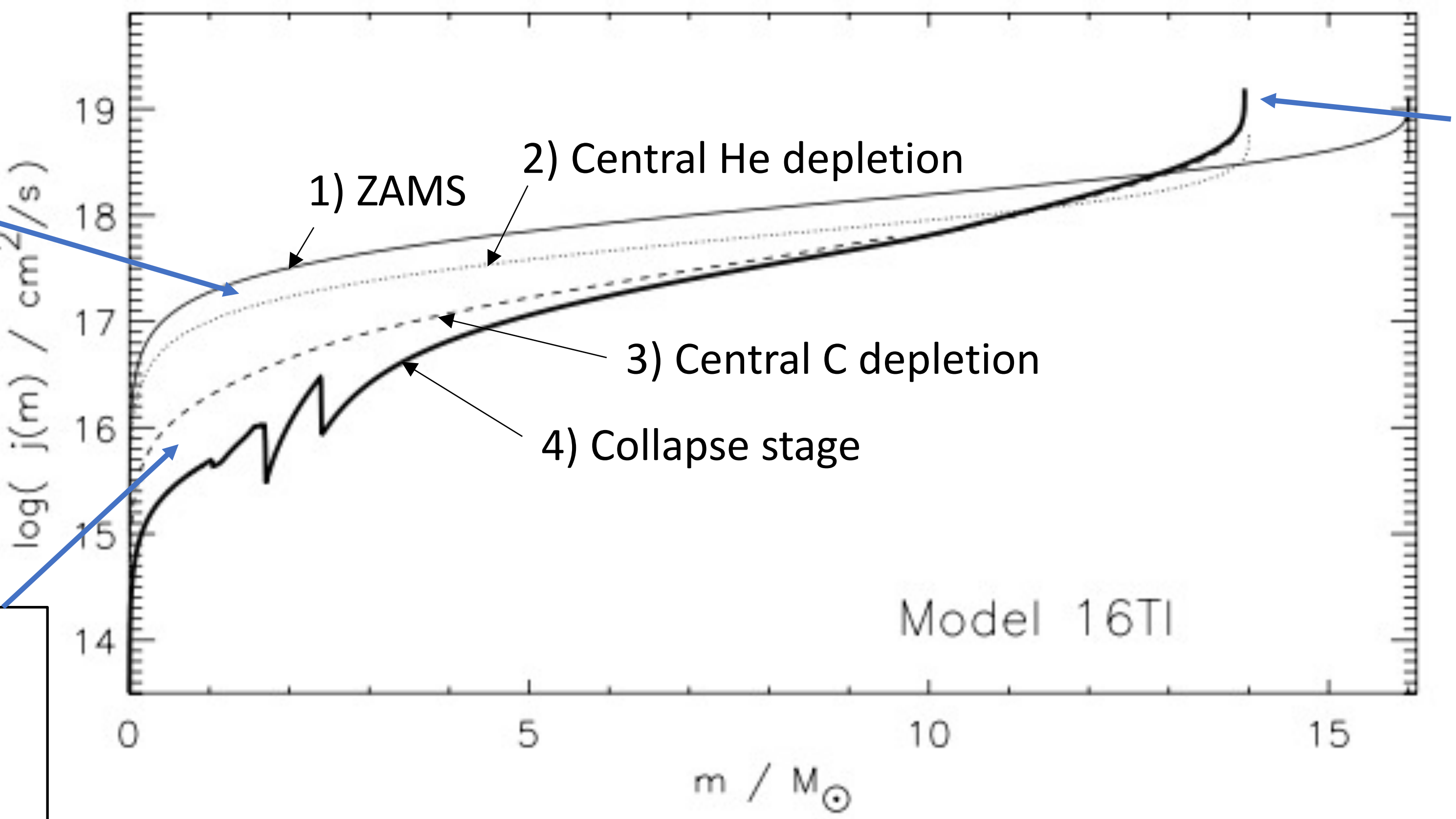

Core region loses factor ~5 angular momentum in last few months between central C depletion and collapse stage.

Only 2 M_{sun} lost to stellar winds over star’s whole life.

Star dies with only 0.3 M_{sun} of He left, and all at the surface, so probably would give a Type Ic SN.

Woosley & Heger 2006

Angular momentum evolution in a star of M_{ZAMS}= 16 M_{sun}, v_{rot} = 400 km/s, Z = 1% of solar, WR mass loss rate suppressed by factor 3.

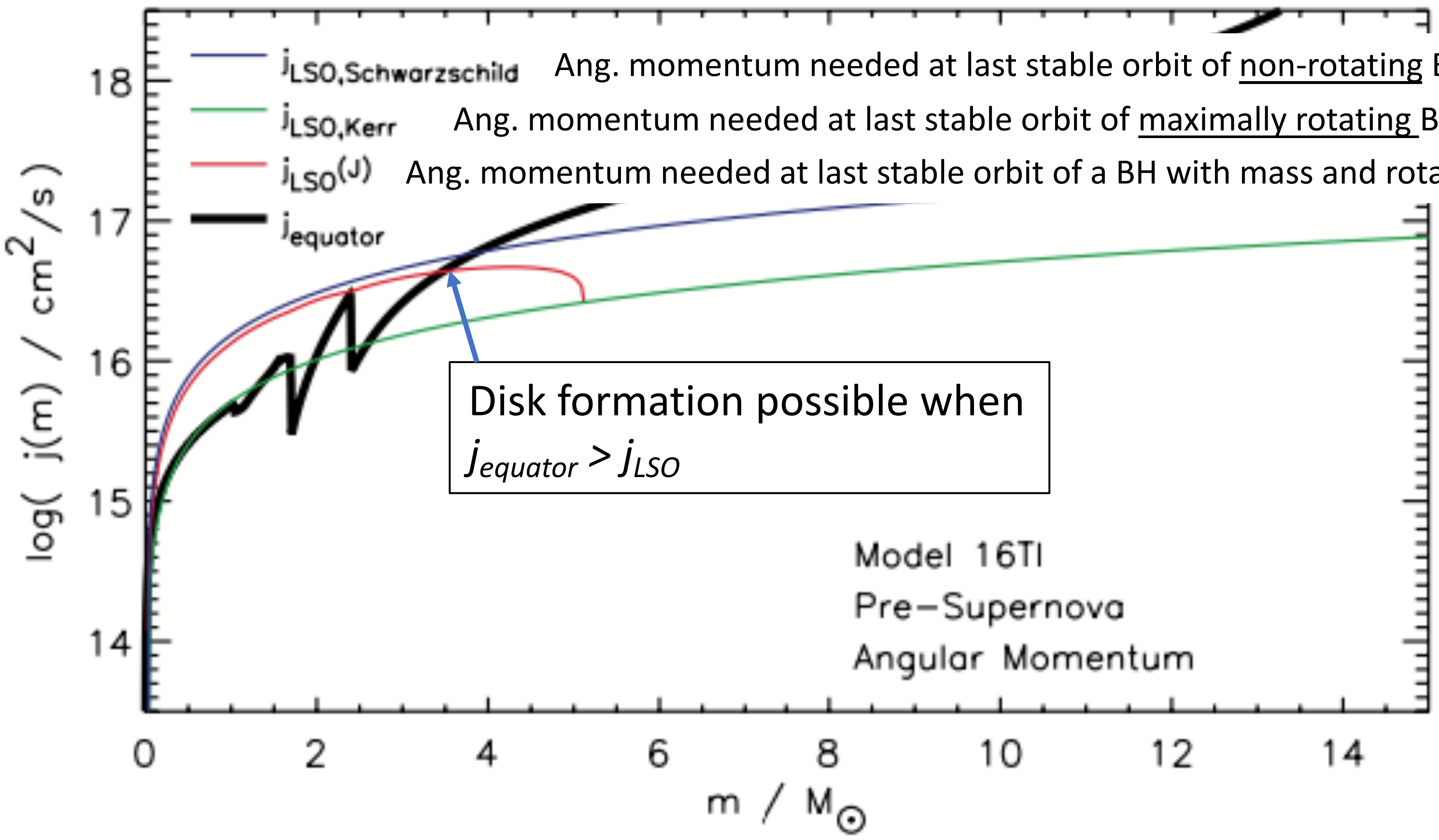

Ang. momentum needed at last stable orbit of non-rotating BH

Ang. momentum needed at last stable orbit of maximally rotating BH

Ang. momentum needed at last stable orbit of a BH with mass and rotation of inner material

Disk formation possible when $j_{equator} > j_{LSO}$

Woosley & Heger 2006

Do GRBs require low metallicity?

Many GRBs have low metallicity host environments, but that is mostly because they are at high redshift.

More recently many GRBs also at high metallicity have been discovered, and its not fully clear whether they form more easily in low-metallicity stars or not.

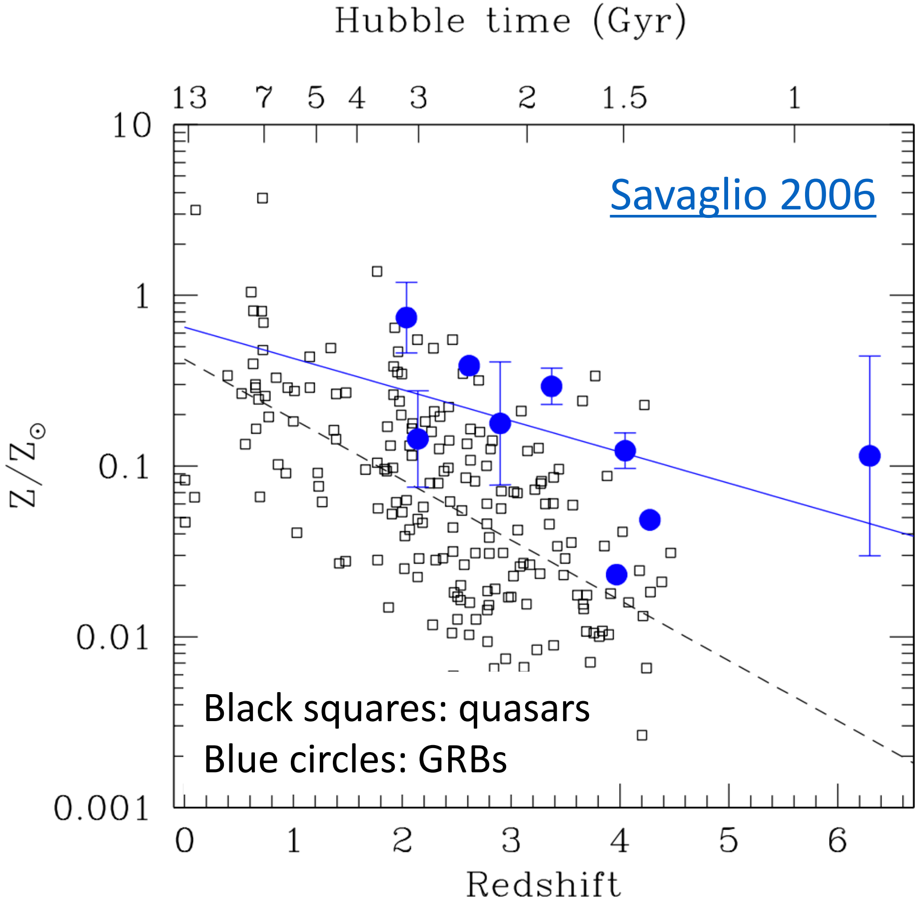

Savaglio 2006

Black squares: quasars

Blue circles: GRBs

Perley 2016

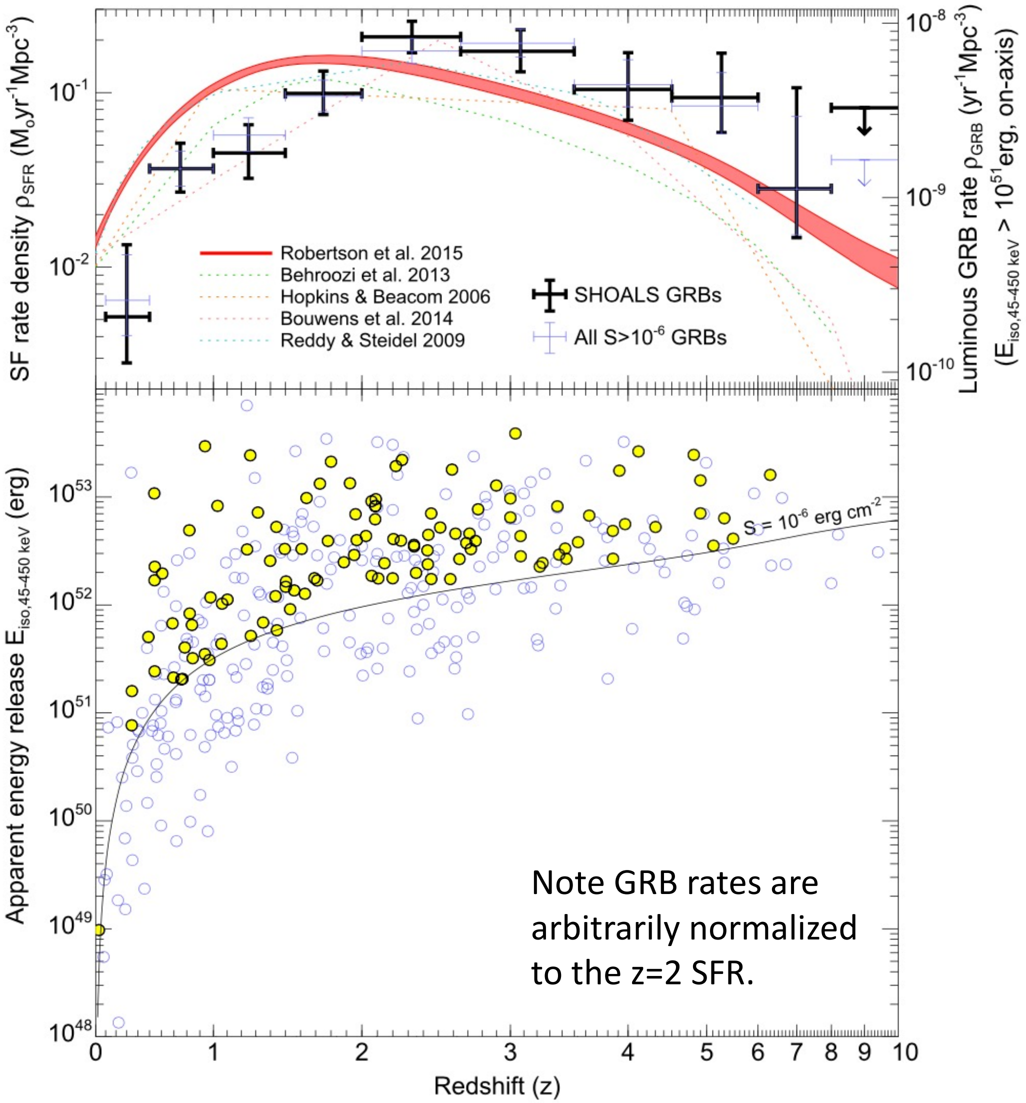

Note GRB rates are arbitrarily normalized to the z=2 SFR.

Short bursts

Radiated energies 1-2 orders of magnitude smaller than long.

<u>Properties consistent with merger of two NSs or a BH-NS:</u>

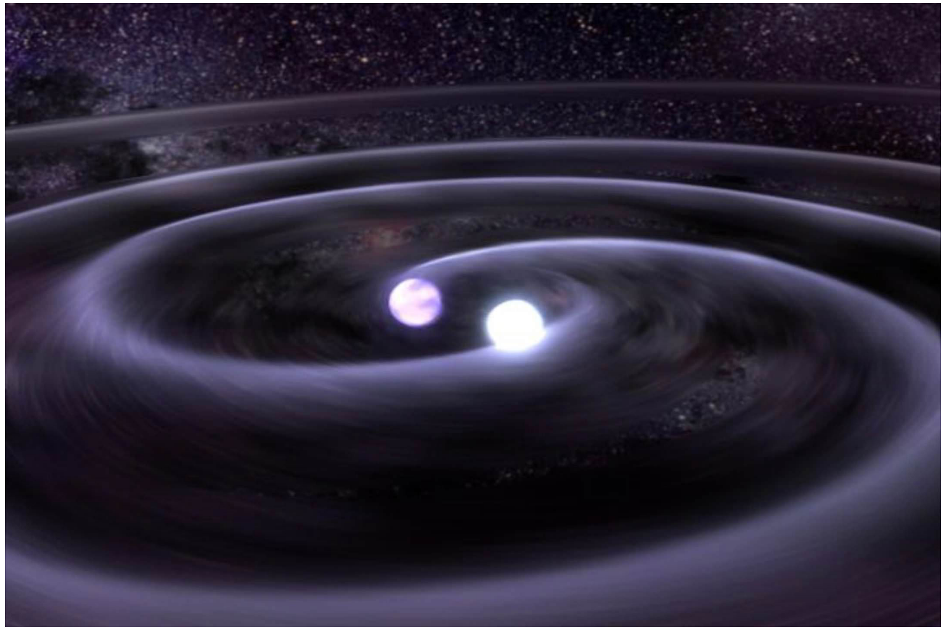

- Simulations of both NS-NS and BH-NS mergers show

that <~ 0.1 M_{sun} of material forms a disk.

- The time-scale of such a ~0.1 M_{sun} *non-resupplied disk* (in contrast to stellar collapse there is no resupply infall here) is <~ 1s agreeing with observed short GRB durations. (Note dynamic timescale of merger itself is too short, <~ ms, need an accretion disk).
- No SNe seen.
- Location often in old elliptical galaxies --> not from massive stars.

One may argue that in this case a BH is almost certainly forms (not a magnetar), so if BH accretion works for the short GRBs, why not for the long ones?

No SNe ever detected in short GRBs, and their weaker afterglows allow for strong limits

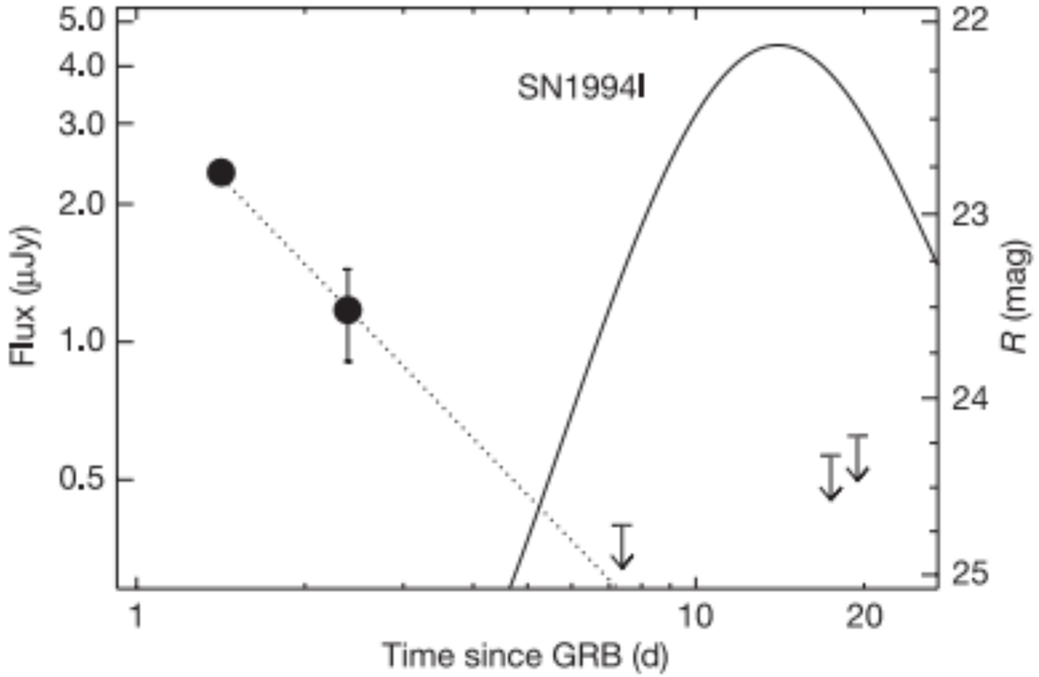

Hjorth 2005

Afterglow of a short GRB : even a normal Ic SN like SN 1994I can be ruled out.

Quentin's lecture: Sometimes though **kilonovae** seen following short GRBs.